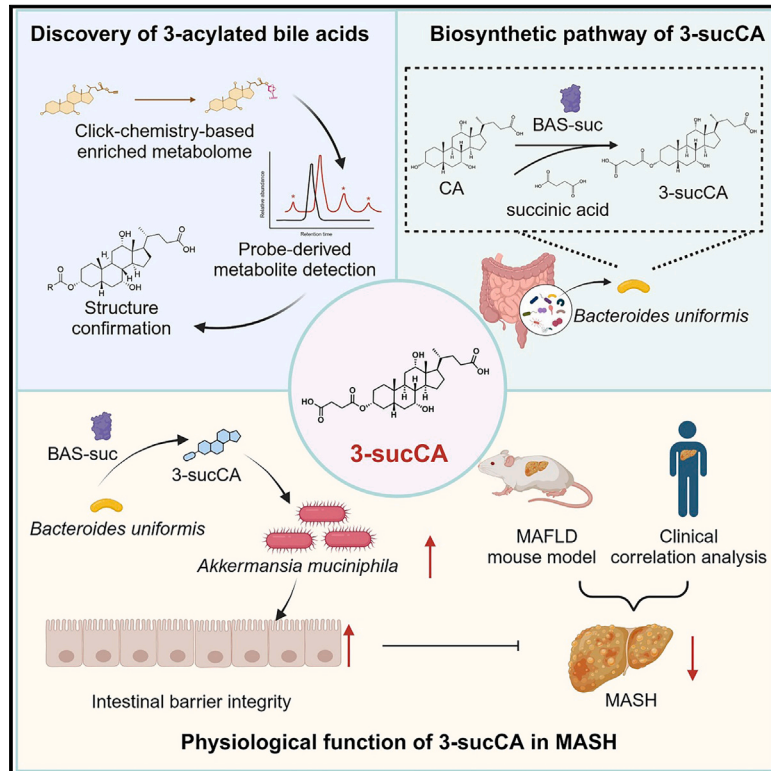


Gut symbionts alleviate MASH through a secondary bile acid biosynthetic pathway

Graphical abstract



Authors

Qixing Nie, Xi Luo, Kai Wang, ..., Yanli Pang, Jie Qiao, Changtao Jiang

Correspondence

yanxingjia@pku.edu.cn (Y.J.), zhengmh@wmu.edu.cn (M.-H.Z.), yanlipang@bjmu.edu.cn (Y.P.), jie.qiao@263.net (J.Q.), jiangchangtao@bjmu.edu.cn (C.J.)

In brief

The microbial bile acid 3-succinylated cholic acid is biosynthesized by BAS-suc, an enzyme annotated as β -lactamase in *Bacteroides uniformis*, and it alleviates MASH progression by enriching the abundance of the beneficial gut bacterium *Akkermansia muciniphila*.

Highlights

- A click-chemistry-based strategy identifies the microbial-derived bile acid 3-sucCA
- *B. uniformis*-expressed BAS-suc is responsible for 3-sucCA biosynthesis
- 3-sucCA is negatively correlated with liver damage in patients with MAFLD
- 3-sucCA alleviates MASH in mice by promoting *A. muciniphila* growth



Article

Gut symbionts alleviate MASH through a secondary bile acid biosynthetic pathway

Qixing Nie,^{1,2,3,16} Xi Luo,^{1,2,16} Kai Wang,^{2,4,16} Yong Ding,^{1,2,16} Shumi Jia,^{5,16} Qixiang Zhao,^{1,2} Meng Li,^{1,2} Jinxin Zhang,^{1,2} Yingying Zhuo,^{1,2} Jun Lin,^{1,2} Chenghao Guo,^{1,2} Zhiwei Zhang,^{1,2} Huiying Liu,^{1,2} Guangyi Zeng,^{1,2} Jie You,⁶ Lulu Sun,^{1,7} Hua Lu,⁸ Ming Ma,⁵ Yanxing Jia,^{5,*} Ming-Hua Zheng,^{9,10,11,*} Yanli Pang,^{1,12,13,14,*} Jie Qiao,^{1,12,13,14,*} and Changtao Jiang^{1,2,4,15,17,*}

¹Department of Physiology and Pathophysiology, School of Basic Medical Sciences, State Key Laboratory of Female Fertility Promotion, Center for Reproductive Medicine, Third Hospital, Peking University, Beijing, China

²Center for Obesity and Metabolic Disease Research, School of Basic Medical Sciences, State Key Laboratory of Vascular Homeostasis and Remodeling, Peking University, Beijing 100191, China

³State Key Laboratory of Food Science and Resources, Key Laboratory of Bioactive Polysaccharides of Jiangxi Province, Nanchang University, Nanchang, China

⁴Department of Immunology, School of Basic Medical Sciences, NHC Key Laboratory of Medical Immunology, Peking University, Beijing, China

⁵State Key Laboratory of Natural and Biomimetic Drugs, School of Pharmaceutical Sciences and Chemical Biology Center, Peking University, Beijing 100191, China

⁶Department of Thyroid Surgery, the First Affiliated Hospital of Wenzhou Medical University, Wenzhou, China

⁷Department of Endocrinology and Metabolism, Peking University Third Hospital, Beijing 100191, China

⁸Beijing National Laboratory for Molecular Sciences, Center for Soft Matter Science and Engineering, Key Laboratory of Polymer Chemistry and Physics of Ministry of Education, College of Chemistry and Molecular Engineering, Peking University, Beijing 100871, People's Republic of China

⁹MAFLD Research Center, Department of Hepatology, the First Affiliated Hospital of Wenzhou Medical University, Wenzhou, China

¹⁰Key Laboratory of Diagnosis and Treatment for the Development of Chronic Liver Disease in Zhejiang Province, Wenzhou, China

¹¹Translational Medicine Laboratory, the First Affiliated Hospital of Wenzhou Medical University, Wenzhou 325035, China

¹²Institute of Advanced Clinical Medicine, Peking University, Beijing 100191, China

¹³National Clinical Research Center for Obstetrics and Gynecology, Peking University Third Hospital, Beijing, China

¹⁴Beijing Key Laboratory of Reproductive Endocrinology and Assisted Reproductive Technology, Beijing, China

¹⁵Center of Basic Medical Research, Institute of Medical Innovation and Research, Peking University Third Hospital, Beijing, China

¹⁶These authors contributed equally

¹⁷Lead contact

*Correspondence: yanxingjia@pku.edu.cn (Y.J.), zhengmh@wmu.edu.cn (M.-H.Z.), yanlipang@bjmu.edu.cn (Y.P.), jie.qiao@263.net (J.Q.), jiangchangtao@bjmu.edu.cn (C.J.)

<https://doi.org/10.1016/j.cell.2024.03.034>

SUMMARY

The gut microbiota has been found to play an important role in the progression of metabolic dysfunction-associated steatohepatitis (MASH), but the mechanisms have not been established. Here, by developing a click-chemistry-based enrichment strategy, we identified several microbial-derived bile acids, including the previously uncharacterized 3-succinylated cholic acid (3-sucCA), which is negatively correlated with liver damage in patients with liver-tissue-biopsy-proven metabolic dysfunction-associated fatty liver disease (MAFLD). By screening human bacterial isolates, we identified *Bacteroides uniformis* strains as effective producers of 3-sucCA both *in vitro* and *in vivo*. By activity-based protein purification and identification, we identified an enzyme annotated as β -lactamase in *B. uniformis* responsible for 3-sucCA biosynthesis. Furthermore, we found that 3-sucCA is a lumen-restricted metabolite and alleviates MASH by promoting the growth of *Akkermansia muciniphila*. Together, our data offer new insights into the gut microbiota-liver axis that may be leveraged to augment the management of MASH.

INTRODUCTION

Metabolic dysfunction-associated fatty liver disease (MAFLD) is the most common chronic liver disorder, with a global prevalence

of approximately 25% among the adult population. And given the global obesity epidemic, it has become a major worldwide public health concern. MAFLD encompasses conditions ranging from the relatively benign metabolic dysfunction-associated fatty liver



(MAFL) to the more pathologically severe metabolic dysfunction-associated steatohepatitis (MASH) and, in some cases, can progress to cirrhosis and/or hepatocellular carcinoma. Currently, there are a few therapeutic drugs for MAFL-MASH, and thus treatment, especially for MASH, represents an important unmet clinical need.^{1,2} An interdependence and tissue crosstalk between the liver and the gut, particularly the gut microbiota, has been found to contribute to the metabolic dysregulation and inflammation that is a hallmark of MASH.^{3–5} However, the clear causal effects between microbial-derived metabolites and MASH progression have not been well established.

Bile acids are pivotal messengers between the host and the gut microbiota, and they play an important role in the regulation of MASH via activation of various receptors, including farnesoid X receptor (FXR) and Takeda G-protein-coupled receptor 5 (TGR5).^{6–9} Although several bile acids may play a role in the improvement of MASH, the overall role of bile acids in MASH pathogenesis remains unclear. The enrichment of bile acid abundance during MASH progression has been observed in multiple studies and is thought to contribute to the lipotoxicity that exacerbates the disease.^{10–13} Additionally, by enhancing a senescence-associated secretome that promotes inflammation in the liver, microbial-derived deoxycholate (DCA) has been linked to hepatocellular carcinoma pathogenesis in MASH,¹⁴ illustrating the complex role of bile acids in MASH progression. In addition, due to their broad affinity for multiple targets, bile acids and their analogs often cause unexpected side effects.¹⁵

Uncovering the underlying microbial metabolic networks is essential for elucidating the physiological significance of bile acids. Recently, several uncharacterized microbial-derived bile acids, referred to as secondary bile acids, have been discovered,^{16–21} and several enzymes were found to be involved in the bile acid metabolism,^{22,23} which reinforces the role of microbiota in shaping the host's bile acid pool.

Here, we used a click-chemistry-based enrichment strategy and identified several secondary bile acids, including 3-succinylated cholic acid (3-sucCA), which we found to be lower in patients with biopsy-confirmed MAFLD compared with controls. We used a screen of human bacterial isolates to identify gut bacteria that produce 3-sucCA. Using activity-based protein purification and identification, we showed that an enzyme annotated as β -lactamase is responsible for 3-sucCA biosynthesis. Importantly, we found that 3-sucCA is a lumen-restricted metabolite and that it alleviates MAFL-MASH progression in mouse models by reshaping the gut microbiota, especially by expanding the population of *Akkermansia muciniphila*. Together, we identified the bacterial producer and biosynthetic enzyme of 3-sucCA and revealed microbial production of 3-sucCA as a potential therapeutic strategy for augmenting the management of MAFL-MASH.

RESULTS

A click-chemistry-based enrichment strategy identifies secondary bile acids

Previous studies have identified a range of microbial amino-acid-conjugated bile acids with amidation at the 24-carboxyl group and their physiological abundance.^{19–21,24–27} We attempted to identify microbial-derived bile acids that are reacted with other

functional groups. To improve sensitivity through enrichment from overwhelming pools of unrelated metabolites and to facilitate recognition of bile acid metabolites by means of a specific fragmentation signature in liquid chromatography-tandem mass spectrometry (LC-MS/MS), we used a click-chemistry-based enrichment strategy²⁸ to investigate the microbial metabolism of bile acids. As cholic acid (CA) is a major primary bile acid in the host, we selected CA as the substrate to construct an alkyne probe for click-chemistry reaction. As shown in the schematic overview (Figure 1A), we synthesized an alkyne probe of CA (alkCA), which added an allylene group at the 24-carboxyl group of CA (Figure S1A). After the click reaction, alkCA is transformed into CA linker (CA-LNK), which displays a higher mass spectrometry response than CA at the same concentration (Figure S1B) and has a characteristic reporter ion at m/z 100.0761 for identification (Figure 1B). By incubating the alkCA probe in human stool-derived *ex vivo* communities (SECs),²⁹ we observed that alkCA probe incubation showed a number of characteristic peaks of derivatives after click reaction (Figure S1C). Our analysis of the tandem mass spectra of several nodes (616.4060, 630.4219, 644.4376, 658.4533, 646.4169, 674.4115, and 688.4276) showed the maintenance of the core CA but with a fragmentation pattern that was characteristic of the presence of several carboxylic acids through an ester bond (Figures S1D and S1E), including several monoacids (formic acid, acetic acid, propionic acid, butyric acid, and glycolic acid), along with two binary acids (malonic acid and succinic acid) harboring a terminal carboxyl group, which is rarely observed in microbial natural products.³⁰

CA possesses three hydroxyl groups (3, 7, and 12) that can undergo an esterification reaction. To determine the exact position of the acylated CAs, we fermented CA with human SECs in a large volume (20 L) and isolated the potential acylated CAs. As determined by one-dimensional and two-dimensional nuclear magnetic resonance (NMR), we obtained 5 acylated CAs, with the acylation reactions all occurring at the 3-hydroxyl group (Figures S1F and S1G). Among these, we validated the stereostructure of 3-sucCA by X-ray single-crystal diffraction (Figure S1H). For further verification, we synthesized all the supposed 3-acylated CAs (Figure S1I) and compared them with CA-incubated human SECs, demonstrating identical LC-MS/MS spectra and retention time with authentic synthetic standard materials (Figure S1J).

All identified 3-acylated CAs were observed in SECs with different prevalence rates (Figures S1K–S1M). We collected fresh fecal samples from 23 healthy volunteers and then detected the content of acylated CAs, and 4 of 7 tested 3-acylated CAs were observed in fecal samples (Figures 1C, 1D, and S1N). In specific-pathogen-free (SPF) mice, only 3-sucCA and 3-acetylated CA (3-aceCA) were observed in the fecal samples, and an antibiotic-treatment group showed a significant decrease in 3-sucCA and 3-aceCA levels (Figures 1D and S1O). Fecal microbiota transplantation (FMT) from SPF mice to antibiotic-treated mice reversed the effect of antibiotics on 3-sucCA and 3-aceCA levels (Figure S1O). Moreover, the above 3-acylated CAs were undetectable in the feces of germ-free (GF) mice, indicating the contribution of the gut microbiota to the levels of 3-acylated CA (Figure S1P).

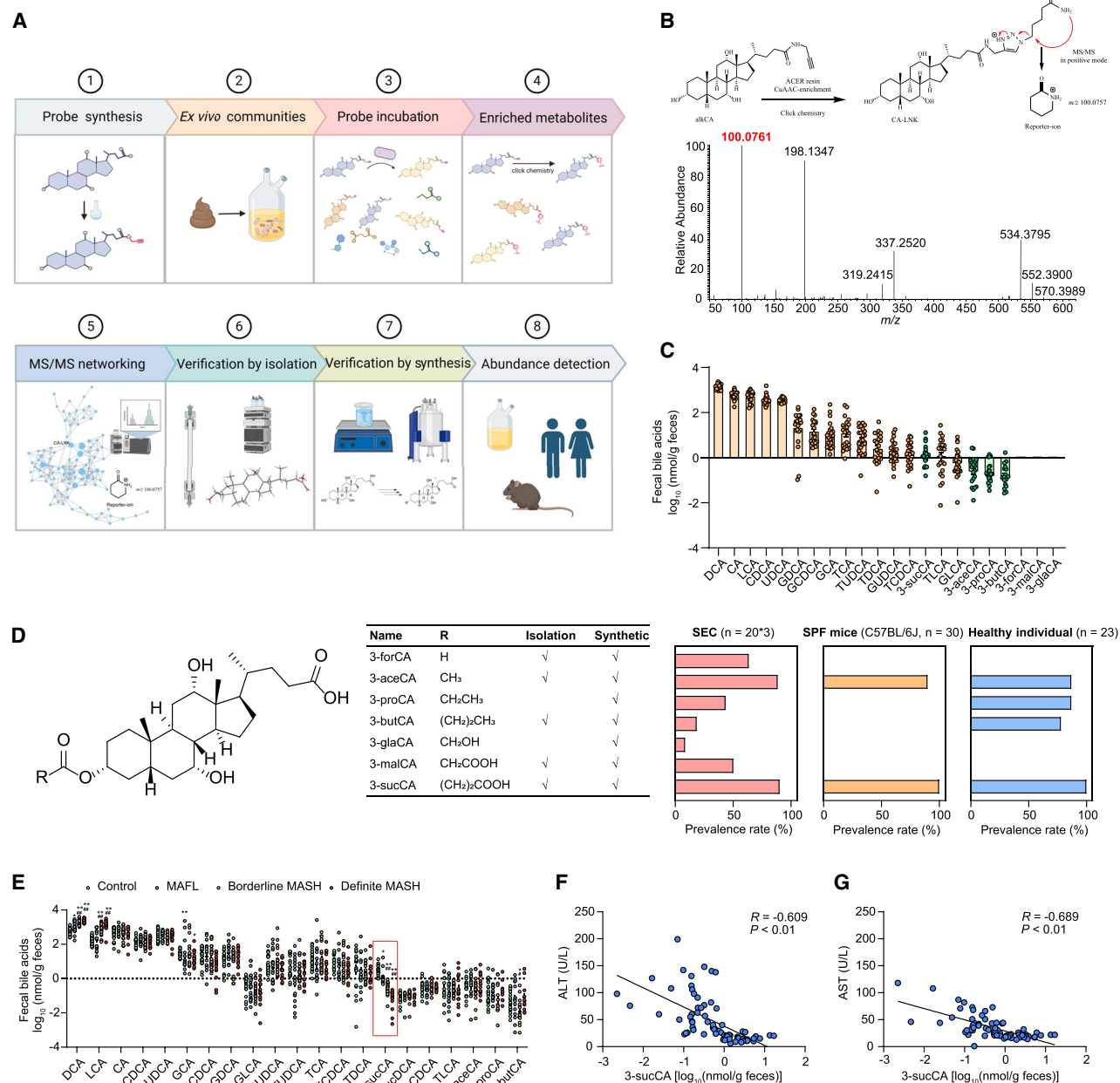


Figure 1. 3-sucCA is lower in patients with biopsy-proven MAFLD

(A) Schematic representation of the microbiota-associated bile acid screening system. The synthesized alkCA probe was incubated in human stool-derived *ex vivo* communities (SECs) after probe incubation and enrichment using the ACER resin. Enriched metabolites (CA-LNK derivatives) are analyzed via LC-MS/MS. Target metabolites were further verified by both isolation- and synthesis-based methods and then analyzed for physiological and pathological abundance.

(B) Characteristic peak of CA-LNK. MS/MS of CA-LNK in positive mode produces a reporter ion at m/z 100.0761 (within 5 ppm, theoretical m/z is 100.0757).

(C) Bile acids profile in feces of 23 healthy volunteers. Orange represents classical bile acids, and green represents bile acids identified by click-chemistry-based enrichment strategy. Missing points indicate that relevant bile acids were not detected in the samples.

(D) Structure, identification process, and prevalence rate in SECs ($n = 20$ individuals with 3 different culture conditions), mice ($n = 30$), or humans ($n = 23$).

(E) Quantification of fecal bile acids in 21 controls and 55 patients with different MAFLD stages (MAFL [$n = 17$], borderline MASH [$n = 23$], or definite MASH [$n = 15$]). Missing points indicate that relevant bile acids were not detected in the samples.

(F and G) Correlative analysis of 3-sucCA concentration with levels of ALT (F) and AST (G). Correlations between variables were assessed by linear regression analysis. Linear correlation index R and p values were calculated.

All data are presented as the means \pm SEMs. In (E), the p values were determined by Kruskal-Wallis test followed by Dunn's post hoc test. * $p < 0.05$ and ** $p < 0.01$ versus the control group. ## $p < 0.01$ and ### $p < 0.01$ versus the MAFL group. See also Figure S1.

3-sucCA levels are lower in patients with biopsy-proven MAFLD

To elucidate the correlation between 3-acylated CAs and human MAFL-MASH progression, we collected data from 55 patients with liver-tissue-biopsy-proven MAFLD, along with 21 controls with similar ages and sexes (Table S1). Fecal and serum samples were collected to measure 3-acylated CA levels and biochemical indicators. In line with previous reports,^{10,31} we observed a significant increase in DCA and lithocholic acid (LCA) with MAFL-MASH progression (Figure 1E). However, lower 3-sucCA levels were observed in the patients with MAFLD compared with controls (Figure 1E), and 3-sucCA levels were negatively correlated with MAFLD severity (MAFL, borderline MASH, and definite MASH), as indicated by various pathology indicators, including the MAFLD activity score (MAS), the steatosis score, the presence of lobular inflammation, the ballooning score, and the fibrosis score (Figures 1E and S1Q–S1T). Furthermore, correlations between 3-sucCA levels and metabolic indicators were further analyzed and shown to be negatively correlated with the serum levels of the liver enzymes alanine aminotransferase (ALT) and aspartate aminotransferase (AST) (Figures 1F and 1G).

To explore whether sucCAs with different acylation positions (7-sucCA and 12-sucCA) and other succinylated bile acids (3-suc-chenodeoxycholic acid [3-sucCDCA], 3-sucDCA, and 3-sucLCA) also existed in individuals, we synthesized the above bile acids (Figures S1U–S1W). We then performed multilevel quantitative analysis, including using SECs as well as fecal samples from healthy individuals and mice, and we found that 7-sucCA, 12-sucCA, and 3-sucLCA were almost undetectable and that 3-sucCDCA and 3-sucDCA showed a lower abundance than 3-sucCA (Figures S1X–S1Z). However, there was no difference in the abundance of these bile acids among the patients with different severities of MAFL-MASH (Figure 1E).

Bacteroides uniformis is the main bacterial source for 3-sucCA production

3-sucCA contains an ester bond that may be degraded by a hydrolase encoded by the gut microbiota. Thus, we incubated 3-sucCA with human SECs for 3 continuous days and found that 3-sucCA is relatively stable in the microecological environment (Figure S2A). As a control, glycocholic acid (GCA) was degraded within 24 h of incubation due to bile salt hydrolase (BSH) activity from various gut bacteria strains³² (Figure S2A).

To identify potential bacterial producers of 3-sucCA, we collected fresh fecal samples for analysis from the 3 healthy volunteers with the highest 3-sucCA levels among the 23 volunteers

mentioned above (Figures 1C and S2B). We picked 315 distinct colonies and identified 97 unique species that broadly covered the bacterial phyla using 16S rRNA gene sequencing (Figure 2A; Table S2). Among the 315 isolates, only 42 bacterial isolates converted CA into 3-sucCA after 48 h incubation (Figure 2A), with all 15 of the tested *Bacteroides uniformis* strains displaying strong 3-sucCA production activity, while the other species belonging to the genus *Bacteroides* failed to produce detectable 3-sucCA (Figures 2A and S2C). The results were reproducible in 5 other medium conditions, including a chemically defined medium (CDM) containing CA and succinic acid (Figure S2D), which may exclude the distribution of trace levels of complex bile acids in the natural medium. The bacterial pellets were resuspended in phosphate-buffered saline (PBS) containing CA and succinic acid and showed 3-sucCA production activity (Figure S2E). Furthermore, we established several mixed-strain cultures with or without the addition of *B. uniformis* JC066 (*Bu*) (Figure S2F). As with the single-strain-level assay, 3-sucCA could be detected only in the presence of *Bu* (Figure S2G).

We next investigated whether *B. uniformis* can affect 3-sucCA levels in mice during colonization. We inoculated GF mice with either *Bu* or control (PBS) once by gavage, and then we measured 3-sucCA levels in the feces by LC-MS/MS 1 week later (Figure 2B). Colonization efficiency of *Bu* was determined by measurements of colony-forming units (CFUs) in feces after 1 week of the single gavage (Figure 2C), and *Bu* colonization significantly improved the level of 3-sucCA (Figure 2D). Moreover, we also inoculated SPF mice with *Bu* to test whether 3-sucCA abundance is increased in a complex microbiota environment (Figure 2E). In line with the observation in GF mice, gavage of SPF mice with *Bu* also induced a successful colonization and an increase in 3-sucCA levels (Figures 2F and 2G).

Activity-based protein purification identifies the enzyme for 3-sucCA production

Next, we sought to identify the biosynthetic pathway of 3-sucCA. Cell lysates of *B. uniformis* retained the ability to convert CA to 3-sucCA, which was lost by boiling or treating the lysate with protease K, indicating that *B. uniformis* produced 3-sucCA by an enzymatic reaction (Figures 3A and 3B). Structural analysis revealed that 3-sucCA may be synthesized via an acyltransferase. We assembled and annotated *B. uniformis* using whole-genome sequencing to identify the potential 3-sucCA-producing gene. In the *B. uniformis* chromosome, there were 16 genes annotated as acyltransferases, including two homologous enzymes of acyl coenzyme A-cholesterol acyltransferase (ACAT) in human (Figure S2H). However, by expression of all

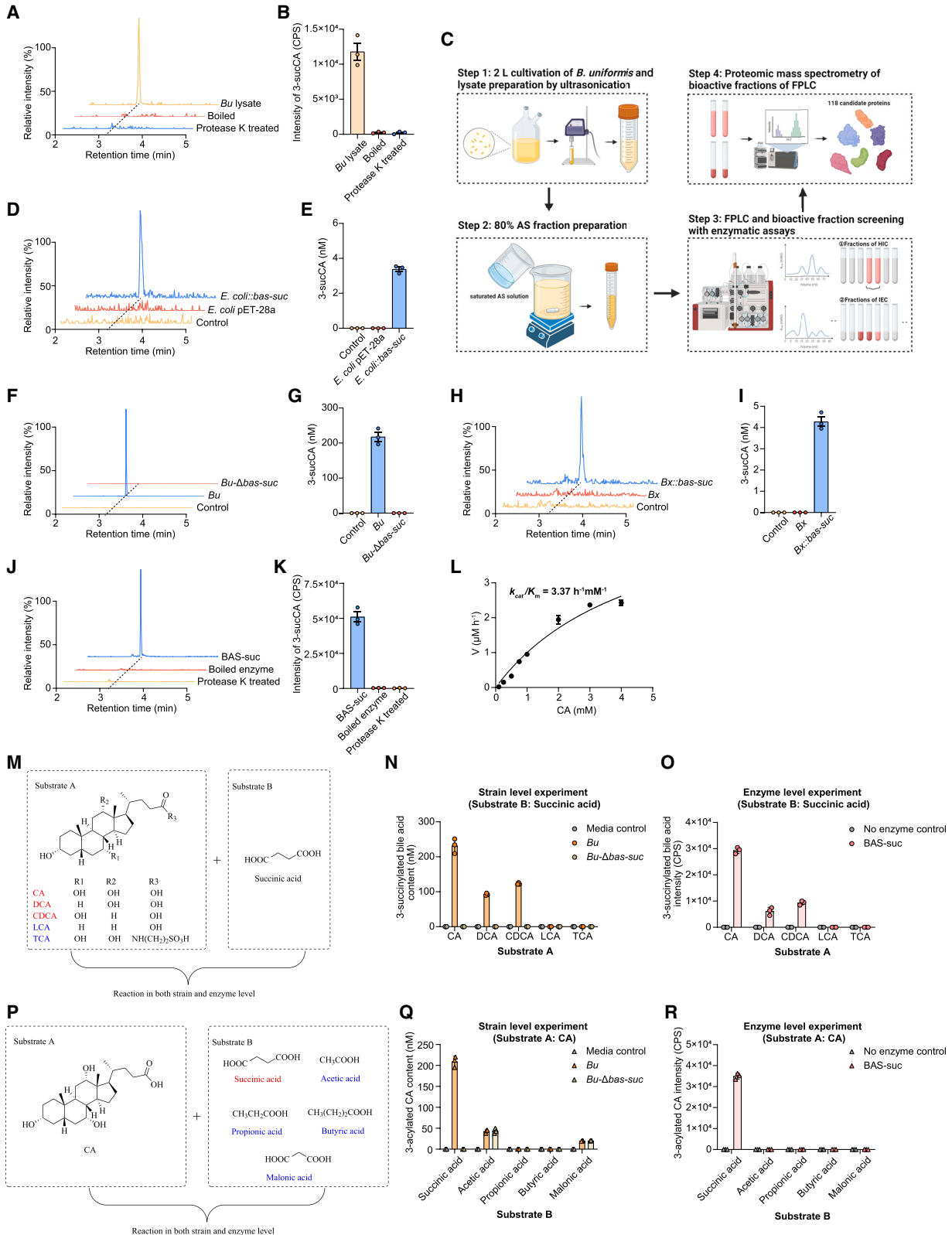
Figure 2. *B. uniformis* produces 3-sucCA both *in vitro* and *in vivo*

(A) Phylogenetic tree of the 315 gut microbial isolates with 97 different species and the yield of 3-sucCA. The tree was colored in terms of the phylum of each node; the inner heatmap displays the number of isolated strains, and the outer heatmap displays the prevalence rate of 3-sucCA-producing strains in the indicated species. The histogram displays the average yield of 3-sucCA.

(B–D) *B. uniformis* colonization efficiency (C) and 3-sucCA concentration (D) in feces of control and *Bu*-treated GF mice, as described in the schematic diagram (B). *n* = 6 mice per group.

(E–G) *B. uniformis* colonization efficiency (F) and 3-sucCA concentration (G) in feces of control and *Bu*-treated SPF mice, as described in the schematic diagram (E). *n* = 6 mice per group.

All data are presented as the means \pm SEMs. In (C) and (D), the *p* values were determined by two-tailed Mann-Whitney U test. In (F) and (G), the *p* values were determined by two-tailed Student's *t* test. ***p* < 0.01 versus the control group. See also Figure S2.



(legend on next page)

the supposed acyltransferase in *E. coli* BL21 (DE3), we found that CA incubation in culture failed to produce 3-sucCA (Figure S2I).

We next attempted to identify the potential 3-sucCA synthetase by activity-based protein purification. We performed sequential activity-based protein purification, which consisted of ammonium sulfate (AS) fractionation, hydrophobic interaction chromatography (HIC), and ion-exchange chromatography (IEC) (Figure 3C). Fraction 4 and fraction 5 from HIC and fractions 4–10 and fractions 4–11 from IEC showed high activity for 3-sucCA production as evaluated by enzymatic assays (Figures S2J–S2N). Mass spectrometry analysis of these active fractions (fraction 4, fraction 5, fractions 4–10, and fractions 4–11) revealed 118 overlapping proteins (Table S3). Next, we individually overexpressed all 118 proteins in *E. coli* BL21 (DE3) (Table S3) and found that only overexpression of homolog of UniProt: A7UYF6, a protein annotated as a β -lactamase, enabled *E. coli* BL21 (DE3) to produce 3-sucCA. We named this enzyme bile acid acyl synthetase for succinyl (BAS-suc) (Figures 3D and 3E).

To further verify BAS-suc as the synthetase of 3-sucCA, we generated a targeted genomic mutation by in-frame deletion utilizing a CRISPR-Cas system (Figures S2O and S2P). We found the growth of the knockout strain to be consistent with wild-type *Bu* in rich media, with or without CA/3-sucCA addition (Figures S2Q and S2R). However, *Bu- Δ bas-suc* showed no 3-sucCA production compared with wild-type *Bu* (Figures 3F and 3G). Next, we heterologously expressed *bas-suc* in *B. xylanisolvens* JC077, a species that belongs to the same genus as *B. uniformis* but is unable to produce 3-sucCA (Figures 2A, S2C, S2S, and S2T). BLAST analysis also confirmed the absence of close homologs of *bas-suc* in the *B. xylanisolvens* genome. The expression of *bas-suc* resulted in measurable production of 3-sucCA (Figures 3H and 3I), without growth defects (Figure S2U).

Next, we synthesized codon-optimized DNA sequences of *bas-suc* for recombinant protein expression in *E. coli* and purified the BAS-suc protein (Figure S2V). BAS-suc catalyzed the conversion of CA and succinic acid into 3-sucCA without other cofactors (Figures 3J and 3K). Kinetic analysis showed that BAS-suc has a Michaelis constant (K_m) of 4.69 mM for CA and a k_{cat} of 15.78 h⁻¹ (Figures 3L and S2W). To evaluate the substrate scope of BAS-

suc, we further incubated a *Bu* strain, a *Bu- Δ bas-suc* strain, or BAS-suc protein with a panel of bile acids and short-chain carboxylic acids and measured the resulting products. When using succinic acid and different bile acids, including CA, DCA, CDCA, LCA, and taurocholic acid (TCA) as substrates, we found that *Bu* and BAS-suc were active on CA, DCA, and CDCA but had little effect on LCA and TCA (Figures 3M–3O). However, when CA and different short-chain carboxylic acids (succinic acid, acetic acid, propionic acid, butyric acid, and malonic acid) were used as substrates, BAS-suc could not catalyze the reaction of CA with malonic acid and monobasic acids, including acetic acid, propionic acid, and butyric acid, although *Bu* shows weak activity for 3-aceCA and 3-malonyl CA (3-malCA) production (Figures 3P–3R).

3-sucCA alleviates MAFL-MASH progression in a gut-microbiota-dependent manner

After the discovery of the enzyme responsible for 3-sucCA, we next explored whether 3-sucCA can alleviate MAFL-MASH progression in mouse models. SPF mice that were administered an 8-week choline-deficient amino-acid-defined and high-fat diet (CDAA-HFD) were divided into two groups and gavaged with PBS or 3-sucCA for the last 3 weeks of the regimen (Figure 4A). The liver weight and the plasma levels of ALT and AST, as well as hepatic triglyceride (TG) levels, of 3-sucCA-gavaged mice were lower than those of PBS-treated mice (Figures 4B–4E). No significant differences in plasma TG or hepatic and plasma total cholesterol (TC) levels were found between the two groups (Figures S3A–S3E). By hematoxylin and eosin (H&E), oil red O, and Sirius red staining, 3-sucCA treatment alleviated MAFL-MASH progression under CDAA-HFD feeding, and this improvement was accompanied by less severe hepatic steatosis, inflammation, and fibrosis (Figures 4F and S3F–S3I). Furthermore, lower levels of relative expression of mRNA involved in hepatic lipid synthesis and uptake (*Srebp1c* and *Cd36*), proinflammatory cytokine production (*Tnfa*, *Il1b*, and *Ccl2*) and collagen synthesis (*Tgfb*, *Sma*, and *Col1a1*) were observed in 3-sucCA-treated mice compared with the controls (Figures S3J–S3L). Hence, 3-sucCA administration improved hepatic steatosis, inflammation, and fibrosis in the CDAA-HFD-induced MASH model.

Figure 3. BAS-suc is responsible for the production of 3-sucCA in *B. uniformis*

(A and B) Representative extracted ion chromatogram (A) and intensity (B) of 3-sucCA in enzymatic assays with *B. uniformis* cell lysate under different conditions. (C) Schematic representation of the activity-guided enzyme purification workflow. See [activity-guided enzyme purification](#) in the [method details](#). (D and E) Representative extracted ion chromatogram (D) and quantified production (E) of 3-sucCA by medium control, culture of *E. coli* pET-28a, or *E. coli::bas-suc*. (F and G) Representative extracted ion chromatogram (F) and quantified production (G) of 3-sucCA by medium control, culture of *B. uniformis*, or *B. uniformis bas-suc* deficiency strain. (H and I) Representative extracted ion chromatogram (H) and quantified production (I) of 3-sucCA by medium control, culture of *B. xylanisolvens*, or *B. xylanisolvens* strain heterologous expression with *bas-suc*. (J and K) Representative extracted ion chromatogram (J) and intensity (K) of 3-sucCA in enzymatic assays with BAS-suc protein under different conditions. (L) Michaelis-Menten saturation curves and k_{cat}/K_m for BAS-suc. CA in different concentration as substrate. $n = 3$. (M–O) Substrates A (bile acids) tested for conversion by *Bu* strains or BAS-suc protein. Positive substrates shown in red and negative substrates shown in blue (M). Quantified production of 3-succinylated bile acids at both strain (N) and enzyme (O) levels. (P–R) Substrates B (short-chain carboxylic acids) tested for conversion by *Bu* strains or BAS-suc protein. Positive substrates shown in red and negative substrates shown in blue (P). Quantified production of 3-acylated CAs at both strain (Q) and enzyme (R) level. All data are presented as the means \pm SEMs. Three biological replicates with 3 independent technical replicates for (A), (B), (D)–(K), (N), (O), (Q), and (R). See also Figure S2.

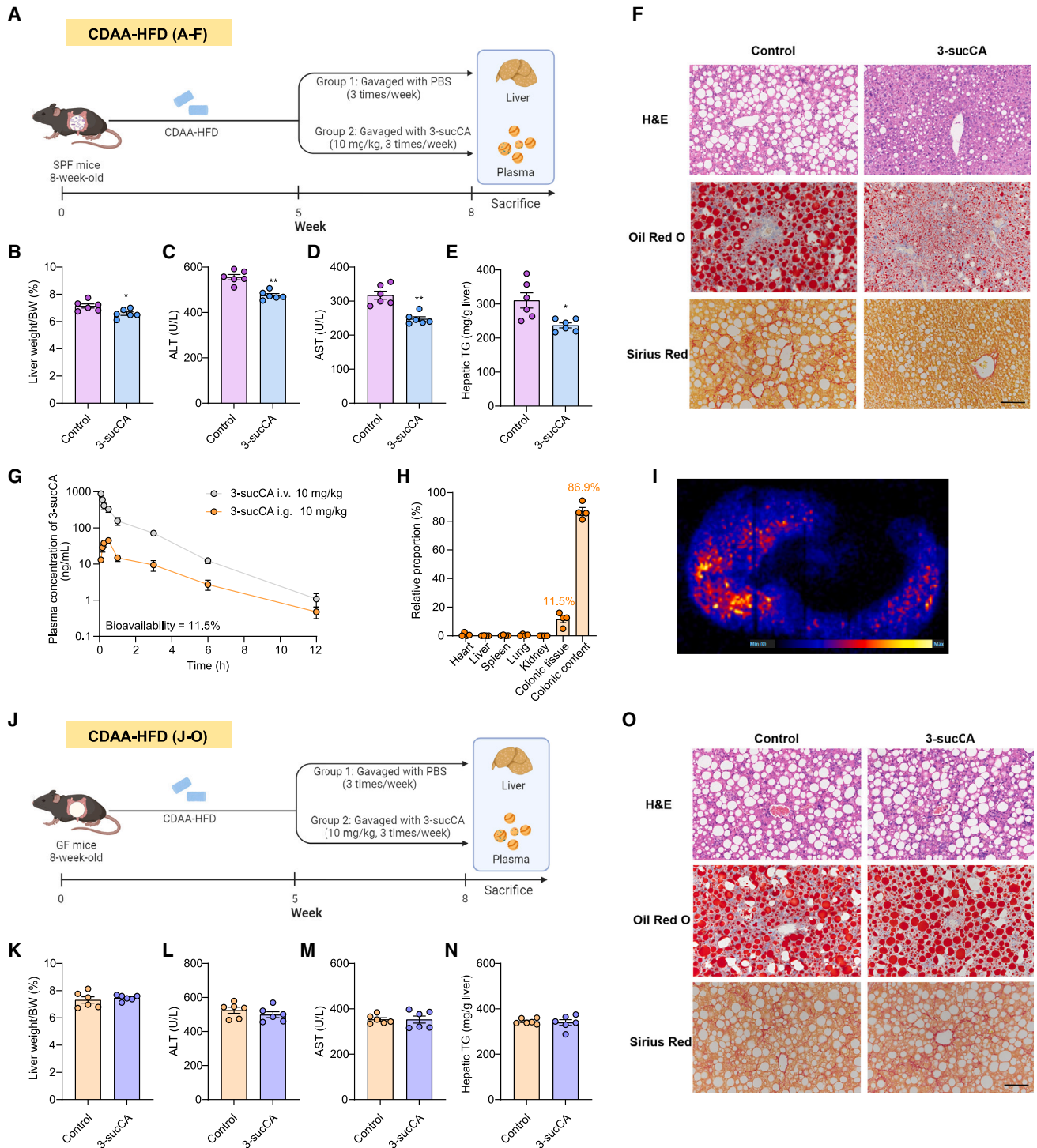


Figure 4. 3-sucCA alleviates MAFL-MASH progression in a gut-microbiota-dependent manner

(A–F) (A) Experimental scheme for (B)–(F), $n = 6$ mice/group. CDAA-HFD-fed SPF mice were treated with PBS (control) or 3-sucCA (10 mg/kg) 3 times per week for the last 3 weeks. (B) Ratios of liver mass to body mass. Plasma ALT (C) and AST (D) levels. (E) Hepatic TG content. (F) Representative hematoxylin and eosin (H&E) (top), oil red O (middle), and Sirius red (bottom) staining of liver sections. $n = 3$ mice per group, 3 images per mouse. Scale bar, 100 μ m. (G) Blood pharmacokinetics of 10 mg/kg 3-sucCA administered by intravenous injection (i.v.) or oral gavage (i.g.) over time. $n = 4$ mice/group. (H) Tissue distribution of 3-sucCA at the time of peak plasma concentration (30 min) after 10 mg/kg 3-sucCA by gavage. $n = 4$ mice/group. (I) Distribution of 3-sucCA in cecal content of SPF mice with 3-sucCA (10 mg/kg) administered once by gavage, based on desorption electrospray ionization-mass spectrometry imaging (DESI-MSI).

(legend continued on next page)

To explore the mechanisms by which 3-sucCA improves MAFL-MASH, we first tested the action site of 3-sucCA in mice. By analyzing 3-sucCA levels in different tissues from untreated SPF mice, we found that 3-sucCA had a higher content in the feces and colonic contents than in other tested tissues and could not be detected in either the plasma or the liver (Figure S3M). Further exploring the pharmacokinetics of 3-sucCA treatment, we found by both intravenous injection (i.v.) and oral gavage (i.g.) that once in mice, 3-sucCA showed a bioavailability of 11.5% (Figure 4G), indicating that 3-sucCA has a poor oral absorption. To further evaluate whether 3-sucCA is a gut-lumen-restricted metabolite, we explored the tissue distribution of 3-sucCA at the time of peak plasma concentration and found that 86.9% of 3-sucCA remained in the colonic content, with 11.5% in the colonic tissue (Figure 4H). We performed mass spectrometry imaging of 3-sucCA on caeca from 3-sucCA-treated mice, and 3-sucCA was seen at a high abundance in the lumen but was absent in the tissues (Figure 4I).

TGR5 and FXR are widely studied bile acid receptors and play an important role in MASH progression.^{6,9} We also tested the effects of 3-sucCA against TGR5 by luciferase reporter gene assay as well as FXR by both luciferase reporter gene assay and time-resolved fluorescence resonance energy transfer (TR-FRET). Other representative bile acids with known TGR5- or FXR-regulating functions were also tested, including a known TGR5 agonist (LCA), FXR agonist (CDCA), and FXR antagonist (tauro- β -muricholic acid [T β MCA]). However, under conditions close to the physiological concentration of 3-sucCA, 3-sucCA failed to affect the activity of either TGR5 or FXR (Figures S3N–S3R).

After we observed that 3-sucCA mainly remains in the gut lumen, we next explored whether 3-sucCA required gut microbiota to ameliorate MAFL-MASH (Figure 4J). In GF mice, the beneficial effects of 3-sucCA on MAFL-MASH progression were totally mitigated, as indicated by liver weights, plasma ALT and AST levels, and hepatic TG levels as well as on histochemical staining results (Figures 4K–4O and S3S–AD). These data indicate that 3-sucCA alleviated MAFL-MASH progression via gut microbiota.

3-sucCA promotes the growth of *A. muciniphila* both *in vitro* and *in vivo*

To explore the effects of 3-sucCA on the gut microbiota, we first analyzed the effects of 3-sucCA treatment on the gut microbiota of CDAA-HFD-fed mice by 16S rRNA gene amplicon sequencing. There was no significant difference between the two groups regarding α -diversity and β -diversity (Figures S4A and S4B). Linear discriminant analysis effect size (LEfSe) identified *Akkermansia* as a distinguishable genus with increased abundances in the 3-sucCA-treated group (Figure 5A), which was further confirmed by volcano plot evaluation (Figure 5B).

We further explored the role of 3-sucCA on a single-strain level. By incubating 3-sucCA with different bacterial strains

covering 97 different species, we found that a physiological level of 3-sucCA resulted in a significantly greater growth yield of *A. muciniphila* (Figure 5C). *A. muciniphila* is a paradigm for next-generation beneficial microorganisms, and it can play a protective role in a variety of metabolic diseases, including MAFLD, and part of the mechanism is dependent on the improvement of the intestinal barrier function.^{33–35} 3-sucCA promoted the growth of three different *A. muciniphila* strains (JC032, ATCC BAA-835, and JCM 30893) in a dose-dependent manner *in vitro* (Figures 5D, S4C, and S4D), while other types of bile acids (CA, DCA, CDCA, TCA, 3-sucDCA, 3-sucCDCA, 3-aceCA, and 3-proCA) or succinic acid at their different concentrations failed to stimulate the growth of *A. muciniphila* JC032 (Figures S4E–S4M). In human SECs, 3-sucCA also specifically enriched the abundance of *A. muciniphila* (Figure 5E). In CDAA-HFD-fed mice, we observed that both 3-sucCA and *A. muciniphila* treatment improved the phenotype of MASH in mice, while cotreatment with 3-sucCA and *A. muciniphila* showed a further increase in fecal *A. muciniphila* levels and a synergistic beneficial effect on MAFL-MASH progression (Figures S4N–AG).

To determine the role of *A. muciniphila* in the beneficial effects of 3-sucCA on MAFL-MASH progression, we next developed an *A. muciniphila* “depletion” system in SPF mice. A previous study provided us with a list of drugs with specific inhibitory effects on *A. muciniphila*.³⁶ By supplementing with 4 identified drugs mentioned above at both single-strain and SEC levels, we found that benzydamine hydrochloride (abbreviated as benzydamine) and benfluorex hydrochloride (abbreviated as benfluorex) have strong effects and specificity on the inhibition of *A. muciniphila*, which may effectively remove *A. muciniphila* with little effect on other bacteria (Figures S4AH and AI). We then administered PBS (control), 3-sucCA, 3-sucCA plus benzydamine, and 3-sucCA plus benfluorex to CDAA-HFD-fed SPF mice for the last 3 weeks of the dietary regimen (Figure 5F). 3-sucCA treatment of these mice significantly enriched the abundance of *A. muciniphila*, and both benzydamine and benfluorex treatment resulted in an extremely low level of *A. muciniphila* (10-fold lower than the control group; Figure S5A). Consistent with the elevated *A. muciniphila* levels, 3-sucCA treatment alleviated intestinal inflammation (*Tnfa* and *Il1b*) (Figure 5B) and intestinal barrier dysfunction, indicated by tight junctions (*Tjp1* and *Cldn3*), antimicrobial peptide secretion (*Reg3g*), and mucoprotein (*Muc2*) levels (Figures S5B and S5C). As indicated by H&E staining and Alcian blue and periodic acid-Schiff (AB-PAS) staining, 3-sucCA treatment also resulted in a greater intestinal mucosal layer thickness and goblet cell number compared with controls (Figures S5D–S5F), which is in line with previous reports exploring the effects of *A. muciniphila* treatment on these parameters.^{37,38} Moreover, intestinal barrier permeability and endotoxemia, as determined by a fluorescein isothiocyanate (FITC)-dextran permeability assay and plasma lipopolysaccharide (LPS) levels, were also improved

(J–O) (J) Experimental scheme for (K)–(O), $n = 6$ mice/group. CDAA-HFD-fed GF mice were treated with PBS (control) or 3-sucCA (10 mg/kg) 3 times per week for the last 3 weeks. (K) Ratios of liver mass to body mass. Plasma ALT (L) and AST (M) levels. (N) Hepatic TG content. (O) Representative H&E (top), oil red O (middle), and Sirius red (bottom) staining of liver sections. $n = 3$ mice per group, 3 images per mouse. Scale bar, 100 μ m. All data are presented as the means \pm SEMs. In (B)–(E) and (K)–(N), the p values were determined by two-tailed Student's t test. In (B)–(E), * $p < 0.05$ and ** $p < 0.01$ versus the control group. See also Figure S3.

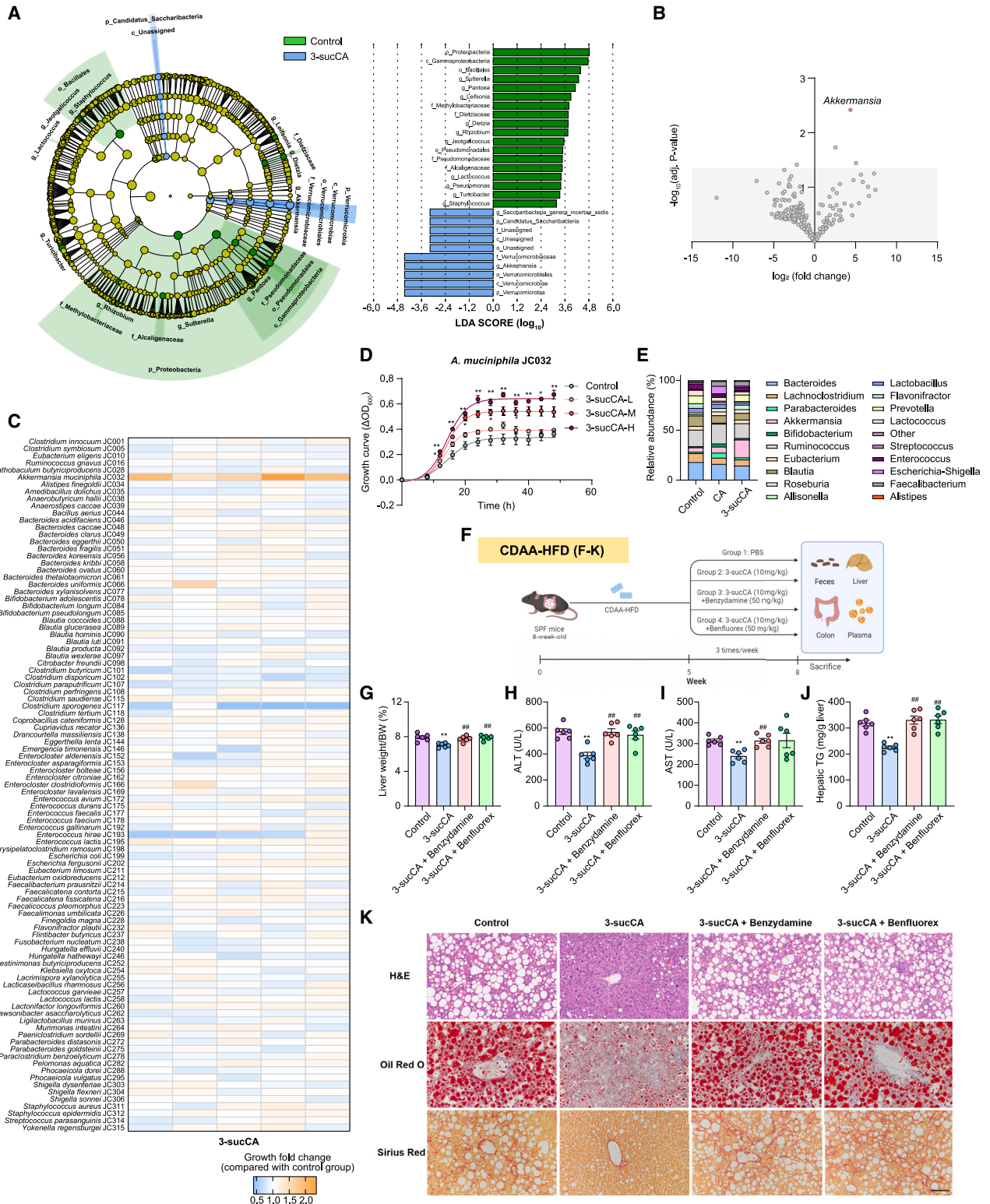


Figure 5. 3-sucCA alleviates MAFL-MASH progression by promoting the expansion of *A. muciniphila*

(A and B) CDAA-HFD-fed SPF mice were treated with PBS (control) or 3-sucCA (10 mg/kg) 3 times per week for the last 3 weeks. The fecal samples in the endpoint were collected, and 16S rRNA gene sequencing was performed. $n = 6$ mice/group. (A) Taxonomic cladogram generated from linear discriminant analysis effect size (LEfSe) analysis. Green and blue represent enriched taxa in the control and 3-sucCA groups, respectively. Each circle's size is proportional to the taxon's

(legend continued on next page)

by 3-sucCA treatment (Figures S5G and S5H), along with significantly improved MAFL-MASH progression (Figures 5G–5K and S5I–S5T). Addition of the *A. muciniphila* “depleters” benzydamine or benfluorex counteracted the beneficial effect of 3-sucCA on intestinal barrier function (Figures S5B–S5H) and MAFL-MASH progression (Figures 5G–5K and S5I–S5T).

Several studies have shown that endotoxemia induced by intestinal barrier damage can aggravate MAFL-MASH progression through the liver Toll-like receptor 4 (TLR4).^{39–41} To further verify whether the beneficial effect of 3-sucCA on MAFL-MASH phenotypes was dependent on the LPS-TLR4 pathway, we constructed *Tlr4* knockout (*Tlr4*^{−/−}) mice and treated them with PBS or 3-sucCA (Figure S5U). In *Tlr4*^{−/−} mice, the beneficial effect of 3-sucCA on MAFL-MASH progression was largely impeded (Figures S5V–AL).

Next, we aimed to explore the potential mechanism underlying the 3-sucCA-mediated increase in *A. muciniphila*. Firstly, we found that 1-week 3-sucCA treatment in SPF mice resulted in significantly greater abundance of *A. muciniphila* compared with control-treated mice (Figure S6A), without a significant change in the bile acid profiles in the feces or plasma (Figures S6B and S6C). Next, 3-sucCA concentration remained unchanged in the culture during the growth period of *A. muciniphila*, indicating that 3-sucCA is not a carbon source for *A. muciniphila* (Figure S6D). Furthermore, we carried out both RNA sequencing (RNA-seq) and untargeted metabolomics analysis of *A. muciniphila* in the culture with or without 3-sucCA, observing an enrichment in amino sugar and nucleotide sugar biosynthesis (Figures S6E and S6F). Targeted metabolomics analysis confirmed the significantly decreased fructose 6-phosphate (Fru-6P) and increased glucosamine, *N*-acetylglucosamine, and glucosamine 6-phosphate (GlcN-6P) (Figure S6G), which is essential for peptidoglycan synthesis.⁴² Also, the peptidoglycan content was significantly increased by 3-sucCA treatment (Figure S6G). By comparing the growth of *A. muciniphila* on different carbon sources with or without 3-sucCA treatment, we found that 3-sucCA exerted significant growth acceleration in the presence of glucose as the sole carbon source and showed minimal effects when glucosamine was sufficient (Figure S6H). The above observations indicate that 3-sucCA may exert growth acceleration effects on *A. muciniphila* by stimulating glucose amination and cell wall synthesis.

Amuc-NagB is the rate-limiting enzyme in *A. muciniphila* for the bidirectional reaction between Fru-6P and GlcN-6P (Figure S6G); however, Amuc-NagB was found to have a weak affini-

ty for the aminating substrate Fru-6P and a strong affinity for the deaminating substrate GlcN-6P, indicating that *A. muciniphila* has a weak aminating ability.⁴² By surface plasmon resonance (SPR) binding experiments, we confirmed the interaction of 3-sucCA and Amuc-NagB (Figure S6I), while other types of bile acids and related metabolites failed to appreciably interact with Amuc-NagB (Figure S6J). To further explore whether 3-sucCA promotes glucosamine production by targeting Amuc-NagB, we simulated the parameter of *A. muciniphila* carbon source utilization in *E. coli* Nissle 1917 by knocking out the *glmS* (the gene encoding an enzyme response for the amination of Fru-6P to GlcN-6P, which is lacking in *A. muciniphila*) and replacing the native *nagB* with Amuc-NagB in the strain to create *E. coli nagB::Amuc-nagB ΔglmS*. Unlike wild-type *E. coli* Nissle 1917, *E. coli nagB::Amuc-nagB ΔglmS* cannot grow in an M9 medium (a synthetic medium with defined chemical composition) without GlcNAc (Figures S6K and S6L), which simulated the nutritional requirements of *A. muciniphila*. However, addition of 3-sucCA at a physiological concentration effectively promoted the growth of *E. coli nagB::Amuc-nagB ΔglmS* in the M9 medium without GlcNAc (Figure S6L).

In addition, we also conducted an animal assay with different bile acids or related metabolites, including 3-sucCA, 3-sucDCA, 3-sucCDCA, 3-aceCA, 3-proCA, CA, and succinic acid, in a CDAA-HFD-induced MASH mouse model, providing the metabolites during the final 3 weeks of the dietary regimen. We found that only 3-sucCA showed strong beneficial effects on MAFL-MASH progression, while the other bile acids or related metabolites at the same dose showed no significant effects on disease progression (Figures S7A–S7R).

B. uniformis alleviates MAFL-MASH progression in a BAS-suc-dependent manner

To explore the beneficial effect of 3-sucCA production in MAFL-MASH progression, we conducted *Bu* or *Bu-Δbas-suc* treatment in CDAA-HFD-fed mice (Figure 6A). The beneficial effects of *Bu* treatment disappeared upon ablation of BAS-suc in *Bu* (Figures 6B–6J and S8A–S8R). Next, we utilized the Gubra-Amylin NASH (GAN) diet model (Figure 6K), another mouse model that simulates MAFL-MASH progression and one that is marked by an impaired intestinal barrier,^{43,44} for further assessment. After successful bacterial colonization and production of 3-sucCA by *Bu* (Figures S8S and S8T), there was significantly higher *A. muciniphila* abundance, greater intestinal barrier

abundance. (B) Volcano plot of 16S rRNA gene sequencing data of control and 3-sucCA groups. The adjusted *p* value threshold was calculated using moderated Student's *t* test followed by Benjamini-Hochberg multiple-test-correction FDR.

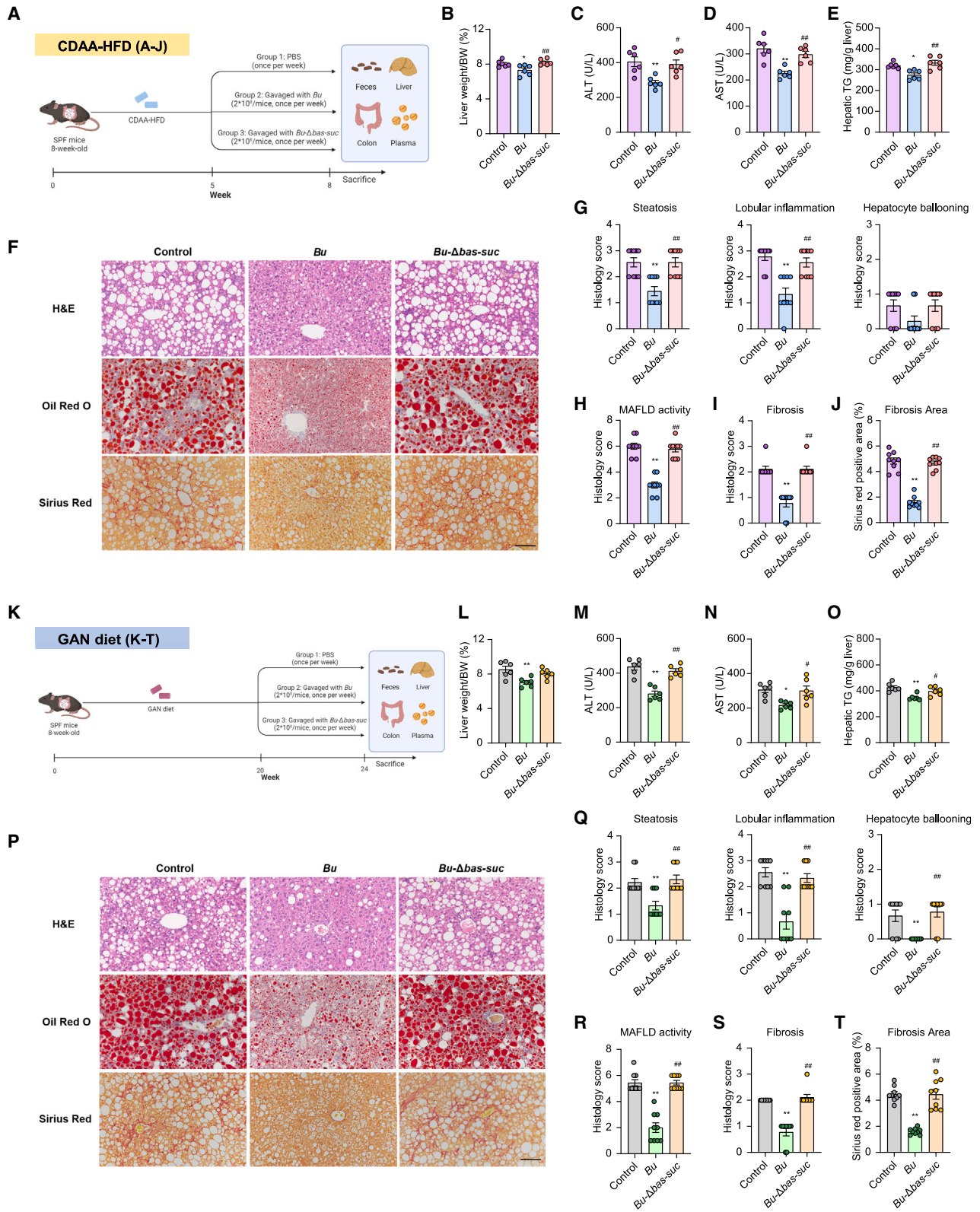
(C) Heatmap shows the effect of 3-sucCA (10 μM) incubation on the growth of gut bacteria at the single-strain level. Each value represents the ratio of OD₆₀₀ value between the 3-sucCA and control groups. *n* = 5.

(D) The growth curve of the *A. muciniphila* JC032 cultured in BHI media supplemented with 3-sucCA at different concentrations or PBS control anaerobically for 48 h. *n* = 3 biological replicates. (L, M, and H indicate 1 μM, 10 μM, and 50 μM, respectively.)

(E) Genus-level compositions of human SECs cultured in mGAM media supplemented with CA (1 mM), 3-sucCA (10 μM), or PBS control anaerobically for 48 h.

(F–K) (F) Experimental scheme for (G)–(K), *n* = 6 mice/group. CDAA-HFD-fed SPF mice were treated with PBS (control), 3-sucCA (10 mg/kg), 3-sucCA plus benzydamine (50 mg/kg), or 3-sucCA plus benfluorex (50 mg/kg) 3 times per week for the last 3 weeks. (G) Ratios of liver mass to body mass. Plasma ALT (H) and AST (I) levels. (J) Hepatic TG content. (K) Representative H&E (top), oil red O (middle), and Sirius red (bottom) staining of liver sections. *n* = 3 mice per group, 3 images per mouse. Scale bar, 100 μm.

All data are presented as the means ± SEMs. In (D), the *p* values were determined by Kruskal-Wallis test followed by Dunn's post hoc test. In (G), (H), and (J), the *p* values were determined by one-way ANOVA with Tukey's post hoc test. In (I), the *p* values were determined by one-way ANOVA with Dunnett's T3 test. In (D), **p* < 0.05 and ***p* < 0.01 versus the control group. In (G)–(J), ***p* < 0.01 versus the control group, ###*p* < 0.01 versus the 3-sucCA group. See also Figures S4–S7.



(legend on next page)

function, and less severe intestinal inflammation as well as lower liver weights, plasma ALT and AST levels, and hepatic TG content in the *Bu*-treated mice compared with those in the PBS-treated mice (Figures 6L–6T and S8U–AJ). The protective effects of *Bu* on MAFL–MASH progression in GAN-fed mice were blunted by *bas-suc* gene deletion (Figures 6L–6T and S8U–AJ).

3-sucCA production is negatively correlated with clinical MAFLD

To elucidate the correlation between our major findings in mice with clinical cases, we performed fecal metagenome sequencing of patients with biopsy-proven MAFLD and controls. Both *A. muciniphila* and *B. uniformis* were lower in the samples from patients with MAFLD compared with those from the controls, and the bacteria gradually disappeared with increasing severity of disease (Figure 7A). Further, we found that the gene abundance of *bas-suc* was negatively correlated with MAFLD severity along the spectrum of controls, MAFL, borderline MASH, and definite MASH, as measured by differences in MAS, steatosis score, ballooning score, lobular inflammation score, and fibrosis score (Figures 7B–7F). *Bas-suc* abundance was found to be positively related to 3-sucCA and *A. muciniphila* abundance (Figures 7G and 7H). Moreover, multivariate correlation analysis also revealed the close correlation between the above gut bacteria (*B. uniformis* and *A. muciniphila*), metabolite (3-sucCA), and clinical indicators (AST and ALT) (Figure 7I). In conclusion, these data establish a negative correlation between intestinal 3-sucCA/*bas-suc* abundance and clinical MAFL–MASH progression while also suggesting, based on the above mouse data, that *B. uniformis*, with its 3-sucCA synthesis activity, could be used as a potential probiotic to prevent MASH.

DISCUSSION

MAFL and its more severe form, MASH, represent a growing worldwide epidemic with a highly unmet medical need.^{45,46} Bile acids are amphipathic molecules synthesized from cholesterol in the pericentral hepatocytes and are key mediators of the enterohepatic circulation, and they are one of the active metabolites most closely related to MAFL–MASH progression.⁸ Although an enrichment of bile acid abundance in MAFLD progression has been observed in multiple studies, its role in MAFL–MASH progression remains unclear.¹¹ Herein, our data suggest a protective role for 3-sucCA in the management of MAFLD. Future large-scale and ethnically diverse clinical cohort

studies are needed to determine the broader role of 3-sucCA in the progression of MAFL–MASH among the general global public.

The 3-hydroxyl group of bile acids was reported to be attached with acyl groups, including the acetyl, propionyl, butyryl, and long-chain fatty acyl groups.^{47–49} However, the 3-acylated bile acids are limited to monocarboxylic acid, and their biosynthetic mechanism is still unclear. Biosynthetic pathway analysis of microbial bile acid metabolism should deepen the understanding of the role of secondary bile acids in health and disease, which is also a key step in achieving a precise regulation of their function. Recent studies have revealed several biosynthetic enzymes for the microbial transformation of bile acids, including 5 α -reduction, 7 α -dehydroxylation, and 24-reconjugation.^{16,17,22,23} Our discovery of BAS-suc revealed an unexplored type of secondary bile acid biosynthetic pathway.

Bile acids have various effects on the gut microbiota.⁵⁰ In addition to indirectly affecting the microbiota composition through the regulation of host intestinal epithelial cells,⁵¹ bile acids are often found to have antibacterial effects on several gram-negative bacteria^{52,53} and have been shown to impact resistance to *Clostridium difficile* infection. We found that 3-sucCA at physiological concentrations can directly promote the growth of *A. muciniphila*. Meanwhile, we also found an inhibitory effect of 3-sucCA on *Clostridium sporogenes* and *Enterococcus hirae*, though its molecular mechanism and biological function require further exploration.

Since its discovery, *A. muciniphila* has been shown to be significantly negatively correlated with the progression of various diseases,³³ and its metabolic benefits to the host have also been verified in mice and in clinical experiments,^{54,55} making it a typical representative of next-generation probiotics derived from the human gut. Multiple studies have focused on interventions to increase the abundance of *A. muciniphila*, including via the diet or polysaccharides.^{56–58} However, due to the complex mechanism of these interventions, it is not clear whether their beneficial effects are due to increased levels of *A. muciniphila* or the intervention itself. By using two *A. muciniphila* depleters, we found that the beneficial effect of 3-sucCA on MAFLD was reversed by *A. muciniphila* depletion. This proof-of-concept assay provides ideas for subsequent functional research on interventions that promote *A. muciniphila* growth.

At present, more than ten clinical trials have been involved to evaluate the effects of *A. muciniphila* on various diseases,

Figure 6. *B. uniformis* alleviates MAFL–MASH progression in a BAS-suc-dependent way

(A–J) (A) Experimental scheme for (B)–(J), $n = 6$ mice/group. CDAA-HFD-fed SPF mice were treated with PBS (control), *Bu*, or *Bu-Δbas-suc* strain 1 time per week for the last 3 weeks. (B) Ratios of liver mass to body mass. Plasma ALT (C) and AST (D) levels. (E) Hepatic TG content. (F) Representative H&E (top), oil red O (middle), and Sirius red (bottom) staining of liver sections. $n = 3$ mice per group, 3 images per mouse. Scale bar, 100 μm . (G) Histology scores of steatosis, lobular inflammation, and hepatocyte ballooning. (H) MAFLD activity score. (I) Histology scores of fibrosis stage. (J) Sirius Red-positive area. (K–T) (K) Experimental scheme for (L)–(T), $n = 6$ mice/group. GAN-diet-fed SPF mice were treated with PBS (control), *Bu*, or *Bu-Δbas-suc* strain 1 time per week for the last 4 weeks. (L) Ratios of liver mass to body mass. Plasma ALT (M) and AST (N) levels. (O) Hepatic TG content. (P) Representative H&E (top), oil red O (middle), and Sirius red (bottom) staining of liver sections. $n = 3$ mice per group, 3 images per mouse. Scale bar, 100 μm . (Q) Histology scores of steatosis, lobular inflammation, and hepatocyte ballooning. (R) MAFLD activity score. (S) Histology scores of fibrosis stage. (T) Sirius Red-positive area. All data are presented as the means \pm SEMs. In (B)–(E), (J), and (L)–(N), the p values were determined by one-way ANOVA with Tukey's post hoc test. In (G)–(I), (O), and (Q)–(S), the p values were determined by Kruskal–Wallis test followed by Dunn's post hoc test. In (T), the p values were determined by one-way ANOVA with Dunnett's T3 test. In (B)–(E), (G)–(J), (L)–(O), and (Q)–(T), * $p < 0.05$ and ** $p < 0.01$ versus the control group, # $p < 0.05$ and ## $p < 0.01$ versus the *Bu* group. See also Figure S8.

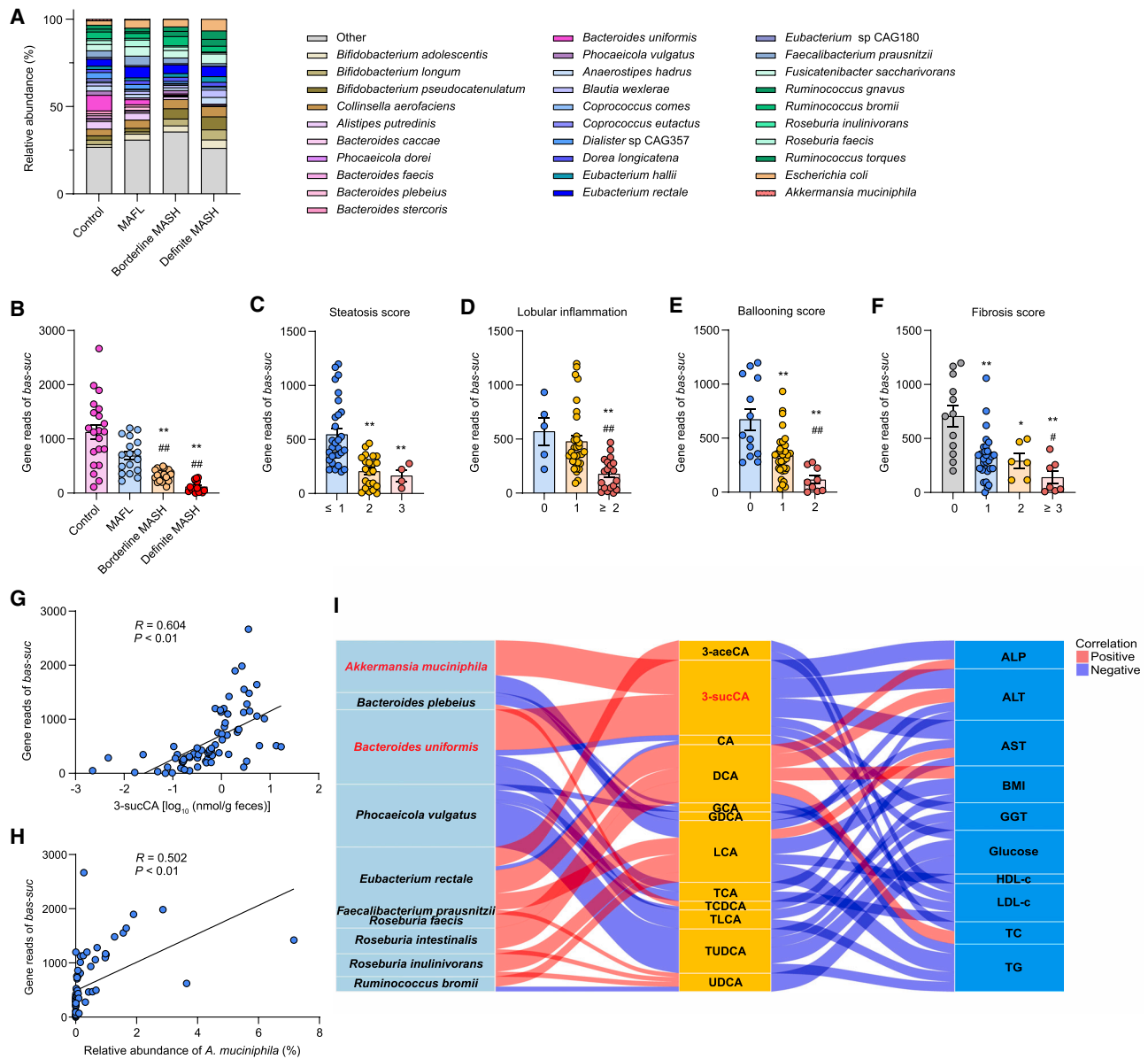


Figure 7. 3-sucCA production is negatively correlated with clinical MAFLD

(A–H) Analysis of controls and patients with different stages of MAFLD. $n = 21$ controls. $n = 55$ patients with MAFLD, including MAFL ($n = 17$), borderline MASH ($n = 23$), and definite MASH ($n = 15$). Bacterial taxonomic profiling of the gut microbiota from controls and different MAFLD stages processed at the species level (A). Gene reads of *bas-suc* associated with controls and patients with different stages of MAFLD (B). Gene reads of *bas-suc* associated with steatosis score (C), lobular inflammation (D), ballooning score (E), and fibrosis stage (F) in patients with MAFLD. Correlative analysis of *bas-suc* gene reads with 3-sucCA (G) and *A. muciniphila* abundance (H). Correlations between variables were assessed by linear regression analysis. Linear correlation index R and p values were calculated.

(I) Interrelationship between gut microbiota, fecal bile acids, and clinical phenotypes of MAFL–MASH progression. Red and blue connections indicate positive or negative correlations, respectively. The thicker the line, the stronger the correlation.

All data are presented as the means \pm SEMs. In (B)–(F), the p values were determined by Kruskal–Wallis test followed by Dunn’s post hoc test. In (B), ** $p < 0.01$ versus the control group, ## $p < 0.01$ versus the MAFL group. In (C), ** $p < 0.01$ versus the steatosis score ≤ 1 group. In (D), ** $p < 0.01$ versus the lobular inflammation = 0 group, ## $p < 0.01$ versus the lobular inflammation = 1 group. In (E), ** $p < 0.01$ versus the ballooning score = 0 group, ## $p < 0.01$ versus the ballooning score = 1 group. In (F), * $p < 0.05$ and ** $p < 0.01$ versus the fibrosis score = 0 group, # $p < 0.05$ versus the fibrosis score = 1 group.

including tumors, metabolic diseases, psychological stress, irritable bowel syndrome, and osteoporosis. Several studies have provided evidence for a beneficial role for *A. muciniphila* in the

prevention of MAFLD^{35,59–61} and alcoholic fatty liver disease⁶² in mouse models. Given the notable effects of 3-sucCA on *A. muciniphila* growth and the beneficial effects of

A. muciniphila on several diseases, it is possible that beyond MAFL-MASH, 3-sucCA could be used as prebiotic in a “drugs for bugs” approach to ameliorate other diseases.

Limitations of the study

In the current study, we demonstrated that 3-sucCA mainly improved MAFL-MASH progression by promoting the abundance of *A. muciniphila*. Several reports have found that *A. muciniphila* can improve MAFL-MASH progression via a variety of pathways,^{35,63,64} but the exact molecular mechanism for these effects remains to be further validated. While we created and utilized *Tlr4* knockout mice to validate a role for this pathway in the beneficial effects of 3-sucCA on MAFL-MASH progression, we cannot rule out a role for other signaling pathways in hepatocytes or other key cell types in these effects, which needs further investigation in the future. Moreover, the detailed mechanism by which 3-sucCA promotes NagB activity to encourage the growth of *A. muciniphila* remains obscure, and identifying this mechanism or validating that 3-sucCA indeed works via NagB is hampered by a lack of a genetic manipulation system for *A. muciniphila*,⁶⁵ which would allow for experimentally induced alterations of *nagB* in the bacterium.

STAR★METHODS

Detailed methods are provided in the online version of this paper and include the following:

- KEY RESOURCES TABLE
- RESOURCE AVAILABILITY
 - Lead contact
 - Materials availability
 - Data and code availability
- EXPERIMENTAL MODEL AND STUDY PARTICIPANT DETAILS
 - Human study
 - Mice and treatments
 - Bacteria
- METHOD DETAILS
 - Synthesis of alkCA
 - Synthesis of ACER resin
 - Stool-derived *ex vivo* communities
 - AlkCA incubation, metabolome extraction and CuAAC-based enrichment
 - Mass spectrometric analysis
 - Molecular networking
 - Probe-derived metabolites identification
 - Extraction and isolation of acylated CAs
 - Synthetic procedures of acylated CAs
 - Targeted metabolomics analysis
 - Quantification of peptidoglycan
 - Stability of 3-sucCA
 - 16S rRNA gene amplicon sequencing and analyses
 - Metagenomic sequencing and analyses
 - Phylogenetic analyses
 - Growth curves of tested strains
 - Biolog microplate analysis
 - Heterologous expression and activity of acyltransferase candidates
 - Activity-guided enzyme purification
 - Proteomic mass spectrometry analysis
 - Construction of *B. uniformis* knockout strain
 - Heterologous expression and purification of BAS-suc
 - Activity assay, kinetics analyses and substrate scope of BAS-suc
 - Surface plasmon resonance (SPR)

- Luciferase reporter gene assays
- TR-FRET FXR coactivator recruitment assay
- Histological analysis
- Measurement of MUC2 content
- Desorption electrospray ionization mass spectrometry imaging (DESI-MSI)
- Quantitative PCR
- Plasma endotoxin detection
- *In vivo* intestinal permeability assay
- Construction of *E. coli nagB::Amuc-nagB ΔglmS*
- QUANTIFICATION AND STATISTICAL ANALYSIS

SUPPLEMENTAL INFORMATION

Supplemental information can be found online at <https://doi.org/10.1016/j.cell.2024.03.034>.

ACKNOWLEDGMENTS

We thank L. Dai (Shenzhen Institute of Synthetic Biology, Shenzhen Institute of Advanced Technology) for providing the *Bacteroides* tool plasmid pB041 and Dr. Xiajuan Zou (Medical and Health Analysis Center, Peking University) for help in proteomic mass spectrometry analysis. Schematic diagrams were generated by [BioRender.com](https://www.biorender.com).

This work was supported by the National Natural Science Foundation of China (nos. 31925021 and 92357305), the National Key Research and Development Program of China (nos. 2018YFA0800700 and 2022YFA0806400), and the National Natural Science Foundation of China (nos. 82130022, 82341226, 82288102, 82370812, 21925101, 92149306, 81921001, 82171627, 32300989, 32202020, 82070588, and 82370577). C.J. acknowledges support from the Tencent Foundation through the Xplorer Prize.

AUTHOR CONTRIBUTIONS

C.J. conceptualized the study. Q.N., X.L., K.W., Y.D., S.J., Q.Z., M.L., J.Z., Y.Z., J.L., C.G., Z.Z., H. Liu, G.Z., J.Y., L.S., H. Lu, and M.M. performed the experiments and analyzed the data. C.J., J.Q., Y.P., M.-H.Z., and Y.J. designed the study, and Q.N., X.L., K.W., Y.D., and C.J. wrote the manuscript. Q.N., X.L., K.W., Y.D., and S.J. contributed equally to this work. All authors edited the manuscript and approved the final manuscript.

DECLARATION OF INTERESTS

The authors declare no competing interests.

Received: July 16, 2023

Revised: February 5, 2024

Accepted: March 23, 2024

Published: April 22, 2024

REFERENCES

1. Powell, E.E., Wong, V.W.-S., and Rinella, M. (2021). Non-alcoholic fatty liver disease. *Lancet* 397, 2212–2224. [https://doi.org/10.1016/s0140-6736\(20\)32511-3](https://doi.org/10.1016/s0140-6736(20)32511-3).
2. Harrison, S.A., Allen, A.M., Dubourg, J., Nouredin, M., and Alkhouri, N. (2023). Challenges and opportunities in NASH drug development. *Nat. Med.* 29, 562–573. <https://doi.org/10.1038/s41591-023-02242-6>.
3. Eslam, M., Sanyal, A.J., and George, J.; International Consensus Panel (2020). MAFLD: A Consensus-Driven Proposed Nomenclature for Metabolic Associated Fatty Liver Disease. *Gastroenterology* 158, 1999–2014.e1. <https://doi.org/10.1053/j.gastro.2019.11.312>.
4. Tilg, H., Adolph, T.E., Dudek, M., and Knolle, P. (2021). Non-alcoholic fatty liver disease: the interplay between metabolism, microbes and immunity. *Nat. Metab.* 3, 1596–1607. <https://doi.org/10.1038/s42255-021-00501-9>.

5. Loomba, R., Friedman, S.L., and Shulman, G.I. (2021). Mechanisms and disease consequences of nonalcoholic fatty liver disease. *Cell* 184, 2537–2564. <https://doi.org/10.1016/j.cell.2021.04.015>.
6. Sun, L., Cai, J., and Gonzalez, F.J. (2021). The role of farnesoid X receptor in metabolic diseases, and gastrointestinal and liver cancer. *Nat. Rev. Gastroenterol. Hepatol.* 18, 335–347. <https://doi.org/10.1038/s41575-020-00404-2>.
7. Masoodi, M., Gastaldelli, A., Hyötyläinen, T., Arretxe, E., Alonso, C., Gagini, M., Brosnan, J., Anstee, Q.M., Millet, O., Ortiz, P., et al. (2021). Metabolomics and lipidomics in NAFLD: biomarkers and non-invasive diagnostic tests. *Nat. Rev. Gastroenterol. Hepatol.* 18, 835–856. <https://doi.org/10.1038/s41575-021-00502-9>.
8. Cai, J., Sun, L., and Gonzalez, F.J. (2022). Gut microbiota-derived bile acids in intestinal immunity, inflammation, and tumorigenesis. *Cell Host Microbe* 30, 289–300. <https://doi.org/10.1016/j.chom.2022.02.004>.
9. Perino, A., and Schoonjans, K. (2022). Metabolic Messengers: bile acids. *Nat. Metab.* 4, 416–423. <https://doi.org/10.1038/s42255-022-00559-z>.
10. Puri, P., Daita, K., Joyce, A., Mirshahi, F., Santhekadur, P.K., Cazanave, S., Luketic, V.A., Siddiqui, M.S., Boyett, S., Min, H.-K., et al. (2018). The presence and severity of nonalcoholic steatohepatitis is associated with specific changes in circulating bile acids. *Hepatology* 67, 534–548. <https://doi.org/10.1002/hep.29359>.
11. Jiao, N., Baker, S.S., Chapa-Rodriguez, A., Liu, W., Nugent, C.A., Tsompana, M., Mastrandrea, L., Buck, M.J., Baker, R.D., Genco, R.J., et al. (2018). Suppressed hepatic bile acid signalling despite elevated production of primary and secondary bile acids in NAFLD. *Gut* 67, 1881–1891. <https://doi.org/10.1136/gutjnl-2017-314307>.
12. Qu, P., Rom, O., Li, K., Jia, L., Gao, X., Liu, Z., Ding, S., Zhao, M., Wang, H., Chen, S., et al. (2023). DT-109 ameliorates nonalcoholic steatohepatitis in nonhuman primates. *Cell Metab.* 35, 742–757. <https://doi.org/10.1016/j.cmet.2023.03.013>.
13. Chávez-Talavera, O., Haas, J., Grzych, G., Tailleux, A., and Staels, B. (2019). Bile acid alterations in nonalcoholic fatty liver disease, obesity, insulin resistance and type 2 diabetes: what do the human studies tell? *Curr. Opin. Lipidol.* 30, 244–254. <https://doi.org/10.1097/mol.0000000000000597>.
14. Yoshimoto, S., Loo, T.M., Atarashi, K., Kanda, H., Sato, S., Oyadomari, S., Iwakura, Y., Oshima, K., Morita, H., Hattori, M., et al. (2013). Obesity-induced gut microbial metabolite promotes liver cancer through senescence secretome. *Nature* 499, 97–101. <https://doi.org/10.1038/nature12347>.
15. Negi, C.K., Babica, P., Bajard, L., Bienertova-Vasku, J., and Tarantino, G. (2022). Insights into the molecular targets and emerging pharmacotherapeutic interventions for nonalcoholic fatty liver disease. *Metabolism* 126, 154925. <https://doi.org/10.1016/j.metabol.2021.154925>.
16. Sato, Y., Atarashi, K., Plichta, D.R., Arai, Y., Sasajima, S., Kearney, S.M., Suda, W., Takeshita, K., Sasaki, T., Okamoto, S., et al. (2021). Novel bile acid biosynthetic pathways are enriched in the microbiome of centenarians. *Nature* 599, 458–464. <https://doi.org/10.1038/s41586-021-03832-5>.
17. Funabashi, M., Grove, T.L., Wang, M., Varma, Y., McFadden, M.E., Brown, L.C., Guo, C., Higginbottom, S., Almo, S.C., and Fischbach, M.A. (2020). A metabolic pathway for bile acid dehydroxylation by the gut microbiome. *Nature* 582, 566–570. <https://doi.org/10.1038/s41586-020-2396-4>.
18. Paik, D., Yao, L., Zhang, Y., Bae, S., D'Agostino, G.D., Zhang, M., Kim, E., Franzosa, E.A., Avila-Pacheco, J., Bisanz, J.E., et al. (2022). Human gut bacteria produce T_H17-modulating bile acid metabolites. *Nature* 603, 907–912. <https://doi.org/10.1038/s41586-022-04480-z>.
19. Gentry, E.C., Collins, S.L., Panitchpakdi, M., Belda-Ferre, P., Stewart, A.K., Carrillo Terrazas, M., Lu, H.-H., Zuffa, S., Yan, T., Avila-Pacheco, J., et al. (2024). Reverse metabolomics for the discovery of chemical structures from humans. *Nature* 626, 419–426. <https://doi.org/10.1038/s41586-023-06906-8>.
20. Mullaney, M.W., Fiebig, A., Schnizlein, M.K., McMillin, M., Rose, A.R., Koval, J., Rubin, D., Dalal, S., Sogin, M.L., Chang, E.B., et al. (2024). Microbially catalyzed conjugation of GABA and tyramine to bile acids. *J. Bacteriol.* 206, e0042623. <https://doi.org/10.1128/jb.00426-23>.
21. Zuffa, S., Schmid, R., Bauermeister, A., Gomes, P.W.P., Caraballo-Rodriguez, A.M., El Abiead, Y., Aron, A.T., Gentry, E.C., Zemlin, J., Meehan, M.J., et al. (2024). microbeMASST: a taxonomically informed mass spectrometry search tool for microbial metabolomics data. *Nat. Microbiol.* 9, 336–345. <https://doi.org/10.1038/s41586-023-01575-9>.
22. Guziar, D.V., Okros, M., Shivel, M., Armwald, B., Bridges, C., Fu, Y., Martin, C., Schillmiller, A.L., Miller, W.M., Ziegler, K.M., et al. (2024). Bile salt hydrolase acyltransferase activity expands bile acid diversity. *Nature* 626, 852–858. <https://doi.org/10.1038/s41586-024-07017-8>.
23. Rimal, B., Collins, S.L., Tanes, C.E., Rocha, E.R., Granda, M.A., Solanki, S., Hoque, N.J., Gentry, E.C., Koo, I., Reilly, E.R., et al. (2024). Bile salt hydrolase catalyses formation of amine-conjugated bile acids. *Nature* 626, 859–863. <https://doi.org/10.1038/s41586-023-06990-w>.
24. Quinn, R.A., Melnik, A.V., Vrbanac, A., Fu, T., Patras, K.A., Christy, M.P., Bodai, Z., Belda-Ferre, P., Tripathi, A., Chung, L.K., et al. (2020). Global chemical effects of the microbiome include new bile-acid conjugations. *Nature* 579, 123–129. <https://doi.org/10.1038/s41586-020-2047-9>.
25. Shalon, D., Culver, R.N., Grembi, J.A., Folz, J., Treit, P.V., Shi, H., Rosenberger, F.A., Dethlefsen, L., Meng, X., Yaffe, E., et al. (2023). Profiling the human intestinal environment under physiological conditions. *Nature* 617, 581–591. <https://doi.org/10.1038/s41586-023-05989-7>.
26. Foley, M.H., Walker, M.E., Stewart, A.K., O'Flaherty, S., Gentry, E.C., Patel, S., Beaty, V.V., Allen, G., Pan, M., Simpson, J.B., et al. (2023). Bile salt hydrolases shape the bile acid landscape and restrict *Clostridioides difficile* growth in the murine gut. *Nat. Microbiol.* 8, 611–628. <https://doi.org/10.1038/s41564-023-01337-7>.
27. Lucas, L.N., Barrett, K., Kerby, R.L., Zhang, Q., Cattaneo, L.E., Stevenson, D., Rey, F.E., and Amador-Noguez, D. (2021). Dominant Bacterial Phyla from the Human Gut Show Widespread Ability To Transform and Conjugate Bile Acids. *mSystems* 6, e00139-18. <https://doi.org/10.1128/mSystems.00805-21>.
28. Hoki, J.S., Le, H.H., Mellott, K.E., Zhang, Y.K., Fox, B.W., Rodrigues, P.R., Yu, Y., Helf, M.J., Baccile, J.A., and Schroeder, F.C. (2020). Deep Interrogation of Metabolism Using a Pathway-Targeted Click-Chemistry Approach. *J. Am. Chem. Soc.* 142, 18449–18459. <https://doi.org/10.1021/jacs.0c06877>.
29. Aranda-Diaz, A., Ng, K.M., Thomsen, T., Real-Ramirez, I., Dahan, D., Dittmar, S., Gonzalez, C.G., Chavez, T., Vasquez, K.S., Nguyen, T.H., et al. (2022). Establishment and characterization of stable, diverse, fecal-derived *in vitro* microbial communities that model the intestinal microbiota. *Cell Host Microbe* 30, 260–272. <https://doi.org/10.1016/j.chom.2021.12.008>.
30. Xiao, F., Dong, S., Liu, Y., Feng, Y., Li, H., Yun, C.-H., Cui, Q., and Li, W. (2020). Structural Basis of Specificity for Carboxyl-Terminated Acyl Donors in a Bacterial Acyltransferase. *J. Am. Chem. Soc.* 142, 16031–16038. <https://doi.org/10.1021/jacs.0c07331>.
31. Ferslew, B.C., Xie, G., Johnston, C.K., Su, M., Stewart, P.W., Jia, W., Brouwer, K.L.R., and Barritt, A.S., IV. (2015). Altered Bile Acid Metabolome in Patients with Nonalcoholic Steatohepatitis. *Dig. Dis. Sci.* 60, 3318–3328. <https://doi.org/10.1007/s10620-015-3776-8>.
32. Sun, L., Pang, Y., Wang, X., Wu, Q., Liu, H., Liu, B., Liu, G., Ye, M., Kong, W., and Jiang, C. (2019). Ablation of gut microbiota alleviates obesity-induced hepatic steatosis and glucose intolerance by modulating bile acid metabolism in hamsters. *Acta Pharm. Sin. B* 9, 702–710. <https://doi.org/10.1016/j.apsb.2019.02.004>.
33. Cani, P.D., Depommier, C., Derrien, M., Everard, A., and de Vos, W.M. (2022). *Akkermansia muciniphila*: paradigm for next-generation beneficial microorganisms. *Nat. Rev. Gastroenterol. Hepatol.* 19, 625–637. <https://doi.org/10.1038/s41575-022-00631-9>.
34. Miura, K., and Ohnishi, H. (2014). Role of gut microbiota and Toll-like receptors in nonalcoholic fatty liver disease. *World J. Gastroenterol.* 20, 7381–7391. <https://doi.org/10.3748/wjg.v20.i23.7381>.

35. Rao, Y., Kuang, Z., Li, C., Guo, S., Xu, Y., Zhao, D., Hu, Y., Song, B., Jiang, Z., Ge, Z., et al. (2021). Gut *Akkermansia muciniphila* ameliorates metabolic dysfunction-associated fatty liver disease by regulating the metabolism of L-aspartate via gut-liver axis. *Gut Microb.* *13*, 1–19. <https://doi.org/10.1080/19490976.2021.1927633>.
36. Maier, L., Pruteanu, M., Kuhn, M., Zeller, G., Telzerow, A., Anderson, E.E., Brochado, A.R., Fernandez, K.C., Dose, H., Mori, H., et al. (2018). Extensive impact of non-antibiotic drugs on human gut bacteria. *Nature* *555*, 623–628. <https://doi.org/10.1038/nature25979>.
37. Shin, N.-R., Lee, J.-C., Lee, H.-Y., Kim, M.-S., Whon, T.W., Lee, M.-S., and Bae, J.-W. (2014). An increase in the *Akkermansia* spp. population induced by metformin treatment improves glucose homeostasis in diet-induced obese mice. *Gut* *63*, 727–735. <https://doi.org/10.1136/gutjnl-2012-303839>.
38. Everard, A., Belzer, C., Geurts, L., Ouwerkerk, J.P., Druart, C., Bindels, L.B., Guiot, Y., Derrien, M., Muccioli, G.G., Delzenne, N.M., et al. (2013). Cross-talk between *Akkermansia muciniphila* and intestinal epithelium controls diet-induced obesity. *Proc. Natl. Acad. Sci. USA* *110*, 9066–9071. <https://doi.org/10.1073/pnas.1219451110>.
39. Henao-Mejia, J., Elinav, E., Jin, C., Hao, L., Mehal, W.Z., Strowig, T., Thaiss, C.A., Kau, A.L., Eisenbarth, S.C., Jurczak, M.J., et al. (2012). Inflammation-mediated dysbiosis regulates progression of NAFLD and obesity. *Nature* *482*, 179–185. <https://doi.org/10.1038/nature10809>.
40. Bessone, F., Razori, M.V., and Roma, M.G. (2019). Molecular pathways of nonalcoholic fatty liver disease development and progression. *Cell. Mol. Life Sci.* *76*, 99–128. <https://doi.org/10.1007/s00018-018-2947-0>.
41. Ye, D., Li, F.Y.L., Lam, K.S.L., Li, H., Jia, W., Wang, Y., Man, K., Lo, C.M., Li, X., and Xu, A. (2012). Toll-like receptor-4 mediates obesity-induced non-alcoholic steatohepatitis through activation of X-box binding protein-1 in mice. *Gut* *61*, 1058–1067. <https://doi.org/10.1136/gutjnl-2011-300269>.
42. van der Ark, K.C.H., Aalvink, S., Suarez-Diez, M., Schaap, P.J., de Vos, W.M., and Belzer, C. (2018). Model-driven design of a minimal medium for *Akkermansia muciniphila* confirms mucus adaptation. *Microb. Biotechnol.* *11*, 476–485. <https://doi.org/10.1111/1751-7915.13033>.
43. Chen, B., Sun, L., Zeng, G., Shen, Z., Wang, K., Yin, L., Xu, F., Wang, P., Ding, Y., Nie, Q., et al. (2022). Gut bacteria alleviate smoking-related NASH by degrading gut nicotine. *Nature* *610*, 562–568. <https://doi.org/10.1038/s41586-022-05299-4>.
44. Gallage, S., Avila, J.E.B., Ramadori, P., Focaccia, E., Rahbari, M., Ali, A., Malek, N.P., Anstee, Q.M., and Heikenwalder, M. (2022). A researcher's guide to preclinical mouse NASH models. *Nat. Metab.* *4*, 1632–1649. <https://doi.org/10.1038/s42255-022-00700-y>.
45. Friedman, S.L., Neuschwander-Tetri, B.A., Rinella, M., and Sanyal, A.J. (2018). Mechanisms of NAFLD development and therapeutic strategies. *Nat. Med.* *24*, 908–922. <https://doi.org/10.1038/s41591-018-0104-9>.
46. Lazarus, J.V., Mark, H.E., Anstee, Q.M., Arab, J.P., Batterham, R.L., Castera, L., Cortez-Pinto, H., Crespo, J., Cusi, K., Dirac, M.A., et al. (2022). Advancing the global public health agenda for NAFLD: a consensus statement. *Nat. Rev. Gastroenterol. Hepatol.* *19*, 60–78. <https://doi.org/10.1038/s41575-021-00523-4>.
47. Takei, H., Narushima, S., Suzuki, M., Kakiyama, G., Sasaki, T., Murai, T., Yamashiro, Y., and Nittono, H. (2022). Characterization of long-chain fatty acid-linked bile acids: a major conjugation form of 3 beta-hydroxy bile acids in feces. *J. Lipid Res.* *63*, 100275. <https://doi.org/10.1016/j.lip.2022.100275>.
48. Garcia, C.J., Kosek, V., Beltrán, D., Tomás-Barberán, F.A., and Hajslova, J. (2022). Production of New Microbially Conjugated Bile Acids by Human Gut Microbiota. *Biomolecules* *12*, 687. <https://doi.org/10.3390/biom12050687>.
49. Liu, C., Du, M.-X., Xie, L.-S., Wang, W.-Z., Chen, B.-S., Yun, C.-Y., Sun, X.-W., Luo, X., Jiang, Y., Wang, K., et al. (2024). Gut commensal *Christensenella minuta* modulates host metabolism via acylated secondary bile acids. *Nat. Microbiol.* *9*, 434–450. <https://doi.org/10.1038/s41564-023-01570-0>.
50. Staley, C., Weingarden, A.R., Khoruts, A., and Sadowsky, M.J. (2017). Interaction of gut microbiota with bile acid metabolism and its influence on disease states. *Appl. Microbiol. Biotechnol.* *101*, 47–64. <https://doi.org/10.1007/s00253-016-8006-6>.
51. Inagaki, T., Moschetta, A., Lee, Y.-K., Peng, L., Zhao, G., Downes, M., Yu, R.T., Shelton, J.M., Richardson, J.A., Repa, J.J., et al. (2006). Regulation of antibacterial defense in the small intestine by the nuclear bile acid receptor. *Proc. Natl. Acad. Sci. USA* *103*, 3920–3925. <https://doi.org/10.1073/pnas.0509592103>.
52. Buffie, C.G., Bucci, V., Stein, R.R., McKenney, P.T., Ling, L., Gobourne, A., No, D., Liu, H., Kinnebrew, M., Viale, A., et al. (2015). Precision microbiome reconstitution restores bile acid mediated resistance to *Clostridium difficile*. *Nature* *517*, 205–208. <https://doi.org/10.1038/nature13828>.
53. Hagi, T., Geerlings, S.Y., Nijssse, B., and Belzer, C. (2020). The effect of bile acids on the growth and global gene expression profiles in *Akkermansia muciniphila*. *Appl. Microbiol. Biotechnol.* *104*, 10641–10653. <https://doi.org/10.1007/s00253-020-10976-3>.
54. Plovier, H., Everard, A., Druart, C., Depommier, C., Van Hul, M., Geurts, L., Chilloux, J., Ottman, N., Duparc, T., Lichtenstein, L., et al. (2017). A purified membrane protein from *Akkermansia muciniphila* or the pasteurized bacterium improves metabolism in obese and diabetic mice. *Nat. Med.* *23*, 107–113. <https://doi.org/10.1038/nm.4236>.
55. Depommier, C., Everard, A., Druart, C., Plovier, H., Van Hul, M., Vieira-Silva, S., Falony, G., Raes, J., Maiter, D., Delzenne, N.M., et al. (2019). Supplementation with *Akkermansia muciniphila* in overweight and obese human volunteers: a proof-of-concept exploratory study. *Nat. Med.* *25*, 1096–1103. <https://doi.org/10.1038/s41591-019-0495-2>.
56. Anhe, F.F., Roy, D., Pilon, G., Dudonné, S., Matamoros, S., Varin, T.V., Garofalo, C., Moine, Q., Desjardins, Y., Levy, E., and Marette, A. (2015). A polyphenol-rich cranberry extract protects from diet-induced obesity, insulin resistance and intestinal inflammation in association with increased *Akkermansia* spp. population in the gut microbiota of mice. *Gut* *64*, 872–883. <https://doi.org/10.1136/gutjnl-2014-307142>.
57. Li, Z., Zhang, B., Wang, N., Zuo, Z., Wei, H., and Zhao, F. (2023). A novel peptide protects against diet-induced obesity by suppressing appetite and modulating the gut microbiota. *Gut* *72*, 686–698. <https://doi.org/10.1136/gutjnl-2022-328035>.
58. Ribo, S., Sánchez-Infantes, D., Martínez-Guino, L., García-Mantrana, I., Ramon-Krauel, M., Tondo, M., Arning, E., Nofrarias, M., Osorio-Conles, Ó., Fernández-Pérez, A., et al. (2021). Increasing breast milk betaine modulates *Akkermansia* abundance in mammalian neonates and improves long-term metabolic health. *Sci. Transl. Med.* *13*, eabb0322. <https://doi.org/10.1126/scitranslmed.abb0322>.
59. Han, Y., Li, L., and Wang, B. (2022). Role of *Akkermansia muciniphila* in the development of nonalcoholic fatty liver disease: current knowledge and perspectives. *Front. Med.* *16*, 667–685. <https://doi.org/10.1007/s11684-022-0960-z>.
60. Kim, S., Lee, Y., Kim, Y., Seo, Y., Lee, H., Ha, J., Lee, J., Choi, Y., Oh, H., and Yoon, Y. (2020). *Akkermansia muciniphila* Prevents Fatty Liver Disease, Decreases Serum Triglycerides, and Maintains Gut Homeostasis. *Appl. Environ. Microbiol.* *86*, e03004–e03019. <https://doi.org/10.1128/aem.03004-19>.
61. Han, Y., Ling, Q., Wu, L., Wang, X., Wang, Z., Chen, J., Zheng, Z., Zhou, Z., Jia, L., Li, L., and Wang, B. (2023). *Akkermansia muciniphila* inhibits non-alcoholic steatohepatitis by orchestrating TLR2-activated $\gamma\delta$ T17 cell and macrophage polarization. *Gut Microb.* *15*, 2221485. <https://doi.org/10.1080/19490976.2023.2221485>.
62. Grander, C., Adolph, T.E., Wieser, V., Lowe, P., Wrzosek, L., Gyongyosi, B., Ward, D.V., Grabherr, F., Gerner, R.R., Pfister, A., et al. (2018). Recovery of ethanol-induced *Akkermansia muciniphila* depletion ameliorates alcoholic liver disease. *Gut* *67*, 891–901. <https://doi.org/10.1136/gutjnl-2016-313432>.

63. Juárez-Fernández, M., Porras, D., Petrov, P., Román-Sagüillo, S., García-Mediavilla, M.V., Soluyanova, P., Martínez-Flórez, S., González-Gallego, J., Nistal, E., Jover, R., and Sánchez-Campos, S. (2021). The Synbiotic Combination of *Akkermansia muciniphila* and Quercetin Ameliorates Early Obesity and NAFLD through Gut Microbiota Reshaping and Bile Acid Metabolism Modulation. *Antioxidants* *10*, 2001. <https://doi.org/10.3390/antiox10122001>.
64. Shi, Z., Lei, H., Chen, G., Yuan, P., Cao, Z., Ser, H.-L., Zhu, X., Wu, F., Liu, C., Dong, M., et al. (2021). Impaired Intestinal *Akkermansia muciniphila* and Aryl Hydrocarbon Receptor Ligands Contribute to Nonalcoholic Fatty Liver Disease in Mice. *mSystems* *6*, e00985-20. <https://doi.org/10.1128/mSystems.00985-20>.
65. Chen, Z., Jin, W., Hoover, A., Chao, Y., and Ma, Y. (2023). Decoding the microbiome: advances in genetic manipulation for gut bacteria. *Trends Microbiol.* *31*, 1143–1161. <https://doi.org/10.1016/j.tim.2023.05.007>.
66. Zhou, Y.-J., Gao, F., Liu, W.-Y., Wong, G.L.-H., Mahadeva, S., Raihan Nik Mustapha, N., Wang, X.-D., Chan, W.-K., Wong, V.W.-S., and Zheng, M.-H. (2021). Screening for compensated advanced chronic liver disease using refined Baveno VI elastography cutoffs in Asian patients with nonalcoholic fatty liver disease. *Aliment. Pharmacol. Ther.* *54*, 470–480. <https://doi.org/10.1111/apt.16487>.
67. Kleiner, D.E., Brunt, E.M., Van Natta, M., Behling, C., Contos, M.J., Cummings, O.W., Ferrell, L.D., Liu, Y.-C., Torbenson, M.S., Unalp-Arida, A., et al. (2005). Design and validation of a histological scoring system for nonalcoholic fatty liver disease. *Hepatology* *41*, 1313–1321. <https://doi.org/10.1002/hep.20701>.
68. Liu, C., Du, M.-X., Abuduaini, R., Yu, H.-Y., Li, D.-H., Wang, Y.-J., Zhou, N., Jiang, M.-Z., Niu, P.-X., Han, S.-S., et al. (2021). Enlightening the taxonomy darkness of human gut microbiomes with a cultured biobank. *Microbiome* *9*, 119. <https://doi.org/10.1186/s40168-021-01064-3>.
69. Wu, Q., Liang, X., Wang, K., Lin, J., Wang, X., Wang, P., Zhang, Y., Nie, Q., Liu, H., Zhang, Z., et al. (2021). Intestinal hypoxia-inducible factor 2 alpha regulates lactate levels to shape the gut microbiome and alter thermogenesis. *Cell Metab.* *33*, 1988–2003.e7. <https://doi.org/10.1016/j.cmet.2021.07.007>.
70. McIver, L.J., Abu-Ali, G., Franzosa, E.A., Schwager, R., Morgan, X.C., Waldron, L., Segata, N., and Huttenhower, C. (2018). bioBakery: a meta'omic analysis environment. *Bioinformatics* *34*, 1235–1237. <https://doi.org/10.1093/bioinformatics/btx754>.
71. Langmead, B., and Salzberg, S.L. (2012). Fast gapped-read alignment with Bowtie 2. *Nat. Methods* *9*, 357–359. <https://doi.org/10.1038/nmeth.1923>.
72. Truong, D.T., Franzosa, E.A., Tickle, T.L., Scholz, M., Weingart, G., Pasolli, E., Tett, A., Huttenhower, C., and Segata, N. (2015). MetaPhlan2 for enhanced metagenomic taxonomic profiling. *Nat. Methods* *12*, 902–903. <https://doi.org/10.1038/nmeth.3589>.
73. Segata, N., Izard, J., Waldron, L., Gevers, D., Miropolsky, L., Garrett, W.S., and Huttenhower, C. (2011). Metagenomic biomarker discovery and explanation. *Genome Biol.* *12*, R60. <https://doi.org/10.1186/gb-2011-12-6-r60>.
74. Nguyen, L.-T., Schmidt, H.A., von Haeseler, A., and Minh, B.Q. (2015). IQ-TREE: A Fast and Effective Stochastic Algorithm for Estimating Maximum-Likelihood Phylogenies. *Mol. Biol. Evol.* *32*, 268–274. <https://doi.org/10.1093/molbev/msu300>.
75. Letunic, I., and Bork, P. (2021). Interactive Tree Of Life (iTOL) v5: an online tool for phylogenetic tree display and annotation. *Nucleic Acids Res.* *49*, W293–W296. <https://doi.org/10.1093/nar/gkab301>.
76. Ha, C.W.Y., Martin, A., Sepich-Poore, G.D., Shi, B., Wang, Y., Gouin, K., Humphrey, G., Sanders, K., Ratnayake, Y., Chan, K.S.L., et al. (2020). Translocation of Viable Gut Microbiota to Mesenteric Adipose Drives Formation of Creeping Fat in Humans. *Cell* *183*, 666–683.e17. <https://doi.org/10.1016/j.cell.2020.09.009>.
77. Zheng, L., Tan, Y., Hu, Y., Shen, J., Qu, Z., Chen, X., Ho, C.L., Leung, E.L.-H., Zhao, W., and Dai, L. (2022). CRISPR/Cas-Based Genome Editing for Human Gut Commensal *Bacteroides* Species. *ACS Synth. Biol.* *11*, 464–472. <https://doi.org/10.1021/acssynbio.1c00543>.
78. Qi, X., Yun, C., Sun, L., Xia, J., Wu, Q., Wang, Y., Wang, L., Zhang, Y., Liang, X., Wang, L., et al. (2019). Gut microbiota-bile acid-interleukin-22 axis orchestrates polycystic ovary syndrome. *Nat. Med.* *25*, 1225–1233. <https://doi.org/10.1038/s41591-019-0509-0>.

STAR★METHODS

KEY RESOURCES TABLE

REAGENT or RESOURCE	SOURCE	IDENTIFIER
Bacterial strains		
<i>E. coli</i> BL21 (DE3)	Thermo Scientific	Cat# EC0114
<i>E. coli</i> DH5 α	Thermo Scientific	Cat# EC0112
<i>E. coli</i> S17-1 λ pir	Beyotime	Cat# D1075S
<i>A. muciniphila</i> JCM 30893	JCM	Cat# 30893
<i>A. muciniphila</i> ATCC BAA-835	ATCC	Cat# BAA-835
Other strains used in this study	This study	Table S2
Chemicals, peptides, and recombinant proteins		
Ampicillin	Sigma-Aldrich	Cat# BP021
Kanamycin	Sigma-Aldrich	Cat# D403
Metronidazole	Sigma-Aldrich	Cat# M1547
Vancomycin	Sigma-Aldrich	Cat# V2002
Gentamicin sulfate	Sigma-Aldrich	Cat# E003632
Methanol	Sigma-Aldrich	Cat# 439193
Acetonitrile	Sigma-Aldrich	Cat# 34851
Formic acid	Sigma-Aldrich	Cat# F0507
Cholic acid-2,2,4,4-d4	Sigma-Aldrich	Cat# 614149
Ursodeoxycholic acid-2,2,4,4-d4	Sigma-Aldrich	Cat# 904171
Lithocholic acid-2,2,4,4-d4	Sigma-Aldrich	Cat# 589349
EtOAc	Beijing FreeMore bioscience	Cat# E116131
NMP	MREDA	Cat# M19219
CuSO ₄	Sigma-Aldrich	Cat# 451657
BTTAA	Acmecc	Cat# B36940
Ascorbic acid	Solarbio	Cat# IA0530
TFA	Sigma-Aldrich	Cat# 302031
TIPS	Adamas	Cat# 011138495
DCM	Acmecc	Cat# D12641
Hexane	Beijing FreeMore bioscience	Cat# H109656
FITC-dextran (4 kDa)	Aladdin	Cat# F491425
Benzylamine hydrochloride	Aladdin	Cat# B129528
Benfluorex hydrochloride	Macklin	Cat# B880127
Coelenterazine	Yeasen biotechnology	Cat# 40904ES02
Cholic acid	Aladdin	Cat# C103690
Deoxycholic acid	Aladdin	Cat# D103697
Chenodeoxycholic acid	Aladdin	Cat# C104902
Lithocholic acid	Aladdin	Cat# L106779
Sodium taurocholate hydrate	Aladdin	Cat# T134625
Succinic acid	Aladdin	Cat# S108855
Ammonium sulfate	Aladdin	Cat# A112103
Anhydrotetracycline	Aladdin	Cat# A276282
GAM broth, modified	Solarbio	Cat# LA4490
Clarified rumen fluid	PERFEMIKER	Cat# PZ01010
BHI medium	Solarbio	Cat# B8130
TSB medium	Solarbio	Cat# RL100111
YCFA medium	Solarbio	Cat# LA4040

(Continued on next page)

Continued

REAGENT or RESOURCE	SOURCE	IDENTIFIER
BB medium	Solarbio	Cat# LA8550
CDM medium	TOPBIO	Cat# MD009C
Yeast extract	Oxoid	Cat# LP0021
Tryptone	Oxoid	Cat# LP0042

Critical commercial assays

Limulus amaebocyte lysate (LAL) kit	Yeasen biotechnology	Cat# EC32545
Peptidoglycan (PG) ELISA kit	Enzyme-linked Biotechnology	Cat# ml024098
Mouse MUC2 ELISA kit	Dogesce	Cat# DG96233Q
AN MicroPlate	Biolog	Cat# 1007
AN Inoculating Fluid	Biolog	Cat# 72007
MultiF Seamless Assembly Mix	Abclonal	Cat# RK21020
2 × Phanta Flash Master Mix (Dye Plus)	Vazyme	Cat# P520-01
FastPure Gel DNA Extraction Mini Kit	Vazyme	Cat# DC301-01
Lipofectamine 3000 transfection reagent	ThermoFisher Scientific	Cat# L3000015
Dual-luciferase assay system	Promega	Cat# E1910
TR-FRET FXR coactivator recruitment assay kit	Thermo Fisher	Cat# A15140
Oil Red O solution	Solarbio	Cat# G1260
Picro Sirius Red Stain Kit	Solarbio	Cat# G1472

Deposited data

Non-targeted metabolome data for CA-LNK derivatives identification	This paper	GNPS: MSV000094115
Non-targeted metabolome data for acylated cholic acid identification	This paper	GNPS: MSV000094116
Metagenome data for patients with MAFLD and controls	This paper	NMDC: NMDC10018735

Experimental models: Cell lines

HEK293T	ATCC	Cat# CRL-3216
---------	------	---------------

Experimental models: Organisms/strains

Mouse: C57BL/6J	GemPharmatech	N/A
Mouse: Germ-free C57BL/6J	GemPharmatech	N/A
Mouse: <i>Tlr4</i> ^{-/-} C57BL/10ScNJ	GemPharmatech	Cat# N000192

Oligonucleotides

Primers used in this study	This study	Table S5
----------------------------	------------	--------------------------

Recombinant DNA

pB041	From Prof. Dai lab	N/A
pB041- <i>Δbas-suc</i>	This study	N/A
pB039:: <i>bas-suc</i>	This study	N/A
pET-28a	Lab stock	N/A
pEcCas	Addgene	Cat# 73227
pEcgRNA	Addgene	Cat# 166581
pEcgRNA- <i>gImS</i>	This study	N/A
pEcgRNA- <i>nagB</i>	This study	N/A
pGL4-Shp-TK firefly luciferase construct	Lab stock	N/A
Human FXR expression plasmid	Lab stock	N/A
Human RXR expression plasmid	Lab stock	N/A
Human ASBT expression plasmid	Lab stock	N/A
pCMVSPORT6/hTGR5	Lab stock	N/A

(Continued on next page)

Continued

REAGENT or RESOURCE	SOURCE	IDENTIFIER
cAMP response element-driven luciferase reporter plasmids	Lab stock	N/A
<i>Renilla</i> luciferase control vector	Lab stock	N/A
Software and algorithms		
GraphPad Prism version 8.0	GraphPad	https://www.graphpad-prism.cn/
ImageJ	ImageJ	https://imagej.net/software/imagej/index
Mega 7	Mega	http://www.megasoftware.net/
SPSS 27.0	SPSS	https://www.ibm.com/spss/
SnapGene Viewer	SnapGene	http://www.snapgene.com/
Blast	NCBI	https://blast.ncbi.nlm.nih.gov/
Other		
NMR system	Bruker	Cat# Avance-500
Quaternary HPLC System	Agilent	Cat# 1200 Infinity
ACQUITY UPLC CSH C18 column	Waters	Cat# 186005297
QTRAP 5500	AB SCIEX	N/A
Choline-deficient amino acid-defined and high-fat diet	Research Diets	Cat# A06071302
Gubra-Amylin NASH diet	Research Diets	Cat# D09100310
ÄKTA pure 25L	Cytiva	Cat# 29018224
SkillPak TOYOPEARL Phenyl-650M 5 mL column	Tosoh Bioscience	Cat# 0045253
SkillPak TOYOPEARL GigaCap Q-650M 5 mL column	Tosoh Bioscience	Cat# 0045239
HisTrap HP	Cytiva	Cat# 17524801
Biacore T200 instrument	GE Healthcare	Cat# BR100649
CM5 sensor chip	GE Healthcare	Cat# BR100012
DESI-Xevo G2-XS QTof	Waters	N/A

RESOURCE AVAILABILITY**Lead contact**

Further information and requests for resources and reagents should be directed to the lead contact, Changtao Jiang (jiangchangtao@bjmu.edu.cn).

Materials availability

Materials in this work are available from the lead contact.

Data and code availability

- Data availability: Non-targeted metabolome data for CA-LNK derivatives identification and non-targeted metabolome data for acylated cholic acid identification are available through GNPS (<https://gnps.ucsd.edu/>) at MSV000094115 or MSV000094116, respectively. Metagenome data for patients with MAFLD and controls is available through NMDC (<https://nmdc.cn/>) at NMDC10018735. These accession numbers for the datasets are listed in the key resources table.
- This paper does not report original code.
- Any additional information required to reanalyze the data reported in this paper is available from the lead contact upon request.

EXPERIMENTAL MODEL AND STUDY PARTICIPANT DETAILS**Human study**

The human study was approved by the Ethical Committee of the First Affiliated Hospital of Wenzhou Medical University [2016-246] and informed written consent was obtained from all participants. Serum and stool samples from 55 patients diagnosed with biopsy-confirmed MAFLD⁶⁶ and 21 controls were obtained. All individuals included in the study are of Han Chinese ethnicity. Their clinical

information, including sex, age, BMI, FBG, TG, TC, HDL-C, LDL-C, ALT, AST, ALP and GGT, is provided in [Table S1](#). For patients with biopsy-confirmed MAFLD, histological specimens were scored according to the MASH-Clinical Research Network (CRN) scoring system.⁶⁷ Briefly, MAFLD activity score (MAS) was calculated as the sum of three histological components, including steatosis (grades 0–3), ballooning (grades 0–2), and lobular inflammation (grades 0–3). Patients with MAS of ≥ 5 correlated with Definite MASH, patients with MAS at 3 or 4 were correlated with Borderline MASH, and biopsies with scores of less than 3 were diagnosed as MAFL. The exclusion criteria were diabetic ketoacidosis or hyperglycemic hyperosmolar state; inflammatory bowel disease; cancer; alcoholism; taking antibiotics, probiotics, prebiotics, proton pump inhibitors, and laxatives taken during the previous 3 months. All clinical information was collected according to standard procedures. Peripheral blood samples were centrifuged at $1000 \times g$ and 4°C for 5 min to obtain the serum. The levels of blood biochemical indicators (i.e., TG, TC, AST and ALT) were measured using an autoanalyzer (BioTek Instruments 800TS). Feces were collected in collection cups and immediately frozen at -80°C until analysis.

Mice and treatments

All animal protocols were approved by the Animal Care and Use Committee of Peking University (permit: PUIRB-LA2023297). C57BL/6J mice and *Tlr4*^{-/-} mice (N000192) on a C57BL/10ScNJ background were purchased from GemPharmatech. Germ-free C57BL/6J mice (GemPharmatech, Nanjing, China) were bred within sterile vinyl isolators and maintained at the gnotobiotic mouse facility in the Department of Experimental Animal Science, Peking University Health Science Center. All mice had free access to food and water under a strict 12-h light/dark cycle at a controlled temperature ($23 \pm 2^\circ\text{C}$).

Age-matched (8-week-old) male mice were used in this study as described in the corresponding figure legends and were randomly assigned to experimental groups, and the groups did not present differences in body weights before the treatments. Mice were euthanized by CO₂ asphyxiation, and no mice were excluded from the analysis.

To detect the content of bile acids in antibiotic-treated (Abx) and fecal microbiota transplant (FMT) mice, 8-week-old SPF male mice were then treated with an oral, poorly absorbed broad-spectrum antibiotic cocktail (vancomycin 0.5 mg/mL, ampicillin 1 mg/mL, kanamycin 1 mg/mL, and metronidazole 1 mg/mL) in drinking water for 1 day. For the FMT group, antibiotics treated mice were transplanted once with fecal microbiota (100 μL per mice) from SPF mice. For FMT, 20 mg feces collected from SPF mice were dissolved in 1 mL of PBS, shaken for 3 min, and centrifuged at $200 \times g$ for 3 min at 4°C and the supernatant was collected.

To investigate the role of *B. uniformis* on the production of 3-sucCA, 8-week-old C57BL/6J male SPF or GF mice were treated with 2×10^8 CFU of *B. uniformis* in 200 μL of sterile anaerobic PBS by gavage once and last for one week, feces were collected for the 3-sucCA detection and verification of colonization efficiency.

To explore the effect of 3-sucCA on MAFL-MASH progression, 8-week-old C57BL/6J male SPF or GF mice were fed 8 weeks of a choline-deficient amino acid-defined and high fat diet (CDAA-HFD, Research Diets, cat# A06071302). Mice were treated with control or 10 mg/kg 3-sucCA by oral gavage 3 times per week for the last 3 weeks.

To test the role of *A. muciniphila* in the alleviation of 3-sucCA on MAFL-MASH progression, 8-week-old SPF male mice were fed a CDAA-HFD for 8 weeks. The mice were administered with control, 10 mg/kg 3-sucCA, 10 mg/kg 3-sucCA combined with 50 mg/kg benzydamine hydrochloride, or 10 mg/kg 3-sucCA combined with 50 mg/kg benfluorex hydrochloride by oral gavage 3 times per week for the last 3 weeks.

To explore the effect of *B. uniformis* on MAFL-MASH progression in the CDAA-HFD model, 8-week-old SPF male mice were fed a CDAA-HFD for 8 weeks. Mice were treated with *Bu*, *Bu- Δ bas-suc* or an equivalent volume of anaerobic PBS once per week for the last 3 weeks. For bacteria colonization, mice were given different strains of *B. uniformis* by gavage at a dose of 2×10^8 CFU in 200 μL sterile anaerobic PBS.

To explore the effect of *B. uniformis* on MAFL-MASH progression in the GAN diet model, 8-week-old SPF male mice were fed a GAN diet [Research Diets, #D09100310, with drinking water containing 23.1 g/L D(-)-fructose (Sigma, #F0127) and D-(+)-glucose (Sigma, #G8270)] for 24 weeks. Mice were treated with *Bu*, *Bu- Δ bas-suc* or an equivalent volume of anaerobic PBS once per week for the last 4 weeks. For bacteria colonization, mice were given different strains of *B. uniformis* by gavage at a dose of 2×10^8 CFU in 200 μL sterile anaerobic PBS.

To explore the effect of Toll-like receptor 4 on the 3-sucCA treated CDAA-HFD mouse model, 8-week-old *Tlr4*^{-/-} SPF male mice were fed a CDAA-HFD for 8 weeks. Mice were treated with control or 10 mg/kg 3-sucCA by oral gavage 3 times per week for the last 3 weeks.

To explore the effect of different bile acids on MAFL-MASH progression, 8-week-old C57BL/6J male SPF mice were fed a CDAA-HFD for 8 weeks. Mice were treated with control or 10 mg/kg compounds (succinic acid/CA/3-sucCA/3-sucCDCA/3-sucDCA/3-aceCA/3-proCA) by oral gavage 3 times per week for the last 3 weeks.

To explore the synergistic beneficial effect of *A. muciniphila* on MAFL-MASH progression, 8-week-old C57BL/6J male SPF mice were fed a CDAA-HFD for 8 weeks. Mice were gavaged with control, 3-sucCA (10 mg/kg) three times per week, *A. muciniphila* one time per week or 3-sucCA plus *A. muciniphila* for the last 3 weeks mice were given strain of *A. muciniphila* by gavage at a dose of 2×10^8 CFU in 200 μL sterile anaerobic PBS.

For biochemical analysis, hepatic and plasma triglyceride and cholesterol were determined with assay kits following the manufacturer's instructions. ALT and AST levels were assessed using commercial ALT and AST assay kits.

Bacteria

Bacteria strains were isolated from human stools, as previously described.⁶⁸ Briefly, human fecal solution (individuals with the highest 3-sucCA production; 10 mg/mL) was diluted 10⁴-fold. Then, 100 μ L of dilution was plated onto modified GAM (mGAM) agar plates for anaerobic (gas mix: 70% N₂, 25% CO₂, 5% H₂) incubation at 37°C. All the single colonies appearing on the agar plates after incubation for 48 h were picked, inoculated into 96-deep well plates containing 200 μ L of mGAM broth medium in each well and incubated at 37°C for 48 h. Then, the bacterial pellet was lysed with 5 μ L of NaOH/SDS lysis buffer and diluted with 150 μ L of deionized water. Two microliters of the templates were used for polymerase chain reaction (PCR)-based amplification of 16S rRNA gene sequences. The PCR products were identified by sequencing. The phylogenies of all the cultured isolates were determined by basic local alignment search tool (BLAST) analysis of the 16S rRNA gene sequences against the NCBI 16S rRNA sequence database.

For the colonization of *B. uniformis* JC066 in mice, the cultures were washed and concentrated in anaerobic PBS and the CFU/mL determined by plate counting using mGAM agar plate.³⁸ Before administration by oral gavage, the bacterial solutions were diluted with anaerobic PBS to a final concentration of 2 \times 10⁸ CFU/0.2 mL.

For the screen of 3-sucCA-producing bacteria, the mGAM medium (contain 1 μ M CA and 1 μ M succinic acid) was inoculated with different strains. The supernatant was harvested after 48 h incubation, which was further processed for LC-MS/MS analysis.

METHOD DETAILS

Synthesis of alkCA

Cholic acid (1.0 g, 2.4 mmol, 1.0 equiv) was dissolved in anhydrous CH₂Cl₂ (6 mL), diisopropylethylamine (DIPEA; 640 μ L, 3.7 mmol, 1.5 equiv), dicyclohexylcarbodiimide (DCC; 760 mg, 3.7 mmol, 1.5 equiv), 1-Hydroxybenzotriazole (HOBt; 360 mg, 2.7 mmol, 1.1 equiv) and propargylamine (185 μ L, 2.7 mmol, 1.1 equiv) were sequentially added to the stirred mixture, which was left at room temperature for 4 h. The reaction mixture was then diluted with CHCl₃, transferred into a separating funnel and washed twice with water. The organic phase, dried over anhydrous Na₂SO₄ and filtered, was then concentrated under reduced pressure and purified by column chromatography. Elution of the column with CHCl₃ containing increasing amounts of CH₃OH (from 1 to 10%) gave pure alkCA in 92% yield.

Synthesis of ACER resin

For ACER resin, synthesis was carried out as previously reported procedure.²⁸ 4-(2',4'-Dimethoxyphenyl-Fmoc-aminomethyl)-phenoxy resin (53.6 mg, 0.0175 mmol, 1.0 equiv) was weighed out into a flame dried 4 mL vial and 20% piperidine in dry *N,N*-dimethylformamide (DMF) was added to remove the fluorenylmethoxycarbonyl (Fmoc) protecting group. Remove the supernatant and add 20% piperidine in dry DMF (3 mL) again for complete cleavage. This step was repeated for 3–4 times and then the resin was washed in dry DMF for three times and stored in 3 mL dry DMF. Finally, a Kaiser test was used to ensure that Fmoc protecting group was removed completely. Valeric acid azide (3.8 mg, 0.027 mmol, 1.5 equiv), benzotriazole tetramethylurea tetrafluoroborate (TBTU; 16.9 mg, 0.053 mmol, 3.0 equiv), and diisopropylethylamine (DIEA; 9 μ L, 0.053 mmol, 3.0 equiv) were added into the flame dried 4 mL vial containing 3 mL dry DMF and Fmoc-removing resin. The vial was capped and rotated on a rotational mixer (25 rpm) at room temperature for half an hour when a Kaiser test was applied to confirm that the reaction was complete. The reaction mixture was then washed in *N*-methyl pyrrolidone (NMP), ddH₂O, NMP, dichloromethane (DCM) ordinally and the resin was air dried and stored in NMP in a final concentration of 10 mg/mL at 4°C.

Stool-derived ex vivo communities

For human fecal microbiota samples, the fecal pellet (10 mg) is suspended in 1 mL sterilized PBS, then the samples were immediately homogenized using a vortex for 1 min. The fecal suspension was centrifuged to remove larger particles (550 \times g for 5 min at room temperature). The supernatant was harvested and ten times diluted for incubation in different medium with inoculum size at 1% and cultured anaerobically at 37°C for indicated period.

AlkCA incubation, metabolome extraction and CuAAC-based enrichment

To explore the microbial transformation of CA, alkCA were incubated in the mGAM medium with fecal bacteria from healthy individuals. Briefly, stool-derived ex vivo communities were added with 100 μ M alkCA before incubation. After two days of culture, samples were centrifuged to get the supernatant (8000 \times g, 10 min), then the supernatant was extracted with ethyl acetate (1:1, v/v) and dried with nitrogen gas.

The incubated alkCA metabolome with fecal bacterial and related incubation control were separately reconstituted in a mixture of NMP/300 mM PBS (1:3, 1 mL). A click chemistry cocktail consisted of 50 mM CuSO₄ (60 μ L), 100 mM BTAA (60 μ L), and fresh 1 M ascorbic acid (100 μ L). The resulting mixture (220 μ L) and 100 μ L of 10 mg/mL ACER resin slurry were then added to the reconstituted samples for click reaction. Reactions were capped and placed on a rotisserie (22°C, 25 rpm) overnight. After 12 h of click reaction, ACER resin from different samples was harvested by centrifugation (500 \times g, 1 min), the resin was washed 3 times with NMP/water (1:3, 1 mL), NMP/water (1:1, 1 mL), NMP (1 mL), and DCM, respectively. Resin was dried with nitrogen gas and probe-derived metabolites were cleaved from the resin with treatment with trifluoroacetic acid (TFA)/water/TIPS (95:2.5:2.5, 50 μ L) for 1 h. Washing was repeated once, and the supernatant was collected. The cleavage reaction supernatant was combined into a tube and evaporated

with nitrogen gas. Residue was dissolved in methanol/water (4:1, 100 μ L), and tubes were centrifuged (12,000 \times g , 5 min) to pellet any remaining beads. The supernatant was filtered through a membrane filter (pore size, 0.22 μ m) for metabolomics analysis.

Mass spectrometric analysis

For the investigation of probe-derived metabolites, high resolution LC-MS analysis was performed on a Vanquish ultra-high performance liquid chromatography (UHPLC) coupled with a Thermo Q-Exactive HF high-resolution mass spectrometer equipped with a heated electrospray ionization source (HESI) ion source. Chromatographic separation was employed with an ACQUITY UPLC CSH C18 column (2.1 \times 100 mm, 1.7 μ m, Waters) at 40°C and a flow rate of 0.3 mL/min. The solvent A is 0.1% formic acid in water, and the solvent B is 0.1% formic acid in acetonitrile (ACN). Samples were eluted using a linear gradient: 0–5 min, 10% B; 5–20 min, 10–100% B; 20–25 min, 100% B; 25–30 min, 100–10% B. Mass spectrometer parameters were: spray voltage 3.0 kV, capillary temperature 380°C, auxiliary gas heater temperature 400°C; sheath, auxiliary, and spare gas flow was 60, 20, and 1, respectively; S-lens RF level 50. MS1 data was collected in both positive and negative modes. Resolution was set at 240,000, and the scan range was set to m/z 100–1000. The detailed instrument parameter setting referred to the description of Hoki et al.²⁸

Molecular networking

Each LC-MS RAW files (Thermo Fisher) was converted to mzXML format using MSConvert (ProteoWizard). The mzXML files were uploaded to the UCSD MassIVE data storage server through WinSCP for GNPS analysis.²⁴ Molecular networks were created using the online workflow at GNPS and visualized in Cytoscape. The molecular networking and MS-cluster parameters were as follows: parent and fragment ion mass tolerance was set to 0.02 Da, minimum cosine score of 0.7, minimum matched fragment ions of 4, and a minimum cluster size of 4 (to minimize detection of more rare nodes found in few samples).

Probe-derived metabolites identification

LC-MS RAW files (Thermo Fisher) from enriched probe-fed and incubation control samples were converted to mzXML format using MSConvert (ProteoWizard), followed by analysis using the XCMS-based software platform for feature extraction. The different features between enriched probe-fed samples and enriched incubation control samples were compared in network of GNPS. The probe-derived metabolites were further identified by comparing the DeltaMZ, the cosine value, node MS2 peaks, as well as similarity of MS/MS. Additionally, peak area minimum intensity for probe-derived metabolites candidates was set to 10000, and maximum intensity for incubation control was set to 2000, which corresponds to the noise level for most of the m/z range. The detailed intensity of probe-derived metabolites was also checked by the analysis of RAW files by Xcaliber software, which was used to monitor original MS spectra.

Extraction and isolation of acylated CAs

The solvents used for extraction and chromatographic separation were of analytical grade. Thin-layer chromatography (TLC) was carried out on silica gel HSGF254, and the spots were visualized by spraying with 10% H₂SO₄ and heating. Silica gel was used for column chromatography. High-performance liquid chromatography (HPLC) separation was performed on an Agilent 1200 HPLC system using an ODS column (C18, 250 \times 9.4 mm; detector: UV) with a flow rate of 2.0 mL/min. NMR spectral data were obtained with a Bruker Avance-500 spectrometer (DMSO-*d*₆, δ_{H} 2.50/ δ_{C} 39.5). The heteronuclear single quantum correlation spectrum (HSQC) and heteronuclear multiple bond correlation spectrum (HMBC) experiments were optimized for 145.0 and 8.0 Hz, respectively.

Stool-derived *ex vivo* communities from 5 healthy individuals were fermented in mGAM media containing 1 mg/mL CA with step-wise amplification (5 mL⁵ individuals as the initial system, and the bacterial suspensions were transferred into 0.2 L and 20 L system respectively, with a 1:200 inoculum). The fermented substrate was extracted repeatedly with ethyl acetate (3 \times 20 L), and the organic solvent was evaporated under vacuum to yield the crude extract (3.1 g). The crude extract was subsequently separated on a silica gel column (50.0 g of silica gel) eluted with hexane–ethyl acetate via gradient elution (v/v, 1:0, 10:1, each 500 mL) and then with dichloromethane–methanol (v/v, 1:0, 20:1, 10:1, 5:1, 3:1, 0:1, each 50 mL). The above fractions were detected by LC-MS for detected acylated CAs, and fraction eluted with dichloromethane–methanol (v/v, 20:1) was further separated by reversed-phase chromatography using 30% methanol in water and followed preparative thin-layer chromatography (PTLC; DCM/EA = 100: 25) to obtain 3-aceCA (3.2 mg) and 3-butCA (4.2 mg); the fraction eluted using 50% methanol in water was performed by PTLC (DCM/EA = 70: 30) to obtain 3-forCA (1.2 mg). The fractions eluted with dichloromethane–methanol (v/v, 5:1 and 3:1) were further separated by reversed-phase chromatography using 30% methanol in water and followed HPLC (23% methanol in water) to obtain 3-sucCA (10.1 mg) and the fraction eluted using 80% methanol in water was performed by HPLC (39% methanol in water) to obtain 3-malCA (1.6 mg).

X-ray Crystallographic Analysis of 3-sucCA: X-ray diffraction data collection was carried out from a 0.25 \times 0.20 \times 0.02 mm³ crystal with an Eos CCD using graphite-monochromated Cu K α radiation (λ = 1.54180 Å at 100.0 K). The structure was solved by direct methods (SHELXS-97) and refined using full-matrix leastsquares difference Fourier techniques. Crystal data of 3-sucCA: C₂₈H₄₄O₈, MW 508.63, space group monoclinic, P2₁2₁2₁; unit cell dimensions a = 10.3006(3) Å, b = 7.6079(3) Å, c = 16.2648(5) Å, α = 90.00°, β = 93.850(3)°, γ = 90.00°, V = 1271.73(7) Å³, Z = 2, D_{calc} = 1.328 mg/m³, μ = 0.783 mm⁻¹, $F(000)$ = 552.0. A total of 21006 reflections were measured, in which 5104 unique ($|F| \geq 2\sigma|F|$) were used in all calculations.

Synthetic procedures of acylated CAs

All reagents for acylated CAs synthesis were obtained from commercial suppliers unless otherwise stated. Tetrahydrofuran (THF), diethyl ether (Et₂O), toluene (PhMe), *N,N*-dimethylformamide (DMF) and dichloromethane (DCM) were purified by solvent purification system. Flasks were flame-dried under vacuum and cooled under a stream of argon. The following abbreviations are used: EA: ethyl acetate; PE: petroleum ether; THF: tetrahydrofuran; MOM: methoxymethyl; EDCI: *N*-(3-dimethylaminopropyl)-*N'*-ethylcarbodiimide hydrochloride; DMAP: 4-dimethylaminopyridine; DIPEA: *N,N*-diisopropylethylamine; FCC: flash column chromatography; PTLC: preparative thin-layer chromatography; rt: room temperature.

Flash chromatography was performed using silica gel (200–300 mesh) with solvents distilled before use.

Nuclear magnetic resonance (¹H and ¹³C NMR) spectra were recorded on Bruker AVIII-400 [¹H NMR (400 MHz), ¹³C NMR (101 MHz)] spectrometers and Bruker AVIII-600 [¹H NMR (600 MHz), ¹³C NMR (151 MHz)] spectrometers. The following abbreviations are used for the multiplicities: s: singlet, d: doublet, t: triplet, q: quartet, dt: double-triplet, td: triple-doublet, pseudo-t: pseudo-triplet, m: multiplet, brs: broad singlet for proton spectra and carbon spectra. Coupling constants (*J*) are reported in Hertz (Hz).

Mass spectra were recorded using a PE SCLEX QSTAR spectrometer.

3-sucCA (3): To a solution of CA (**1**, 0.5 g, 1.2 mmol, 1.0 equiv) in dry pyridine (5 mL) was added succinic anhydride (0.2 g, 1.7 mmol, 1.4 equiv) and DMAP (0.2 g, 1.3 mmol, 1.1 equiv). The mixture was heated to 80°C and stirred for 7 h. Additional succinic anhydride (0.2 g, 1.7 mmol, 1.4 equiv) was added at room temperature (rt). Next, the mixture was heated to 80°C and stirred for additional 7 h. The reaction was quenched with 2 N HCl (50 mL) and diluted with EA (100 mL), then the mixture was separated, and the aqueous phase was extracted with EA (3 × 100 mL). The combined organic layers were washed with brine (100 mL), dried over Na₂SO₄, filtered, and concentrated under reduced pressure. The residue was purified by FCC (DCM/MeOH/AcOH = 100: 4: 1) to afford **3** (0.50 g, 80%) as a white amorphous solid.

¹H NMR (400 MHz, CD₃OD): δ 4.62–4.49 (m, 1H), 3.96 (brs, 1H), 3.80 (d, *J* = 1.8 Hz, 1H), 2.63–2.49 (m, 4H), 2.49–2.15 (m, 4H), 2.05–1.94 (m, 2H), 1.91–1.71 (m, 5H), 1.69–1.50 (m, 6H), 1.50–1.22 (m, 5H), 1.20–1.04 (m, 2H), 1.02 (d, *J* = 6.3 Hz, 3H), 0.94 (s, 3H), 0.72 (s, 3H).

¹³C NMR (101 MHz, CD₃OD): δ 178.3, 176.1, 173.9, 76.4, 74.0, 69.0, 48.0, 47.5, 43.0, 42.9, 41.0, 36.8, 36.4, 36.1, 35.9, 35.6, 32.3, 32.0, 30.5, 29.9, 29.5, 28.7, 27.9, 27.6, 24.2, 23.0, 17.6, 13.0.

HRMS (ESI) calcd. for C₂₈H₄₃O₈[M – H][–]: 507.2958, found: 507.2952.

Benzyl cholate (4): To a suspension of CA (**1**, 5.0 g, 12.2 mmol, 1.0 equiv) and K₂CO₃ (3.4 g, 24.5 mmol, 2.0 equiv) in dry DMF (50 mL) at 0°C was added benzyl bromide (4.2 g, 24.5 mmol, 2.0 equiv) in portions. The mixture was stirred at rt for 12 h. The reaction was quenched with saturated NaHCO₃ (200 mL) and diluted with DCM (400 mL). The mixture was then separated, and the aqueous phase was extracted with DCM (3 × 200 mL). The combined organic layers were washed with 1 N HCl (200 mL) and brine (200 mL), dried over Na₂SO₄, filtered, and concentrated under reduced pressure. The residue was purified by FCC (DCM/MeOH = 100: 5) to afford **4** (5.80 g, 95%) as a white amorphous solid.

¹H NMR (400 MHz, CDCl₃): δ 7.44–7.26 (m, 5H), 5.17–5.05 (m, 2H), 3.95 (brs, 1H), 3.83 (brs, 1H), 3.52–3.36 (m, 1H), 2.53–2.35 (m, 3H), 2.35–2.14 (m, 4H), 1.98–1.80 (m, 4H), 1.79–1.62 (m, 5H), 1.61–1.45 (m, 4H), 1.44–1.32 (m, 4H), 1.29–1.21 (m, 1H), 1.16–1.03 (m, 1H), 0.97 (d, *J* = 5.8 Hz, 3H), 1.02–0.92 (m, 1H), 0.88 (s, 3H), 0.65 (s, 3H).

¹³C NMR (101 MHz, CDCl₃): δ 174.2, 136.3, 128.7 (2C), 128.4 (2C), 128.3, 73.2, 72.1, 68.6, 66.2, 47.2, 46.6, 41.9, 41.6, 39.7 (2C), 35.4, 35.3, 34.9, 34.8, 31.5, 31.0, 30.6, 28.4, 27.6, 26.6, 23.3, 22.6, 17.4, 12.6.

HRMS (ESI) calcd. for C₃₂H₄₇O₇[M + HCO₂][–]: 543.3322, found: 543.3322.

Benzyl 3-O-formyl cholate (5): To a solution of benzyl cholate (**4**, 0.6 g, 1.2 mmol, 1.0 equiv) in dry DCM (10 mL) was added formic acid (64.4 mg, 1.4 mmol, 1.2 equiv), EDCI (0.3 g, 1.8 mmol, 1.5 equiv) and DMAP (0.2 g, 1.8 mmol, 1.5 equiv). The mixture was stirred overnight at rt. The reaction was quenched with water (80 mL) and diluted with DCM (100 mL). The mixture was then separated, and the aqueous phase was extracted with DCM (3 × 100 mL). The combined organic layers were washed with 1 N HCl (100 mL), saturated NaHCO₃ (100 mL) and brine (100 mL), dried over Na₂SO₄, filtered, and concentrated under reduced pressure. The residue was purified by FCC (PE/EA = 100: 40) to afford **5** (0.37 g, 58%) as a white amorphous solid.

¹H NMR (400 MHz, CDCl₃): δ 8.01 (s, 1H), 7.42–7.27 (m, 5H), 5.17–5.01 (m, 2H), 4.78–4.63 (m, 1H), 3.97 (brs, 1H), 3.85 (d, *J* = 1.6 Hz, 1H), 2.51–2.14 (m, 4H), 2.00–1.64 (m, 11H), 1.63–1.48 (m, 6H), 1.43–1.31 (m, 2H), 1.30–1.22 (m, 1H), 1.18–1.00 (m, 2H), 0.97 (d, *J* = 6.0 Hz, 3H), 0.91 (s, 3H), 0.66 (s, 3H).

¹³C NMR (101 MHz, CDCl₃): δ 174.2, 161.1, 136.2, 128.7 (2C), 128.4 (2C), 128.3, 74.5, 73.0, 68.4, 66.3, 47.4, 46.7, 42.1, 41.3, 39.6, 35.2 (2C), 34.9, 34.8, 34.5, 31.4, 31.0, 28.4, 27.6, 26.8, 26.7, 23.3, 22.6, 17.5, 12.6.

HRMS (ESI) calcd. for C₃₃H₄₇O₈[M + HCO₂][–]: 571.3271, found: 571.3279.

3-forCA (6): To a solution of benzyl 3-O-formyl cholate (**5**, 0.3 g, 0.6 mmol, 1.0 equiv) in THF (20 mL) was added 10% Pd/C (10 wt % of **5**, 30.0 mg) and the suspension was hydrogenated (1 atm, balloon) overnight at 55°C. Thin-layer chromatography (TLC) indicated completion. The suspension was filtered through a pad of Celite, and the filter cake was rinsed with THF (3 × 30 mL). The combined filtrate and rinses were concentrated. The residue was purified by FCC (DCM/MeOH/AcOH = 100: 2: 1) to afford **6** (0.25 g, 95%) as a white amorphous solid.

¹H NMR (400 MHz, CD₃OD): δ 8.06 (s, 1H), 4.72–4.57 (m, 1H), 3.96 (brs, 1H), 3.81 (brs, 1H), 2.48 (q, *J* = 12.8 Hz, 1H), 2.41–2.15 (m, 3H), 2.08–1.63 (m, 10H), 1.62–1.56 (m, 3H), 1.53–1.24 (m, 5H), 1.20–1.05 (m, 2H), 1.02 (d, *J* = 6.2 Hz, 3H), 0.95 (s, 3H), 0.72 (s, 3H).

^{13}C NMR (101 MHz, CD_3OD): δ 178.3, 162.8, 76.0, 74.0, 68.9, 48.0, 47.5, 43.0, 42.9, 41.0, 36.8, 36.5, 36.0, 35.9, 35.6, 32.3, 32.1, 29.6, 28.7, 27.9, 27.7, 24.2, 23.0, 17.6, 13.0.

HRMS (ESI) calcd. for $\text{C}_{25}\text{H}_{39}\text{O}_6[\text{M} - \text{H}]^-$: 435.2747, found: 435.2755.

(Benzyl cholate-3-) 2-(benzyloxy) acetate (7) was prepared following the same procedure as shown in the synthesis of **5** and was obtained in 41% isolated yield as a colorless oil.

^1H NMR (400 MHz, CDCl_3): δ 7.44–7.26 (m, 10H), 5.20–5.02 (m, 2H), 4.75–4.65 (m, 1H), 4.62 (s, 2H), 4.04 (s, 2H), 3.98 (brs, 1H), 3.85 (d, $J = 1.2$ Hz, 1H), 2.50–2.11 (m, 4H), 2.02–1.60 (m, 9H), 1.58–1.44 (m, 7H), 1.44–1.33 (m, 2H), 1.31–1.24 (m, 2H), 1.19–1.02 (m, 2H), 0.97 (d, $J = 6.0$ Hz, 3H), 0.91 (s, 3H), 0.67 (s, 3H).

^{13}C NMR (101 MHz, CDCl_3): δ 174.1, 170.1, 137.4, 136.3, 128.7 (2C), 128.6 (2C), 128.4 (2C), 128.3 (3C), 128.1, 75.1, 73.5, 73.0, 68.3, 67.6, 66.3, 47.4, 46.7, 42.2, 41.3, 39.7, 35.3, 35.2, 35.0, 34.8, 34.4, 31.4, 31.0, 28.6, 27.5, 26.9, 26.8, 23.3, 22.7, 17.5, 12.7.

HRMS (ESI) calcd. for $\text{C}_{41}\text{H}_{55}\text{O}_9[\text{M} + \text{HCO}_2]^-$: 691.3846, found: 691.3855.

3-glaCA (8) was prepared following the same procedure as shown in the synthesis of **6** and was obtained in 98% isolated yield as a white amorphous solid.

^1H NMR (600 MHz, CD_3OD): δ 4.67–4.60 (m, 1H), 4.05 (s, 2H), 3.96 (brs, 1H), 3.80 (d, $J = 2.6$ Hz, 1H), 2.45 (dd, $J = 25.1, 13.0$ Hz, 1H), 2.35–2.18 (m, 2H), 2.05–1.94 (m, 3H), 1.93–1.83 (m, 3H), 1.83–1.64 (m, 4H), 1.63–1.50 (m, 5H), 1.49–1.39 (m, 2H), 1.37–1.29 (m, 2H), 1.18–1.03 (m, 2H), 1.02 (d, $J = 6.5$ Hz, 3H), 0.94 (s, 3H), 0.72 (s, 3H).

^{13}C NMR (151 MHz, CD_3OD): δ 178.5, 174.0, 76.7, 73.9, 68.9, 61.2, 48.1, 47.5, 43.0, 42.9, 41.0, 36.8, 36.4, 36.0, 35.9, 35.6, 32.5 (2C), 29.5, 28.7, 27.9, 27.6, 24.2, 23.0, 17.6, 13.0.

HRMS (ESI) calcd. for $\text{C}_{26}\text{H}_{41}\text{O}_7[\text{M} - \text{H}]^-$: 465.2852, found: 465.2862.

(Benzyl cholate-3-) benzyl malonate (9) was prepared following the same procedure as shown in the synthesis of **5** and was obtained in 40% isolated yield as a colorless oil.

^1H NMR (400 MHz, CDCl_3): δ 7.42–7.26 (m, 10H), 5.18 (s, 2H), 5.15–5.06 (m, 2H), 4.70–4.58 (m, 1H), 3.98 (brs, 1H), 3.84 (d, $J = 2.4$ Hz, 1H), 3.38 (s, 2H), 2.52–2.24 (m, 3H), 2.23–2.11 (m, 1H), 1.99–1.84 (m, 3H), 1.84–1.63 (m, 5H), 1.62–1.56 (m, 2H), 1.55–1.31 (m, 8H), 1.30–1.23 (m, 2H), 1.19–1.00 (m, 2H), 0.98 (d, $J = 6.1$ Hz, 3H), 0.90 (s, 3H), 0.67 (s, 3H).

^{13}C NMR (101 MHz, CDCl_3): δ 174.1, 166.7, 166.2, 136.3, 135.5, 128.7 (4C), 128.5 (3C), 128.4 (2C), 128.3, 75.9, 73.0, 68.3, 67.3, 66.3, 47.4, 46.7, 42.2, 42.1, 41.3, 39.7, 35.2, 35.1, 34.9, 34.8, 34.4, 31.4, 31.0, 28.6, 27.5, 26.9, 26.6, 23.3, 22.7, 17.5, 12.7.

HRMS (ESI) calcd. for $\text{C}_{41}\text{H}_{53}\text{O}_8[\text{M} - \text{H}]^-$: 673.3740, found: 673.3738.

3-malCA (10) was prepared following the same procedure as shown in the synthesis of **6** and was obtained in 87% isolated yield as a white amorphous solid.

^1H NMR (600 MHz, $\text{DMSO}-d_6$): δ 4.50–4.43 (m, 1H), 4.15 (brs, 1H), 4.12 (brs, 1H), 3.78 (brs, 1H), 3.62 (brs, 1H), 3.26 (s, 2H), 2.42 (q, $J = 12.9$ Hz, 1H), 2.28–2.19 (m, 1H), 2.18–2.05 (m, 2H), 1.98 (td, $J = 11.9, 7.7$ Hz, 1H), 1.87–1.60 (m, 6H), 1.59–1.51 (m, 2H), 1.50–1.26 (m, 7H), 1.25–1.12 (m, 2H), 1.03–0.93 (m, 2H), 0.92 (d, $J = 6.4$ Hz, 3H), 0.84 (s, 3H), 0.59 (s, 3H).

^{13}C NMR (151 MHz, $\text{DMSO}-d_6$): δ 175.0, 168.2, 166.7, 74.8, 71.0, 66.1, 46.1, 45.8, 42.4, 41.3, 41.0, 40.1, 35.0, 34.8, 34.5 (2C), 34.3, 30.9, 30.8, 28.4, 27.3, 26.2, 26.1, 22.8, 22.3, 17.0, 12.3.

HRMS (ESI) calcd. for $\text{C}_{27}\text{H}_{41}\text{O}_8[\text{M} - \text{H}]^-$: 493.2801, found: 493.2806.

Benzyl 3-O-acetyl cholate (11): To a solution of benzyl cholate (**4**, 0.3 g, 0.6 mmol, 1.0 equiv) in dry pyridine (3 mL) at 0°C was added acetic anhydride (60.0 μL , 0.7 mmol, 1.1 equiv) and DMAP (78.0 mg, 0.7 mmol, 1.1 equiv). The mixture was stirred at 0°C for 2 h. Next, the mixture was stirred at rt for 8 h. The reaction was quenched with water (50 mL) and diluted with EA (100 mL). The mixture was then separated, and the aqueous phase was extracted with EA (3×100 mL). The combined organic layers were washed with 1 N HCl (100 mL) and brine (100 mL), dried over Na_2SO_4 , filtered, and concentrated under reduced pressure. The residue was purified by FCC (PE/EA = 100: 38) to obtain **11** (0.16 g, 51%) as a white amorphous solid.

^1H NMR (400 MHz, CDCl_3): δ 7.41–7.26 (m, 5H), 5.20–5.03 (m, 2H), 4.63–4.50 (m, 1H), 3.97 (brs, 1H), 3.85 (d, $J = 2.3$ Hz, 1H), 2.49–2.14 (m, 4H), 2.00 (s, 3H), 1.98–1.56 (m, 13H), 1.53–1.42 (m, 4H), 1.42–1.31 (m, 2H), 1.31–1.24 (m, 1H), 1.19–1.01 (m, 2H), 0.97 (d, $J = 6.0$ Hz, 3H), 0.90 (s, 3H), 0.67 (s, 3H).

^{13}C NMR (101 MHz, CDCl_3): δ 174.1, 170.9, 136.3, 128.7 (2C), 128.4 (2C), 128.3, 74.4, 73.0, 68.4, 66.3, 47.4, 46.7, 42.2, 41.3, 39.7, 35.3, 35.2, 35.0, 34.8, 34.5, 31.5, 31.0, 28.5, 27.5, 26.9, 26.8, 23.3, 22.7, 21.6, 17.5, 12.7.

HRMS (ESI) calcd. for $\text{C}_{34}\text{H}_{49}\text{O}_8[\text{M} + \text{HCO}_2]^-$: 585.3427, found: 585.3423.

3-aceCA (12) was prepared following the same procedure as shown in the synthesis of **6** and was obtained in 98% isolated yield as a white amorphous solid.

^1H NMR (400 MHz, CD_3OD): δ 4.62–4.46 (m, 1H), 3.96 (brs, 1H), 3.80 (d, $J = 2.4$ Hz, 1H), 2.51–2.13 (m, 4H), 2.06–1.99 (m, 1H), 1.98 (s, 3H), 1.98–1.92 (m, 1H), 1.92–1.61 (m, 7H), 1.61–1.25 (m, 9H), 1.21–1.03 (m, 2H), 1.02 (d, $J = 6.4$ Hz, 3H), 0.94 (s, 3H), 0.72 (s, 3H).

^{13}C NMR (101 MHz, CD_3OD): δ 178.4, 172.7, 76.2, 74.0, 68.9, 48.1, 47.5, 43.0, 42.9, 41.0, 36.8, 36.4, 36.1, 35.9, 35.6, 32.4, 32.1, 29.5, 28.7, 27.9, 27.6, 24.2, 23.0, 21.3, 17.6, 13.0.

HRMS (ESI) calcd. for $\text{C}_{26}\text{H}_{41}\text{O}_6[\text{M} - \text{H}]^-$: 449.2903, found: 449.2902.

Benzyl 3-O-propionyl cholate (13) was prepared following the same procedure as shown in the synthesis of **11** and was obtained in 43% isolated yield as a white amorphous solid.

^1H NMR (400 MHz, CDCl_3): δ 7.42–7.26 (m, 5H), 5.18–5.05 (m, 2H), 4.65–4.52 (m, 1H), 3.97 (brs, 1H), 3.84 (d, $J = 1.3$ Hz, 1H), 2.47–2.38 (m, 1H), 2.37–2.16 (m, 5H), 2.01–1.58 (m, 12H), 1.55–1.32 (m, 7H), 1.30–1.23 (m, 1H), 1.18–1.08 (m, 4H), 1.08–1.00 (m, 1H), 0.97 (d, $J = 5.8$ Hz, 3H), 0.90 (s, 3H), 0.67 (s, 3H).

^{13}C NMR (101 MHz, CDCl_3): δ 174.3, 174.1, 136.3, 128.7 (2C), 128.4 (2C), 128.3, 74.2, 73.0, 68.4, 66.3, 47.4, 46.7, 42.2, 41.3, 39.7, 35.4, 35.2, 35.0, 34.8, 34.5, 31.4, 31.0, 28.5, 28.1, 27.6, 26.9, 26.8, 23.3, 22.7, 17.5, 12.7, 9.3.

HRMS (ESI) calcd. for $\text{C}_{35}\text{H}_{51}\text{O}_8[\text{M} + \text{HCO}_2]^-$: 599.3584, found: 599.3577.

3-proCA (14) was prepared following the same procedure as shown in the synthesis of **6** and was obtained in 98% isolated yield as a white amorphous solid.

^1H NMR (400 MHz, CD_3OD): δ 4.66–4.45 (m, 1H), 3.96 (brs, 1H), 3.80 (brs, 1H), 2.53–2.14 (m, 6H), 2.07–1.93 (m, 2H), 1.92–1.52 (m, 11H), 1.51–1.41 (m, 2H), 1.40–1.24 (m, 3H), 1.21–1.04 (m, 5H), 1.02 (d, $J = 6.0$ Hz, 3H), 0.94 (s, 3H), 0.72 (s, 3H).

^{13}C NMR (101 MHz, CD_3OD): δ 178.4, 176.0, 76.1, 74.0, 69.0, 48.1, 47.5, 43.0, 42.9, 41.0, 36.8, 36.5, 36.1, 35.9, 35.6, 32.4, 32.1, 29.5, 28.8, 28.7, 27.9, 27.6, 24.2, 23.0, 17.6, 13.0, 9.5.

HRMS (ESI) calcd. for $\text{C}_{27}\text{H}_{43}\text{O}_6[\text{M} - \text{H}]^-$: 463.3060, found: 463.3055.

Benzyl 3-O-butyryl cholate (15) was prepared following the same procedure as shown in the synthesis of **11** and was obtained in 47% isolated yield as a white amorphous solid.

^1H NMR (400 MHz, CDCl_3): δ 7.42–7.26 (m, 5H), 5.19–5.04 (m, 2H), 4.66–4.51 (m, 1H), 3.97 (brs, 1H), 3.84 (d, $J = 2.1$ Hz, 1H), 2.48–2.16 (m, 6H), 1.98–1.57 (m, 14H), 1.55–1.23 (m, 8H), 1.18–1.02 (m, 2H), 1.02–0.88 (m, 9H), 0.66 (s, 3H).

^{13}C NMR (101 MHz, CDCl_3): δ 174.2, 173.5, 136.2, 128.7 (2C), 128.4 (2C), 128.3, 74.1, 73.1, 68.4, 66.3, 47.4, 46.7, 42.2, 41.4, 39.7, 36.8, 35.4, 35.2, 35.0, 34.8, 34.5, 31.4, 31.0, 28.5, 27.6, 26.9, 26.8, 23.3, 22.7, 18.7, 17.5, 13.8, 12.7.

HRMS (ESI) calcd. for $\text{C}_{35}\text{H}_{51}\text{O}_6[\text{M} - \text{H}]^-$: 567.3686, found: 567.3693.

3-butCA (16) was prepared following the same procedure as shown in the synthesis of **6** and was obtained in 98% isolated yield as a white amorphous solid.

^1H NMR (600 MHz, CD_3OD): δ 4.62–4.48 (m, 1H), 3.96 (brs, 1H), 3.80 (brs, 1H), 2.54–2.14 (m, 6H), 2.07–1.94 (m, 3H), 1.93–1.72 (m, 5H), 1.71–1.56 (m, 7H), 1.54–1.51 (m, 1H), 1.49–1.40 (m, 2H), 1.38–1.28 (m, 2H), 1.18–1.05 (m, 2H), 1.02 (d, $J = 6.1$ Hz, 3H), 0.99–0.84 (m, 6H), 0.72 (s, 3H).

^{13}C NMR (151 MHz, CD_3OD): δ 178.5, 175.2, 76.0, 74.0, 69.0, 48.1, 47.5, 43.0, 42.9, 41.0, 37.5, 36.8, 36.5, 36.1, 35.9, 35.6, 32.4, 32.2, 29.5, 28.7, 27.9, 27.7, 24.2, 23.0, 19.5, 17.6, 13.9, 13.0.

HRMS (ESI) calcd. for $\text{C}_{28}\text{H}_{45}\text{O}_6[\text{M} - \text{H}]^-$: 477.3216, found: 477.3217.

Benzyl 3-O-benzyl cholate (17): To a solution of benzyl cholate (**4**, 1.5 g, 3.0 mmol, 1.0 equiv) in DIPEA (30 mL) was added benzyl bromide (0.8 g, 4.5 mmol, 1.5 equiv) and dry DMF (2 mL). The mixture was heated to 100°C and stirred overnight. The reaction was quenched with water (50 mL) and diluted with DCM (100 mL), then the mixture was separated and the aqueous phase was extracted with DCM (3 × 100 mL). The combined organic layers were washed with 1 N HCl (100 mL), saturated NaHCO_3 (100 mL) and brine (100 mL), dried over Na_2SO_4 , filtered, and concentrated under reduced pressure. The residue was purified by FCC (PE/EA = 3: 1) to afford **17** (1.01 g, 57%) as a white amorphous solid.

^1H NMR (400 MHz, CDCl_3): δ 7.40–7.23 (m, 10H), 5.17–5.05 (m, 2H), 4.66–4.45 (m, 2H), 3.95 (brs, 1H), 3.80 (brs, 1H), 3.30–3.12 (m, 1H), 2.49–2.38 (m, 1H), 2.36–2.13 (m, 3H), 1.98–1.91 (m, 1H), 1.90–1.75 (m, 6H), 1.75–1.71 (m, 1H), 1.70–1.56 (m, 3H), 1.54–1.46 (m, 3H), 1.45–1.32 (m, 4H), 1.31–1.14 (m, 2H), 1.14–1.04 (m, 1H), 0.97 (d, $J = 5.9$ Hz, 3H), 0.95–0.90 (m, 1H), 0.88 (s, 3H), 0.65 (s, 3H).

^{13}C NMR (101 MHz, CDCl_3): δ 174.2, 139.4, 136.3, 128.7 (2C), 128.4 (4C), 128.3, 127.7 (2C), 127.4, 78.8, 73.0, 69.8, 68.4, 66.2, 47.2, 46.6, 42.1, 41.6, 39.7, 36.4, 35.4, 35.2 (2C), 34.8, 31.4, 31.0, 28.5, 27.5, 27.4, 26.8, 23.3, 22.8, 17.4, 12.7.

HRMS (ESI) calcd. for $\text{C}_{39}\text{H}_{53}\text{O}_7[\text{M} + \text{HCO}_2]^-$: 633.3791, found: 633.3785.

(Benzyl 3-O-benzyl cholate-7-) benzyl succinate (18) was prepared following the same procedure as shown in the synthesis of **5** and was obtained in 77% isolated yield as a colorless oil.

^1H NMR (400 MHz, CDCl_3): δ 7.40–7.25 (m, 15H), 5.21–5.06 (m, 4H), 4.92 (d, $J = 2.1$ Hz, 1H), 4.61–4.46 (m, 2H), 3.96 (brs, 1H), 3.29–3.13 (m, 1H), 2.78–2.55 (m, 4H), 2.49–2.36 (m, 1H), 2.35–2.16 (m, 2H), 2.07–1.16 (m, 21H), 1.09–1.00 (m, 1H), 0.96 (d, $J = 5.8$ Hz, 3H), 0.90 (s, 3H), 0.64 (s, 3H).

^{13}C NMR (101 MHz, CDCl_3): δ 174.1, 172.2, 172.0, 139.4, 136.2, 136.0, 128.7 (4C), 128.4 (6C), 128.3 (2C), 127.6 (2C), 127.4, 78.7, 72.8, 71.6, 69.9, 66.6, 66.2, 47.2, 46.7, 42.1, 41.2, 38.3, 35.7, 35.3, 35.1, 34.8, 31.7, 31.4, 31.0, 29.8, 29.4, 28.7, 28.2, 27.5, 27.4, 23.1, 22.7, 17.4, 12.6.

HRMS (ESI) calcd. for $\text{C}_{50}\text{H}_{63}\text{O}_{10}[\text{M} + \text{HCO}_2]^-$: 823.4421, found: 823.4419.

7-sucCA (19): was prepared following the same procedure as shown in the synthesis of **6** and was obtained in 77% isolated yield as a white amorphous solid.

^1H NMR (400 MHz, Acetone- d_6): δ 4.89 (d, $J = 2.1$ Hz, 1H), 3.99 (brs, 1H), 3.47–3.32 (m, 1H), 2.71–2.51 (m, 4H), 2.43–2.27 (m, 2H), 2.25–2.13 (m, 1H), 2.12–2.05 (m, 2H), 2.03–1.92 (m, 2H), 1.92–1.82 (m, 1H), 1.81–1.74 (m, 2H), 1.73–1.65 (m, 1H), 1.65–1.49 (m, 5H), 1.48–1.35 (m, 4H), 1.35–1.21 (m, 2H), 1.16–1.04 (m, 1H), 1.02 (d, $J = 6.4$ Hz, 3H), 1.00–0.95 (m, 1H), 0.94 (s, 3H), 0.71 (s, 3H).

^{13}C NMR (101 MHz, CD_3OD): δ 178.2, 175.9, 173.9, 73.6, 73.1, 72.5, 48.0, 47.6, 43.3, 42.7, 39.9, 39.5, 36.7, 36.3, 35.5, 32.5, 32.3, 32.0, 31.2, 30.7, 29.9, 29.8, 29.4, 28.5, 24.1, 23.1, 17.6, 12.9.

HRMS (ESI) calcd. for $\text{C}_{28}\text{H}_{43}\text{O}_8[\text{M} - \text{H}]^-$: 507.2958, found: 507.2959.

Benzyl 3-O-benzyl-7-O-MOM cholate (20): To a solution of benzyl 3-O-benzyl cholate (**17**, 2.5 g, 4.2 mmol, 1.0 equiv) in dry DCM (50 mL) was added DIPEA (1.5 mL, 8.5 mmol, 2.0 equiv). Then the mixture was cooled to 0°C. MOMBr (0.5 mL, 6.4 mmol, 1.5 equiv) was dissolved in dry DCM (15 mL) and added dropwise to the above solution. Then the mixture was stirred at rt for 2 h. Additional MOMBr (0.2 mL, 2.6 mmol, 0.6 equiv) was added dropwise at 0°C. The mixture was stirred at rt overnight. The reaction was quenched with water (50 mL) and diluted with DCM (100 mL), then the mixture was separated and the aqueous phase was extracted with DCM (3 × 100 mL). The combined organic layers were washed with saturated NH₄Cl (100 mL), saturated NaHCO₃ (100 mL) and brine (100 mL), dried over Na₂SO₄, filtered, and concentrated under reduced pressure. The residue was purified by FCC and PTLC (DCM/EA = 100: 25) to obtain **20** (1.00 g, 37%) as a white amorphous solid.

¹H NMR (400 MHz, CDCl₃): δ 7.42–7.26 (m, 10H), 5.19–5.04 (m, 2H), 4.74–4.48 (m, 4H), 3.95 (s, 1H), 3.61 (s, 1H), 3.37 (s, 3H), 3.28–3.14 (m, 1H), 2.51–2.37 (m, 1H), 2.36–2.13 (m, 3H), 1.96 (td, *J* = 11.9, 7.7 Hz, 1H), 1.90–1.77 (m, 4H), 1.75–1.64 (m, 4H), 1.61–1.57 (m, 1H), 1.55–1.43 (m, 3H), 1.43–1.33 (m, 4H), 1.32–1.11 (m, 2H), 1.10–1.01 (m, 1H), 0.97 (d, *J* = 5.3 Hz, 3H), 0.96–0.92 (m, 1H), 0.90 (s, 3H), 0.65 (s, 3H).

¹³C NMR (101 MHz, CDCl₃): δ 174.2, 139.5, 136.3, 128.7 (2C), 128.4 (4C), 128.3, 127.6 (2C), 127.4, 95.6, 78.9, 74.4, 73.0, 69.9, 66.2, 56.3, 47.3, 46.5, 41.8, 41.7, 39.7, 35.9, 35.4, 35.2, 35.1, 31.5, 31.0 (2C), 28.5, 27.5, 27.3, 27.2, 23.3, 22.9, 17.5, 12.7.

HRMS (ESI) calcd. for C₄₁H₅₇O₈[M + HCO₂]⁻: 677.4053, found: 677.4063.

(Benzyl 3-O-benzyl-7-O-MOM cholate-12-) benzyl succinate (21): To a solution of benzyl 3-O-benzyl-7-O-MOM cholate (**20**, 0.8 g, 1.3 mmol, 1.0 equiv) in dry DCM (20 mL) was added monobenzyl succinate (0.8 g, 3.8 mmol, 3.0 equiv), EDCI (0.8 g, 4.1 mmol, 3.2 equiv), DMAP (0.5 g, 4.1 mmol, 3.2 equiv) and DIPEA (1.1 mL, 6.3 mmol, 5.0 equiv). Then the mixture was stirred at 50°C overnight. The reaction was quenched with water (80 mL) and diluted with DCM (100 mL), then the mixture was separated and the aqueous phase was extracted with DCM (3 × 100 mL). The combined organic layers were washed with 1 N HCl (100 mL), saturated NaHCO₃ (100 mL) and brine (100 mL), dried over Na₂SO₄, filtered, and concentrated under reduced pressure. The residue was purified by PTLC (PE/EA = 100: 35) to obtain **21** (0.57 g, 55%) as a yellow oil.

¹H NMR (400 MHz, CDCl₃): δ 7.40–7.25 (m, 15H), 5.19–5.05 (m, 5H), 4.73–4.49 (m, 4H), 3.62 (d, *J* = 1.8 Hz, 1H), 3.37 (s, 3H), 3.24–3.13 (m, 1H), 2.79–2.59 (m, 4H), 2.46–2.35 (m, 1H), 2.34–2.20 (m, 2H), 2.17–1.99 (m, 2H), 1.94–1.79 (m, 2H), 1.78–1.60 (m, 8H), 1.58–1.42 (m, 2H), 1.42–1.30 (m, 3H), 1.30–1.18 (m, 2H), 1.13–0.98 (m, 1H), 0.97–0.90 (m, 1H), 0.88 (s, 3H), 0.80 (d, *J* = 5.8 Hz, 3H), 0.69 (s, 3H).

¹³C NMR (101 MHz, CDCl₃): δ 174.1, 172.1, 171.9, 139.4, 136.3, 136.1, 128.7 (2C), 128.6 (2C), 128.4 (4C), 128.3 (4C), 127.7 (2C), 127.5, 95.6, 79.1, 76.0, 74.4, 70.0, 66.6, 66.2, 56.3, 47.5, 45.1, 42.9, 41.8, 39.4, 36.0, 35.3, 35.1, 34.9, 31.4, 31.0 (2C), 29.7, 29.3, 28.1, 27.5, 27.4, 25.6, 23.1, 22.8, 17.6, 12.4.

HRMS (ESI) calcd. for C₅₁H₆₅O₉[M - H]⁻: 821.4629, found: 821.4623.

(Benzyl 3-O-benzyl cholate-12-) benzyl succinate (22): To a solution of hydrochloric acid (2.0 mol/L) in ethyl acetate (10 mL) was added (benzyl 3-O-benzyl-7-O-MOM cholate-12-) benzyl succinate (**21**, 0.5 g, 0.6 mmol, 1.0 equiv). Then the mixture was stirred at rt for 6 h. The reaction was quenched with water (50 mL) and diluted with EA (100 mL), then the mixture was separated and the aqueous phase was extracted with EA (3 × 100 mL). The combined organic layers were washed with saturated NaHCO₃ (100 mL) and brine (100 mL), dried over Na₂SO₄, filtered, and concentrated under reduced pressure. The residue was purified by PTLC (DCM/MeOH = 100: 3.5) to obtain **22** (0.45 g, 90%) as a yellow oil.

¹H NMR (400 MHz, CDCl₃): δ 7.40–7.25 (m, 15H), 5.18–5.05 (m, 5H), 4.60–4.49 (m, 2H), 3.86 (d, *J* = 2.5 Hz, 1H), 3.27–3.12 (m, 1H), 2.77–2.59 (m, 4H), 2.45–2.34 (m, 1H), 2.33–2.18 (m, 2H), 2.09 (td, *J* = 12.6, 4.4 Hz, 1H), 2.02–1.88 (m, 3H), 1.87–1.79 (m, 2H), 1.78–1.61 (m, 5H), 1.59–1.44 (m, 3H), 1.43–1.32 (m, 4H), 1.31–1.23 (m, 2H), 1.20–1.06 (m, 1H), 1.00–0.90 (m, 1H), 0.88 (s, 3H), 0.80 (d, *J* = 6.1 Hz, 3H), 0.71 (s, 3H).

¹³C NMR (101 MHz, CDCl₃): δ 174.1, 172.1, 171.8, 139.4, 136.3, 136.1, 128.7 (2C), 128.6 (2C), 128.4 (4C), 128.3 (4C), 127.7 (2C), 127.4, 78.9, 76.0, 69.9, 68.3, 66.6, 66.2, 47.5, 45.3, 43.5, 41.6, 39.5, 36.5, 35.2, 35.1, 34.8 (2C), 31.3, 30.9, 29.7, 29.4, 27.7, 27.5 (2C), 25.6, 23.1, 22.8, 17.5, 12.4.

HRMS (ESI) calcd. for C₅₀H₆₃O₁₀[M + HCO₂]⁻: 823.4421, found: 823.4419.

12-sucCA (23) was prepared following the same procedure as shown in the synthesis of **6** and was obtained in 91% isolated yield as a yellow amorphous solid.

¹H NMR (400 MHz, CD₃OD): δ 5.11 (brs, 1H), 3.83 (brs, 1H), 3.40–3.34 (m, 1H), 2.79–2.51 (m, 4H), 2.41–2.06 (m, 5H), 2.03–1.88 (m, 2H), 1.88–1.64 (m, 6H), 1.63–1.48 (m, 4H), 1.44–1.24 (m, 5H), 1.21–1.10 (m, 1H), 1.04–0.97 (m, 1H), 0.92 (s, 3H), 0.86 (d, *J* = 5.4 Hz, 3H), 0.78 (s, 3H).

¹³C NMR (151 MHz, CD₃OD): δ 178.4, 176.0, 173.7, 77.5, 72.8, 68.7, 46.2, 44.5, 43.1, 40.6, 40.4, 36.4, 36.2, 35.7 (3C), 32.1, 32.0, 31.1, 30.8, 30.0, 28.7, 28.5, 26.3, 23.9, 23.1, 17.9, 12.6.

HRMS (ESI) calcd. for C₂₈H₄₃O₈[M - H]⁻: 507.2958, found: 507.2966.

Benzyl deoxycholate (25): was prepared following the same procedure as shown in the synthesis of **4** and was obtained in 90% isolated yield as a white amorphous solid.

¹H NMR (400 MHz, CDCl₃): δ 7.42–7.26 (m, 5H), 5.18–4.98 (m, 2H), 3.96 (brs, 1H), 3.68–3.51 (m, 1H), 2.48–2.35 (m, 1H), 2.34–2.21 (m, 1H), 1.91–1.62 (m, 10H), 1.61–1.53 (m, 2H), 1.53–1.47 (m, 3H), 1.45–1.30 (m, 6H), 1.29–1.19 (m, 2H), 1.19–0.97 (m, 3H), 0.95 (d, *J* = 5.7 Hz, 3H), 0.90 (s, 3H), 0.64 (s, 3H).

^{13}C NMR (101 MHz, CDCl_3): δ 174.2, 136.3, 128.7 (2C), 128.3 (3C), 73.2, 71.9, 66.2, 48.4, 47.4, 46.6, 42.2, 36.6, 36.2, 35.3, 35.2, 34.2, 33.8, 31.5, 31.0, 30.6, 28.8, 27.6, 27.3, 26.2, 23.8, 23.3, 17.4, 12.8.

HRMS (ESI) calcd. for $\text{C}_{32}\text{H}_{47}\text{O}_6[\text{M} + \text{HCO}_2]^-$: 527.3373, found: 527.3376.

(Benzyl deoxycholate-3-) benzyl succinate (26): was prepared following the same procedure as shown in the synthesis of **5** and was obtained in 96% isolated yield as a colorless oil.

^1H NMR (400 MHz, CDCl_3): δ 7.44–7.28 (m, 10H), 5.21–5.04 (m, 4H), 4.79–4.65 (m, 1H), 3.96 (brs, 1H), 2.75–2.53 (m, 4H), 2.49–2.36 (m, 1H), 2.36–2.23 (m, 1H), 1.90–1.57 (m, 10H), 1.54–1.33 (m, 10H), 1.29–1.19 (m, 2H), 1.16–1.00 (m, 3H), 0.96 (d, $J = 6.0$ Hz, 3H), 0.91 (s, 3H), 0.65 (s, 3H).

^{13}C NMR (101 MHz, CDCl_3): δ 174.1, 172.3, 171.8, 136.2, 135.9, 128.6 (4C), 128.3 (6C), 74.8, 73.2, 66.6, 66.2, 48.4, 47.5, 46.6, 42.0, 36.1, 35.1, 35.0, 34.2, 33.7, 32.2, 31.4, 31.0, 29.6, 29.4, 28.8, 27.5, 27.0, 26.6, 26.1, 23.7, 23.2, 17.4, 12.8.

HRMS (ESI) calcd. for $\text{C}_{43}\text{H}_{57}\text{O}_9[\text{M} + \text{HCO}_2]^-$: 717.4003, found: 717.4009.

3-sucDCA (27): was prepared following the same procedure as shown in the synthesis of **6** and was obtained in 97% isolated yield as a white amorphous solid.

^1H NMR (400 MHz, CD_3OD): δ 4.75–4.65 (m, 1H), 3.97 (brs, 1H), 2.66–2.46 (m, 4H), 2.43–2.29 (m, 1H), 2.28–2.12 (m, 1H), 2.02–1.73 (m, 7H), 1.69–1.24 (m, 14H), 1.23–1.04 (m, 3H), 1.01 (d, $J = 6.2$ Hz, 3H), 0.95 (s, 3H), 0.72 (s, 3H).

^{13}C NMR (101 MHz, CD_3OD): δ 178.2, 176.0, 173.8, 76.1, 74.0, 49.3, 48.1, 47.6, 43.4, 37.4, 36.7, 36.0, 35.3, 34.7, 33.3, 32.3, 32.0, 30.5, 29.8 (2C), 28.6, 28.2, 27.4, 27.3, 24.8, 23.6, 17.6, 13.2.

HRMS (ESI) calcd. for $\text{C}_{28}\text{H}_{43}\text{O}_7[\text{M} - \text{H}]^-$: 491.3009, found: 491.3015.

Benzyl chenodeoxycholate (29) was prepared following the same procedure as shown in the synthesis of **4** and was obtained in 96% isolated yield as a white amorphous solid.

^1H NMR (400 MHz, CDCl_3): δ 7.47–7.28 (m, 5H), 5.22–4.98 (m, 2H), 3.84 (brs, 1H), 3.55–3.36 (m, 1H), 2.48–2.34 (m, 1H), 2.33–2.12 (m, 2H), 2.05–1.92 (m, 2H), 1.91–1.76 (m, 4H), 1.75–1.65 (m, 2H), 1.65–1.57 (m, 3H), 1.55–1.44 (m, 3H), 1.43–1.22 (m, 7H), 1.22–1.06 (m, 3H), 1.05–0.96 (m, 1H), 0.91 (d, $J = 6.3$ Hz, 3H), 0.90 (s, 3H), 0.63 (s, 3H).

^{13}C NMR (101 MHz, CDCl_3): δ 174.2, 136.3, 128.7 (2C), 128.3 (3C), 72.1, 68.6, 66.3, 55.9, 50.6, 42.8, 41.6, 40.0, 39.8, 39.5, 35.4 (2C), 35.2, 34.7, 33.0, 31.4, 31.1, 30.8, 28.3, 23.8, 22.9, 20.7, 18.4, 11.9.

HRMS (ESI) calcd. for $\text{C}_{31}\text{H}_{45}\text{O}_4[\text{M} - \text{H}]^-$: 481.3318, found: 481.3320.

(Benzyl chenodeoxycholate-3-) benzyl succinate (30) was prepared following the same procedure as shown in the synthesis of **5** and was obtained in 90% isolated yield as a colorless oil.

^1H NMR (400 MHz, CDCl_3): δ 7.46–7.28 (m, 10H), 5.20–5.05 (m, 4H), 4.68–4.51 (m, 1H), 3.84 (d, $J = 2.0$ Hz, 1H), 2.74–2.54 (m, 4H), 2.48–2.22 (m, 3H), 2.01–1.77 (m, 6H), 1.74–1.64 (m, 2H), 1.63–1.56 (m, 1H), 1.52–1.24 (m, 11H), 1.23–1.14 (m, 2H), 1.13–1.08 (m, 1H), 1.07–0.97 (m, 1H), 0.92 (d, $J = 6.4$ Hz, 3H), 0.91 (s, 3H), 0.64 (s, 3H).

^{13}C NMR (101 MHz, CDCl_3): δ 174.2, 172.3, 171.9, 136.2, 136.0, 128.6 (4C), 128.3 (6C), 74.9, 68.5, 66.6, 66.2, 55.9, 50.5, 42.8, 41.3, 39.7, 39.5, 35.4, 35.3, 35.2, 35.1, 34.5, 32.9, 31.4, 31.1, 29.7, 29.4, 28.2, 26.8, 23.8, 22.8, 20.7, 18.4, 11.9.

HRMS (ESI) calcd. for $\text{C}_{43}\text{H}_{57}\text{O}_9[\text{M} + \text{HCO}_2]^-$: 717.4003, found: 717.4009.

3-sucCDCA (31) was prepared following the same procedure as shown in the synthesis of **6** and was obtained in 76% isolated yield as a white amorphous solid.

^1H NMR (400 MHz, CD_3OD): δ 4.61–4.49 (m, 1H), 3.80 (d, $J = 1.3$ Hz, 1H), 2.62–2.48 (m, 4H), 2.47–2.28 (m, 2H), 2.26–2.14 (m, 1H), 2.04–1.64 (m, 9H), 1.58–1.40 (m, 7H), 1.39–1.01 (m, 7H), 0.97 (d, $J = 6.7$ Hz, 3H), 0.95 (s, 3H), 0.70 (s, 3H).

^{13}C NMR (101 MHz, CD_3OD): δ 178.2, 176.0, 173.9, 76.4, 69.0, 57.3, 51.5, 43.7, 42.9, 41.0, 40.7, 36.7, 36.4, 36.2, 36.1, 35.7, 34.0, 32.3, 32.0, 30.5, 29.8, 29.2, 27.8, 24.6, 23.3, 21.8, 18.8, 12.2.

HRMS (ESI) calcd. for $\text{C}_{28}\text{H}_{43}\text{O}_7[\text{M} - \text{H}]^-$: 491.3009, found: 491.3015.

3-sucLCA (33) was prepared following the same procedure as shown in the synthesis of **3** and was obtained in 96% isolated yield as a white amorphous solid.

^1H NMR (400 MHz, CD_3OD): δ 4.75–4.65 (m, 1H), 2.71–2.43 (m, 4H), 2.41–2.27 (m, 1H), 2.26–2.12 (m, 1H), 2.08–1.98 (m, 1H), 1.98–1.73 (m, 5H), 1.72–1.58 (m, 2H), 1.57–1.37 (m, 8H), 1.37–1.00 (m, 10H), 1.00–0.87 (m, 6H), 0.70 (s, 3H).

^{13}C NMR (101 MHz, CD_3OD): δ 178.2, 176.1, 173.8, 76.0, 57.8, 57.4, 43.9, 43.3, 41.8, 41.5, 37.2, 36.7, 36.1, 35.7, 33.3, 32.3, 32.0, 30.5, 29.8, 29.2, 28.2, 27.6 (2C), 25.3, 23.8, 22.0, 18.8, 12.5.

HRMS (ESI) calcd. for $\text{C}_{28}\text{H}_{43}\text{O}_6[\text{M} - \text{H}]^-$: 475.3060, found: 475.3058.

Targeted metabolomics analysis

Quantification of different acylated CAs was performed by a liquid chromatography-tandem mass spectrometry (LC-MS/MS) system that composed of a Acquity Ultra-Performance Liquid Chromatography (UPLC) system (Waters Corporation, Milford, USA) coupled to a Sciex 5500 triple quadrupole linear ion trap mass spectrometer (AB SCIEX, Framingham, MA, USA). Chromatographic separation was employed with an ACQUITY UPLC CSH C18 column (2.1 × 100 mm, 1.7 μm , Waters) at 40°C and a flow rate of 0.25 mL/min. The injection volume was 5 μL , Mobile phase A was 0.1% FA in water and mobile phase B was 0.1% FA in acetonitrile. All analytes were detected in negative ion multiple reaction monitoring (MRM) mode. Chromatographic separation was performed using a linear gradient as follows: 0–1 min, 40% B; 1–6 min, 40–100% B; 6–7 min, 100% B; 7–8 min, 100–40% B. The detailed MRM parameters was listed in Table S4. The standard curves with internal calibration were constructed using mixed working standard solutions with

gradient dilution (0.1, 1, 10, 100, 1000 nM), CA-d4 (0.2 μ M) was used as internal standard for each concentration. Operational control of the LC-MS/MS was performed with Analyst version 1.6.2, and quantitative analysis was performed using MultiQuant software (version 3.0.1).

For the quantification of acylated CAs from different biological samples (intestine, intestinal contents, feces), accurately weighed samples (20 mg) were placed in tube and add 400 μ L of ice-cold methanol containing 0.2 μ M internal standards. The samples were thoroughly homogenized with a tissue homogenizer. Samples were subsequently ultrasonic extraction for 20 min for metabolites extraction. All samples were subsequently centrifuged at 14,000 rpm for 20 min at 4°C. The supernatant was filtered through a membrane filter (pore size, 0.22 μ m) for LC-MS/MS analysis.

For the quantification of acylated CAs from plasma or culture supernatant from bacteria, samples were diluted with ice-cold methanol (1:4) containing 0.2 μ M internal standards (CA-d4). Then the samples were vortex for 10 min and were incubated at –20°C for 1 h. All samples were subsequently centrifuged at 14,000 rpm for 20 min at 4°C. The supernatant was filtered through a membrane filter (pore size, 0.22 μ m) for LC-MS/MS analysis.

For analysis of 3-sucDCA and 3-sucDCA, chromatographic separation was achieved by reverse-phase C30 column (2.1 \times 150 mm, 3 μ m, ChromCore) with gradient elution. The solvent A is 0.1% FA in water, and the solvent B is 0.1% FA in ACN. Samples were eluted using a linear gradient: 0–0.5 min, 30% B; 0.5–13 min, 30–100% B; 13–14 min, 100–30% B; 14–15 min, 30% B.

For the quantification of core metabolites related to amino sugar metabolism, *A. muciniphila* JC032 were cultured in BHI media supplemented with 3-sucCA (10 μ M) or PBS control, then grew anaerobically for 48 h. The cultured samples were diluted with ice-cold methanol (1:4), which were lysed by sonication and then centrifuged at 14,000 rpm for 20 min at 4°C. The supernatant was filtered through a membrane filter (pore size, 0.22 μ m) for LC-MS/MS analysis.

Quantification of peptidoglycan

The peptidoglycan content of *Akkermansia muciniphila* JC032 was determined using the bacterial peptidoglycan ELISA Kit according to the manufacturer's instructions. Briefly, *A. muciniphila* JC032 were cultured in BHI media supplemented with 3-sucCA (10 μ M) or PBS control, then grew anaerobically for 48 h. The bacteria were harvested through centrifugation at 14,000 rpm for 20 min, which was resuspended in 500 μ L PBS buffer and lysed by sonification. The samples were used for the quantification of peptidoglycan.

Stability of 3-sucCA

Stool-derived *ex vivo* communities in mGAM (10 mL) was added with 20 μ M 3-sucCA before incubation, and GCA was used as control. Then the two bile acids were incubated for continuous 3 days, and samples were collected at appropriate time. The level of 3-sucCA at different time points was analyzed by LC-MS/MS.

16S rRNA gene amplicon sequencing and analyses

DNA for 16S rRNA amplicon sequencing was extracted from *ex vivo* human fecal culture or mice feces and subjected to 16S rRNA gene high-throughput sequencing using the Illumina NovaSeq PE250 platform. The 16S rRNA gene V3-V4 region was amplified using the primers F341 (CCTACGGGGRSGCAGCAG) and R806 (GGACTACVVGGGTATCTAATC). The quality of the data obtained from Illumina NovaSeq sequencing was assessed using FastQC and analyzed using the DADA2 software package. The DADA2 output sequence table was converted to biom format using biomformat software and this data used to assess sequence variant abundances, producing counts for each sample. Full analysis workflows were performed by MicrobiomeAnalyst (<https://www.microbiomeanalyst.ca/>).

Metagenomic sequencing and analyses

Metagenomic sequencing was performed as previously described⁶⁹. Sequencing libraries were established by the Ultra DNA Library Prep Kit for Illumina; the manufacturer's recommendations and index codes were adopted to attribute sequences to each sample. The fragmented DNA ends were repaired, polyA-tailed, and ligated with a sequencing adaptor for Illumina sequencing. PCR amplification and purification (AMPure XP system) were performed. DNA concentrations were measured by a Qubit DNA Assay Kit in a Qubit 2.0 fluorometer and diluted to 2 ng/ μ L. The insert size of the library was assessed using an Agilent Bioanalyzer 2100 system. qPCR was performed to ensure an accurate concentration (> 3 nM) of the library. The clustering of the index-coded samples was performed on a cBot Cluster Generation System using a HiSeq 4000 PE Cluster Kit according to the manufacturer's instructions. After cluster generation, the library preparations were sequenced on an Illumina HiSeq 4000 platform, and 150-bp paired-end reads were generated.

bioBakery tools⁷⁰ were used to process metagenomic reads (in fastq format) by trimming the reads to PHRED quality 30 and removing Illumina adapters. Following trimming, the KneadData integrated Bowtie2 tool⁷¹ was used to remove reads that aligned to the human genome. Subsequently, taxonomic composition of metagenomes was profiled by MetaPhlAn2⁷² tool using the MetaPhlAn database of mpa_v30_CHOCOPhAn_201901. All the parameters of MetaPhlAn utilized default settings. The α -diversity was estimated based on the gene profile of each sample according to the ACE, Chao1 and Shannon indices. The LEfSe analysis was performed with Galaxy.⁷³

Phylogenetic analyses

The phylogenetic tree of stool isolates was calculated by maximum likelihood method using IQ-TREE software,⁷⁴ with the 16S sequences of the stool isolates. The diagram was visualized using iTOL.⁷⁵

Growth curves of tested strains

Fresh strains (2×10^7 CFU/mL) at 0.2 mL were inoculated anaerobically into freshly prepared medium (10 mL) containing control or compounds at different concentrations, then growth anaerobically for 48 h. The medium for bacteria growth was listed in Table S2. The bacterial growth kinetics were analyzed using a Spectra Max 190 microplate reader (Molecular Devices Inc.) by measuring the optical density (OD₆₀₀).

Biolog microplate analysis

The Biolog AN MicroPlate test panel contains 94 wells with different carbon compounds and one well with water (control). Iodonitro-tetrazolium (INT) violet was used as a redox dye to colorimetrically measure the mitochondrial respiration activity resulting from the oxidation of metabolizable carbon sources. The oxidation of succinate to fumarate causes the irreversible reduction of INT to a red-colored formazan dye. The absorbance reading 750 nm measures the turbidity.⁷⁶ Bacteria resuspended in inoculating fluid (Biolog) were added to AN MicroPlate (Biolog) with distinct carbon sources as per manufacturer's instruction. Plates were incubated in GasPak EZ anaerobic pouch system (BD) at 37°C. Growth was measured colorimetrically by microplate reader (BMG LABTECH) after 48 h incubation.

Heterologous expression and activity of acyltransferase candidates

The candidates were amplified from genome of *B. uniformis* JC066 with primers listed in Table S5 using Phanta Super-Fidelity DNA Polymerase (Vazyme) and cloned into pET28a. Confirmed plasmids were transformed into *E. coli* BL21 (DE3) strains. Single colony for each aimed gene was incubated in 5 mL LB medium containing 50 µg/mL kanamycin at 37°C, 220 rpm overnight. And then 40 µL of the cultures were inoculated respectively into 4 mL fresh LB medium with 50 µg/mL kanamycin, 1 µM CA, 1 µM succinic acid. When the OD₆₀₀ reached 0.6, 0.25 mM isopropyl β-*d*-1-thiogalactopyranoside (IPTG) was added to induce the protein expression. Cultures were cultured for additional 16 h at 25°C before being harvested for detection of 3-sucCA formation by LC-MS.

Activity-guided enzyme purification

In general, 2 L culture of *B. uniformis* was lysed by ultrasonication to obtain the cell lysate, in which saturated ammonium sulfate (AS) solution was added for preparation of AS fraction. The crude protein was loaded on a fast protein liquid chromatography (FPLC), including hydrophobic interaction chromatography (HIC) and ion exchange chromatography (IEC) for purification. Finally, 118 candidate proteins were confirmed by proteomic mass spectrometry of bioactive fractions of FPLC.

Enzymatic assays during the activity-guided enzyme purification were performed following the same procedures. A reaction mixture containing 2 mM CA and 2 mM succinic acid as substrates supplemented with 10 µg protein of each fraction in 50 mM PB buffer (pH 7.0) in a final volume of 100 µL was incubated for 30 min at 37°C. The reactions were terminated by the addition of 300 µL ice-cold methanol containing 0.2 µM internal standards (CA-*d*4). The samples were vortexed for 10 min and were incubated at -20°C for 1 h. All samples were subsequently centrifuged at 12,000 × *g* for 20 min at 4°C. The supernatant was filtered through a membrane filter (pore size, 0.22 µm) for LC-MS/MS analysis. Each fraction was quantified by BCA Protein Assay Kit (Thermo Scientific). All samples were prepared in triplicate.

All procedures described below were carried out at 4°C. 2 L fresh culture of the strain *B. uniformis* was incubated for 2 days to reach the stationary phase before harvested by centrifugation at 4°C. The pellets were resuspended in cold PBS supplemented with 1 mM phenylmethanesulfonyl fluoride (PMSF) as protease inhibitor and lysed by ultrasonication. The lysate was clarified by centrifugation at 9,000 × *g* for 30 min at 4°C.

The saturated ammonium sulfate (AS) solution was added into the remained lysate at a ratio of 4:1 (v/v) to 80% saturation. The mixture was stirred softly at 4°C overnight before centrifuging at 16,000 × *g* for 30 min and the pellets were suspended in the storage buffer (50 mM Tris-HCl, 20% glycerol, pH 7.5) as 80% AS fraction for long-time storage and enzymatic assays.

Hydrophobic interaction chromatography (HIC): A Skillpak 5 mL TOYOPEARL Phenyl-650M (Tosoh Bioscience) was equilibrated with 10 column volumes (CV) of 50 mM sodium phosphate buffer, pH 7.0, which contained 1.5 M AS. The 80% AS fraction obtained as above was buffer-changed to equilibrium liquid (50 mM PB, 1.5 M AS, pH 7.0) and loaded on the equilibrated column at a flow rate of 1.3 mL/min via a fast protein liquid chromatography (FPLC) system of ÄKTA pure. A linear gradient to 50 mM sodium phosphate buffer, pH 7.0, from 0% to 100% (v/v) was applied to protein separation within 40 min at a flow rate of 1.3 mL/min while 7 fractions of every 10 mL were collected. Each fraction was concentrated and buffer changed to storage buffer using Amicon Ultra-10K (Millipore) for long-time storage and enzymatic assays.

Ion-exchange chromatography (IEC): A Skillpak 5 mL TOYOPEARL Gigacap Q-650M (Tosoh Bioscience) was equilibrated with 10 column volumes (CV) of 20 mM Tris-HCl, pH 8.5. The active fractions of HIC were buffer-changed into 20 mM Tris-HCl, pH 8.5, and loaded on the equilibrated column at a flow rate of 1 mL/min via FPLC. A linear gradient to 20 mM Tris-HCl,

pH 8.5, which contained 1 M NaCl, from 0% to 100% (v/v) was applied for protein elution within 40 min at a flow rate of 1 mL/min while fractions of every 2 mL were collected. Each fraction was concentrated and buffer-changed to storage buffer for storage or analysis.

Proteomic mass spectrometry analysis

For the preparation of fractions digestion, 10 μ g protein of each fraction, 12.5 μ L of Tris-HCl buffer (pH 8.8), 21 μ L of 30% acrylamide solution, 0.5 μ L 10% SDS and 5 μ L of 10% ammonium persulfate were added to a 1.5 mL Eppendorf tube. The mixture was vortexed for 0.5 min. Then 0.2 μ L TEMED was added.

The gel was fixed with 50% methanol, 12% acetic acid for 30 min at room temperature and cut into small pieces. The gel pieces were dehydrated with ACN and reduced with 10 mM TCEP for 10 min at 67°C, then alkylated with 50 mM iodoacetamide at room temperature in the dark for 45 min. Gel pieces were washed with 50% ACN/50 mM NH_4HCO_3 buffer and dehydrated with ACN. The gel was rehydrated with 100 μ L of 10 ng/ μ L trypsin in 25 mM NH_4HCO_3 buffer at 4°C for 2 h and then incubated at 37°C overnight. After enzyme digestion, the peptides mixture was extracted with ACN/5% FA (2:1) twice and lyophilized to dryness.

nano-LC-MS/MS: The digested peptides were loaded on a C18 pre-column loaded on a C18-A1 pre-column (100 μ m \times 2 cm, Thermo Scientific, No. SC100) and subsequently separated on the analytical column (C18-A2, 75 μ m \times 10 cm, Thermo Scientific, No. SC 200) using an Easy-LC nano-HPLC (Thermo Scientific). For a gradient separation, $\text{H}_2\text{O}/\text{FA}$ (99.9:0.1) was used as the mobile phase A while ACN/FA (99.9:0.1) was mobile phase B. At first, a gradient of 5%–32% solvent B for 68 min, 30%–45% solvent B for 9 min, then 50%–100% solvent B for 10 min, and held at 100% solvent B for 3 min. The flow rate was 300 nL/min. Mass spectrometric analysis was performed using an LTQ Orbitrap Velos pro (Thermo Scientific, Bremen, Germany). The spray voltage was operated at 2.5 kV with the ion transfer capillary at 250°C. The MS/MS spectra were obtained in a data-dependent collision induced dissociation (CID) mode, and the full MS was acquired from m/z 350 to 2000 with resolution 60,000. The top 15 most intense ions were selected to for MS/MS. Parameters for acquiring CID were as follows: activation time = 10 ms, normalized energy = 35, Q-activation = 0.25. The dynamic exclusion was set as follows: repeat count 1, duration 30 s, exclusion list size 500 and an exclusion duration 30 s.

Raw files were analyzed using MaxQuant software (version 1.5.8.0, <http://www.maxquant.org/>). MS/MS spectra were searched against UniProt *Bacteroides uniformis* database using the Andromeda search engine. The search parameters were set as follows: fixed modification of cysteine residues, variable modification of methionine oxidation, and full trypsin cleavage, at most two missed tryptic cleavage sites. False discovery rates were calculated by decoy database searching.

Construction of *B. uniformis* knockout strain

The construction of mutant was performed using inducible CRISPR-Cas system according to the protocol described previously.⁷⁷ During the process, the strain *B. uniformis* JC066 was used to generate *bas-suc* knockout strain. Briefly, the whole experimental process contained 4 steps: plasmid construction, conjugation and selection, CRISPR-Cas induction and identification of mutants, and plasmid curing. Firstly, the *Bacteroides-E. coli* shuttle plasmid was constructed using Gibson assembly. The sgRNA which targeted *bas-suc* was designed as 'GGAAGCAAGCAGTTGCTCCCGGC' in the website: <https://benchling.com/>. The 1 kb DNA fragments, which were upstream and downstream homology arms of the target gene, sgRNA fragment and linearization plasmid of pB041 were amplified by PCR using DNA polymerase with primer pairs listed in Table S5 and assembled by MultiF Seamless Assembly Mix (Ab-clonal). The resulting construct was transformed into *E. coli* S17-1 λ pir and confirmed by sequencing. Secondly, the plasmid was introduced into *B. uniformis* JC066 via *E. coli-Bacteroides* conjugation. After 24 h anaerobic incubation at 37°C, the transconjugants were selected on gentamicin (200 μ g/mL) and erythromycin (25 μ g/mL) plates. Thirdly, the *B. uniformis* colonies which were proved to contain the constructed plasmid by PCR were incubated anaerobically in GAM medium with gentamicin and erythromycin overnight and diluted 1:100 into GAM medium containing gentamicin (200 μ g/mL), erythromycin (25 μ g/mL) and aTc (100 ng/mL) to induce the editing of genome for 24 h. Cultures were plated on GAM-aTc plate and incubated anaerobically for 2 days. Colonies were picked and screened by PCR using the diagnostic primers listed in Table S5, and confirmed by DNA sequencing to ensure that the candidates had lost the genes. Lastly, the mutants were passaged for more than 5 times without antibiotics for plasmid curing.

Heterologous expression and purification of BAS-suc

The signal peptide free codon-optimized DNA sequence of *bas-suc* was synthesized by Azenta Life Science, cloned into pET28a expression vectors with a C-terminal 6-histidine affinity tag. The expression and purification of BAS-suc were carried out according to the following protocol. The confirmed plasmid was transformed into *E. coli* BL21 (DE3) strains and single colony was picked and grown at 37°C in 10 mL of LB with kanamycin overnight. The seed culture was then diluted 1:100 into 2 L LB containing kanamycin and cultured at 37°C, 220 rpm to reach an appropriate optical density at OD_{600} of 0.6, at which time protein expression was induced by the addition of 0.2 mM IPTG. Then the culture was incubated at 20°C for additional 16 h before harvested by centrifugation at 5,000 \times g for 10 min at 4°C. The pellets were resuspended in lysis buffer (50 mM Tris-HCl, 300 mM NaCl, 20 mM imidazole, pH 8.0) supplemented with 1 mM protease inhibitor PMSF and lysed by ultrasonication. The lysate was clarified by centrifugation at 12,000 \times g for 30 min at 4°C. And then the supernatant was applied to a pre-equilibrated Ni-NTA (5 mL HisTrap HP, Cytiva) column via an FPLC system. After washed with lysis buffer, the captured protein was eluted by elution buffer (50 mM Tris-HCl, 300 mM NaCl,

500 mM imidazole, pH 8.0). The elution peak was confirmed by SDS-PAGE and stored into storage buffer (50 mM Tris-HCl, 20% glycerol, pH 7.5) by centrifugal ultrafiltration using an Amicon Ultra-10K tube (Millipore). Finally, BAS-suc concentration was determined by BCA Protein Assay Kit (Thermo Scientific).

Activity assay, kinetics analyses and substrate scope of BAS-suc

In catalytic activity assays of BAS-suc, 2 μ g purified enzyme was added to 100 μ L reaction mixture which contained 50 mM PB buffer (pH 7.0) and required substrates (2 mM CA, 2 mM succinic acid) and incubated at 37°C for 30 min. The reactions were quenched with the addition of 300 μ L ice-cold methanol containing 0.2 μ M internal standards (CA-d4). The samples were vortexed for 10 min and were incubated at -20°C for 1 h. All samples were subsequently centrifuged at 12,000 \times g for 20 min at 4°C. The supernatant was filtered through a membrane filter (pore size, 0.22 μ m) for LC-MS/MS analysis. Besides, corresponding negative controls were undergone in the same conditions except for boiled or proteinase K treated protein. All samples were prepared in triplicate for analysis.

For kinetics analyses of BAS-suc, catalytic activity assays were conducted with a series of substrates concentrations. Kinetic studies of the enzyme were performed by changing the CA concentrations from 0.1 mM to 4 mM with the saturating succinic acid (6 mM) and 2 μ g purified enzyme in the reaction buffer (50 mM PB, pH 7.0) in a total volume of 100 μ L for 30 s at 37°C. The catalytic reactions were stopped by addition of 300 μ L methanol and prepared for LC-MS/MS.

For investigation for the substrate scope of BAS-suc, various substrates were applied to the assay to test whether BAS-suc possessed promiscuous catalytic activity. 2 mM of specific substrates (DCA, CDCA, LCA, and TCA) and 2 mM of specific SFCAs (acetic acid, propionic acid, butyric acid, malonic acid) were added into reaction buffer supplemented with 2 μ g enzyme and incubated for 30 min at 37°C. Samples were prepared in triplicate and sent for LC-MS/MS analysis.

Surface plasmon resonance (SPR)

The SPR assay based on the phenomenon in which incident light is strongly absorbed by the surface plasma at the incident angle and incident wavelength, resulting in a resonance spectrum. Changes in the molecular mass of the biomarker bound to the sensor surface shift the resonance wavelength or resonance angle, enabling quantitative real-time monitoring of the biomarker, and widely used in the interaction of small molecules with proteins, due to its sensitivity to changes in surface refractive index for the label-free, highly sensitive and rapid detection of biomarkers. Firstly, the DNA sequence of Amuc-NagB was amplified from genome of *Akkermansia muciniphila* JC032 and cloned into pET-28a and the purified protein was obtained as described above. SPR experiments were performed at 25°C using a Biacore T200 instrument (GE Healthcare). The purified protein Amuc-NagB was immobilized onto CM5 sensor chips. Serial dilutions of different compounds were injected, ranging in concentrations from 0.39 μ M to 12.5 μ M. Data were analyzed using the Biacore T200 evaluation software (GE Healthcare) and indicative K_D and R_{max} values were obtained by nonlinear curve fitting of a 1:1 Langmuir interaction model.

Luciferase reporter gene assays

The luciferase reporter gene assays of FXR and TGR5 were carried out according to the protocol described below. HEK293 cells were co-transfected with human FXR expression vector, human ASBT expression vector, human RXR expression vector, pGL4-Shp-TK firefly luciferase construct and a Renilla luciferase control vector for FXR luciferase assay, or pCMVSPORT6/hTGR5 and cAMP response element-driven luciferase reporter plasmids for TGR5 luciferase assay. After 24 h post-transfection, the cells were exposed to different concentrations of various bile acids for 16 h. Luciferase assays were performed using the dual-luciferase assay system for FXR or assay buffer with coelenterazine for TGR5.

TR-FRET FXR coactivator recruitment assay

TR-FRET FXR coactivator recruitment assay was carried out according to the manufacturer's instruction of the commercial TR-FRET FXR coactivator recruitment assay kit.

Histological analysis

For histological analysis of liver, after mice sacrifice, liver tissues of mice were preserved in 10% formalin. Formalin-fixed paraffin-embedded liver tissue slides were subjected to hematoxylin and eosin (H&E) and Sirius red staining to assess lipid accumulation, inflammation severity and liver fibrosis degree, respectively. The frozen liver sections were stained with oil red O for visualizing lipid droplets. All the processes were according to standard protocols followed by microscopic examination. The histology scores were evaluated according to a reported MAFLD scoring system⁶⁷ and Sirius red positive areas were measured by ImageJ.

For histological analysis of colonic tissue, proximal colon segments were immediately removed and fixed in Carnoy's solution for 24 h at room temperature. Post Carnoy's fixation, the colon samples were routinely dehydrated, and then embedded in paraffin and thin sections (5 μ m) were cut and deposited on glass slides. The paraffin sections were stained with H&E or AB-PAS. Quantification of mucus thickness and colonic goblet cell density were identified by AB-PAS reaction of colon paraffin sections.

Measurement of MUC2 content

For measurement of MUC2 content, mice extra-luminal proximal colon tissues were frozen in liquid nitrogen and stored at -80°C. The colon tissues were homogenized in ice-cold RIPA buffer with protease and phosphatase inhibitors. After centrifugation, samples

were prepared for measurement of MUC2 content according to the manufacturer's instruction of MUC2 ELISA kit. Each sample was quantified by BCA Protein Assay Kit.

Desorption electrospray ionization mass spectrometry imaging (DESI-MSI)

Caecum of SPF mice was used for mass spectrometry imaging. The carboxymethylcellulose (CMC) solution (4% w/v) was prepared using distilled water (Milli-Q, 95°C) and with vigorous stirring. Caecum of SPF mice were embedded in a CMC solution and frozen at -80°C for further analysis. Samples were then cryosectioned to a 10 µm thickness for DESI-MS imaging. The 3-sucCA distribution was evaluated on a Xevo G2-XS ToF mass spectrometer with the DESI source in negative mode (Waters Corporation). The MS images were created by spraying N₂ gas-focused solvent stream directly onto the sample to produce the MS spectra from the surface, which was then rastered across the sample at regular intervals to build a 2D image. Image creation was performed using high-definition imaging 1.6 (HDI) software (Waters Corporation) with the following parameters: X and Y pixel size was 100 µm; raster speed was 400 µm/s; spray solvent was 49% methanol, 49% acetonitrile, and 2% H₂O delivered at 2 µL/min. The mass spectrometer was operated in negative-ion mode with 1.05 kV capillary voltage, and mass range *m/z* 50–1,200 Da. The DESI-MS/MS images were created for 3-sucCA (*m/z* 507.2962, -H adduct), and the collision energy is 30 eV. For the mass spectrometry imaging of 3-sucCA, we optimized the mass spectrometry conditions. The theoretical mass-to-charge ratio (*m/z*) of the 3-sucCA is 507.2963 Da (fragment ions: 407.2803 Da, 99.0088 Da) during negative ion mode, and the *m/z* of synthetic standards is measured at 507.2962 (fragment ions: 407.2804 Da, 99.0086 Da), indicating the high accuracy of mass spectrometry imaging method. Then we performed mass spectrometry imaging by DESI-MS/MS (507.2963 → 407.2803).

Quantitative PCR

For detection of gene expression (including intestinal barrier indicators and MAFLD related genes in the liver in mice), we used reverse transcription quantitative PCR (RT-qPCR). Mice extra-luminal colon and liver tissues were frozen in liquid nitrogen and stored at -80°C. A standard phenol-chloroform extraction was performed to isolate total RNA from frozen tissues with TRIzol reagent. cDNA was synthesized from 2 µg of total RNA with a Reverse Transcription Kit. RT-qPCR primer sequences were included in Table S5, the relative amount of each mRNA was calculated after normalization to the corresponding *Actb* gene, and the results are expressed as fold changes relative to the control group.

For detecting bacteria abundance, DNA was extracted from mouse fecal pellet using a CTAB-based DNA extraction protocol. For each sample, the fecal pellet was resuspended in 600 µL CTAB lysis buffer, then the samples were lysed using a tissue laser. The tubes were then vortexed and then incubated for 1 h at 65°C. Seven hundred microliters of chloroform-isoamyl alcohol (24:1) was added to each tube, and the tubes were vortexed and then centrifuged at 13,000 rpm for 15 min at room temperature. 500 µL of supernatant was transferred in a 1.5 mL tube, 330 µL isopropanol was added and inverted gently to mix. The genomic DNA was precipitated at 12000 × *g* for 2 min in a microcentrifuge. The DNA pellet was washed with 400 µL 70% ethanol twice and then subjected to dried vacuum centrifugation, upon which it was resuspended in 50 µL nuclease-free water. The genomic DNA of *A. muciniphila* and *B. uniformis* was extracted to establish a standard curve by RT-qPCR. KAPA SYBR FAST qPCR Kit was used for the reactions (2 × KAPA SYBR FAST qPCR Master Mix: 10 µL, 10 µM forward/reverse Primer: 0.4 µL, Template gDNA: 1 µL, Water to 20 µL). Reaction conditions were conducted at 95°C for 3 min followed by 40 cycles of [95°C for 3 s, 60°C for 20 s, 72°C for 20 s]. This was followed by one cycle of 65°C for 5 s and 95°C for holding to calculate the disassociation curves. Different concentration of gDNA was used as the template to get a corresponding Ct value.

Plasma endotoxin detection

Plasma endotoxin was quantified using an endpoint chromogenic limulus amoebocyte lysate (LAL) assays (Yeasen biotechnology Co., Ltd, China) according to the manufacturer's instructions. Briefly, 50 µL of plasma sample and known standards were placed in pyrogen-free tubes. These samples were incubated with 50 µL of LAL reagent for 8 min and 50 µL of chromogenic solution for 6 min at 37°C, respectively. After incubation, 250 µL of stop solution was added to each tube and then allowed to stand for 5 min at room temperature, the absorbance was then measured at 545 nm.

In vivo intestinal permeability assay

Mice were fasted for 6 h then orally administered fluorescein isothiocyanate (FITC)-dextran 4 kDa (400 mg/kg body weight). After 90 min, 100 µL of blood were collected from the tip of the tail vein. The blood was kept in the dark and centrifuged at 3000 × *g* for 10 min to collect plasma. Plasma aliquots (40 µL) were plated in 96-well plates and diluted to 200 µL with PBS (pH = 7.4). The fluorescence intensity in the plasma was measured at an excitation wavelength of 485 nm and an emission wavelength of 530 nm using a spectrofluorometer.

Construction of *E. coli* *nagB::Amuc-nagB ΔglmS*

A two-plasmid-mediated CRISPR-Cas9 genome editing system was used to edit genes in *E. coli*. The gRNAs which targeted *E. coli* Nissle 1917 *glmS* and *nagB* were designed using benchling according to the illustration (<https://benchling.com/>, gRNA for *glmS*: gggttcgccagactgtgaca; gRNA for *nagB*: gtactgggctgcccactgg). Then the gRNAs were integrated into the plasmid pEcgRNA by PCR to generate the plasmids pEcgRNA-*glmS* and pEcgRNA-*nagB*, respectively. Subsequently, the pEcCas plasmid was

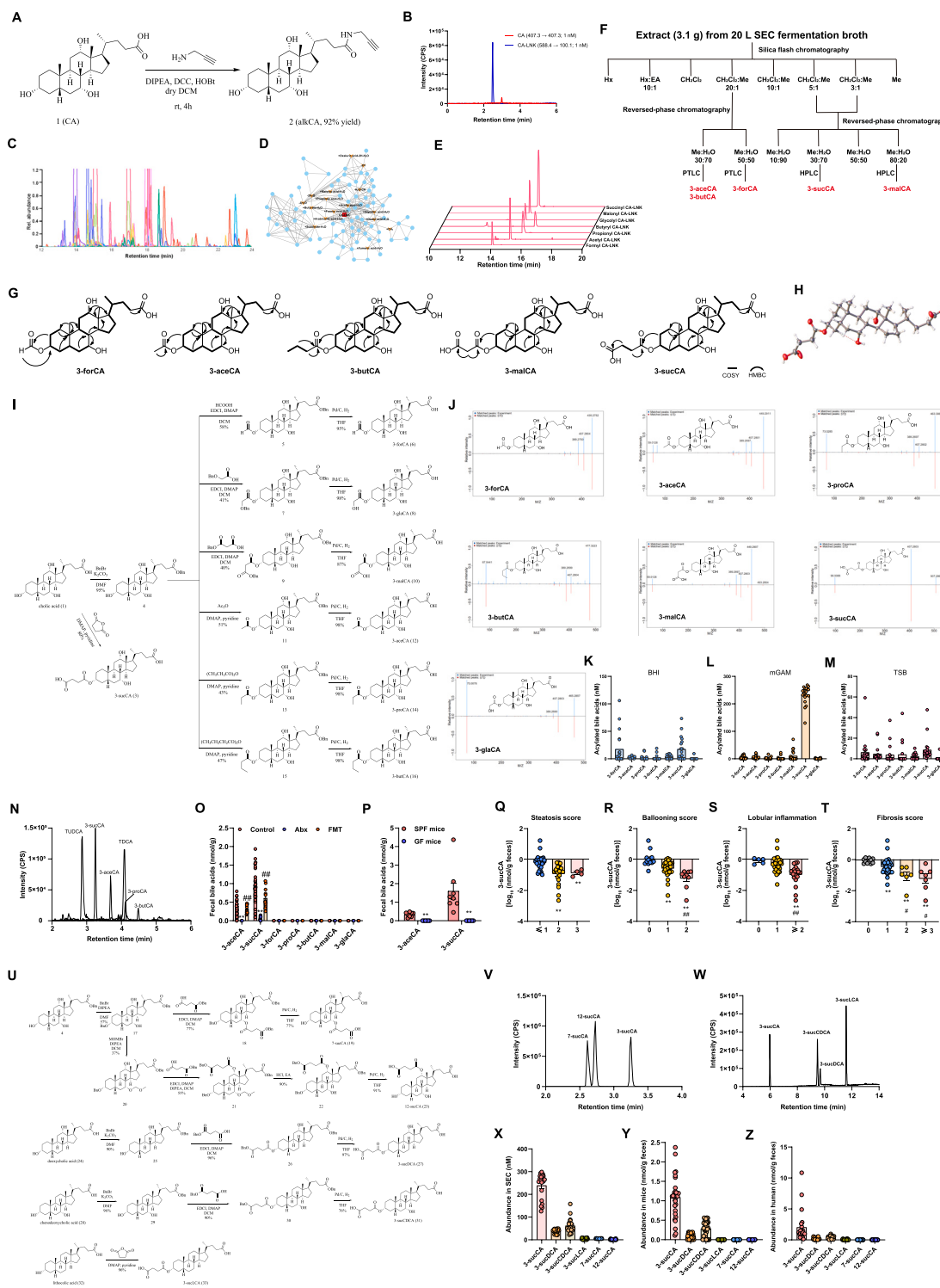
introduced into *E. coli* Nissle 1917 by electrotransformation to form strain *E. coli*-pEcCas. For knock out of the gene *glmS*, 500 bp up-homologous and down-homologous arms of *glmS* were acquired by PCR and ligated through overlapping PCR. Then 100 ng of pEcgRNA-*glmS* DNA and 400 ng of up-down homologous arm DNA were coelectroporated into competent cells of *E. coli*-pEcCas (10 mM arabinose was added to the culture for λ -Red system induction for competent cell preparation). Cells were recovered at 37°C for 1 h before being spread onto LB agar containing kanamycin (50 μ g/mL), spectinomycin (50 μ g/mL) and GlcNAc (5 g/L) and incubated overnight at 37°C. Transformants were identified by colony PCR and DNA sequencing. To eliminate the pEcgRNA-*glmS* plasmid, a colony of the edited clone containing both pEcCas and pEcgRNA-*glmS* was inoculated in 2 mL of LB medium containing rhamnose (10 mM), kanamycin (50 μ g/mL) and GlcNAc (5 g/L). The culture was incubated overnight with shaking at 220 rpm, and then diluted and spread on solid LB medium containing kanamycin (50 μ g/mL) and GlcNAc (5 g/L). The colonies that grew on kanamycin LB plates (GlcNAc, 5 g/L) after incubation overnight at 37°C were randomly picked and screened on LB plates (GlcNAc, 5 g/L) carrying kanamycin (50 μ g/mL) and spectinomycin (50 μ g/mL). The colonies that were sensitive to spectinomycin were cured of pEcgRNA-*glmS* and the clone was defined as *E. coli* Δ *glmS*.

Similarly, we replaced the native *nagB* with *A. muciniphila nagB* by two-plasmid-mediated CRISPR-Cas9 system. In brief, 500 bp up-homologous, down-homologous arms of *nagB* and *A. muciniphila nagB* were acquired by PCR and ligated through overlapping PCR. Then 100 ng of pEcgRNA-*nagB* DNA and 400 ng of up-Am-*nagB*-down repair template DNA were co-electroporated into competent cells of *E. coli* Δ *glmS*. Transformants were identified by colony PCR and DNA sequencing. After verification of *nagB* replacement, the plasmids pEcgRNA-*nagB* and pEcCas were eliminated successively and the final strain was defined as *E. coli* *nagB::Am-nagB* Δ *glmS*.

QUANTIFICATION AND STATISTICAL ANALYSIS

GraphPad Prism version 9.0 and SPSS version 27.0 were used for statistical analysis. The experimental data were shown as the mean \pm SEMs. The sample size was estimated based on previous experience, sample availability and previously reported studies.⁷⁸ No data were excluded from the data analysis. The normal distribution of the data was determined by the Shapiro-Wilk normality test. For statistical comparisons, Student's t test (between two groups) or one-way ANOVA (between multiple groups) with Tukey's (the same standard deviation) or with Dunnett's T3 test (different standard deviation) analysis was used to compare normally distributed variables. Nonnormally distributed data were compared by the Mann-Whitney *U* test (between two groups) or the Kruskal-Wallis test (between multiple groups). $p < 0.05$ was considered significant.

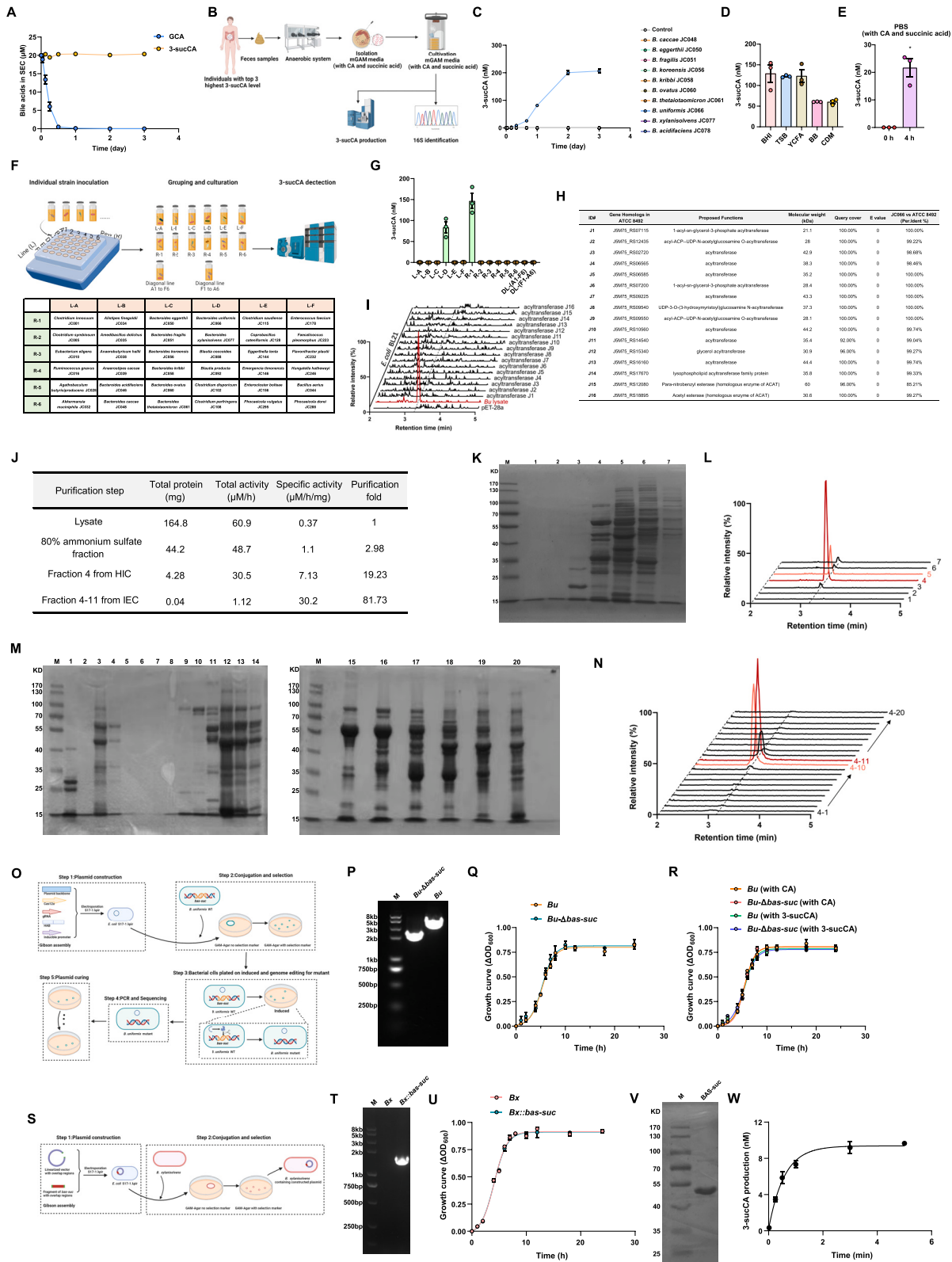
Supplemental figures



(legend on next page)

Figure S1. Click-chemistry-based enrichment strategy identifies 3-sucCA, and it is lower in patients with biopsy-proven MAFLD, related to Figure 1

- (A) The synthesis route of alkyne probe of CA (alkCA).
- (B) Extracted ion chromatograms of CA and CA-LNK with the same concentration shown differentiated mass spectrometry response.
- (C) Extracted ion chromatogram for the reporter ion m/z 100.0761 of a probe-enriched metabolites in the stool-derived *ex vivo* community (SEC) culture.
- (D) Molecular networks of probe-derived metabolites. Each node represents a clustered tandem mass spectrum, and connections between the nodes indicate relationships through the cosine score (cut-off minimum of 0.7).
- (E) Extracted ion chromatograms of presumptive CA-LNK-derived metabolites.
- (F) Flow diagram for fractionation of CA (0.1 mg/mL) incubated SECs. Acylated CAs are shown in red. Hx, hexane; EA, ethyl acetate; CH_2Cl_2 , dichloromethane; Me, methanol.
- (G) Key ^1H - ^1H COSY and HMBC correlations of isolated acylated CAs.
- (H) Thermal ellipsoid representation of 3-sucCA by X-ray crystallographic analysis.
- (I) The synthesis routes of CA derivatives, including 3-forCA, 3-aceCA, 3-proCA, 3-butCA, 3-malCA, 3-sucCA, and 3-glaCA.
- (J) Comparison of LC-MS/MS data of 3-acylated CAs from synthetic standards and bacteria cultured samples.
- (K–M) 3-acylated CAs production in the SEC anaerobic cultured in BHI (K), mGAM (L), and TSB media (M). $n = 20$ individuals.
- (N) Representative extracted ion chromatograms of 3-acylated CAs, TUDCA, and TDCA in fecal sample from healthy individual (separated by C18 column).
- (O) 8-week-old SPF mice were divided into three groups: drinking water control ($n = 30$ mice), antibiotics in the drinking water ($n = 12$ mice), or mice transplanted with SPF fecal microbiota after antibiotic treatment ($n = 12$ mice). The feces were collected for the quantification of fecal 3-acylated CAs.
- (P) Feces of 8-week-old SPF ($n = 8$ mice) and GF ($n = 6$ mice) mice were collected and detected for the concentrations of fecal 3-acylated CAs.
- (Q–T) Patients with MAFLD ($n = 55$), including MAFL ($n = 17$), borderline MASH ($n = 23$), and definite MASH ($n = 15$). Concentrations of 3-sucCA associated with steatosis score (Q), ballooning score (R), lobular inflammation (S), and histology scores of fibrosis stage (T) in patients with MAFLD.
- (U) The synthesis routes of 7-sucCA, 12-sucCA, 3-sucCDCA, 3-sucDCA, and 3-sucLCA.
- (V) Extracted ion chromatograms of sucCAs with substitution of hydroxyl group in different positions (separated by C18 column).
- (W) Extracted ion chromatograms of 3-sucCA, 3-sucCDCA, 3-sucDCA, and 3-sucLCA (separated by C30 column).
- (X–Z) Concentrations of 3-sucCA, 7-sucCA, 12-sucCA, 3-sucCDCA, 3-sucDCA, and 3-sucLCA in SECs (mGAM, $n = 20$) (X), SPF mice ($n = 30$) (Y), and human ($n = 23$) (Z). Points falling on X axis indicated that relevant bile acids were not detected.
- All data are presented as the means \pm SEMs. In (O) and (Q)–(T), the p values were determined by Kruskal-Wallis test followed by Dunn's post hoc test. In (P), the p values were determined by two-tailed Mann-Whitney U test. In (O), $**p < 0.01$ versus the control group, $##p < 0.01$ versus the Abx group. In (P), $**p < 0.01$ versus SPF mice group. In (Q), $**p < 0.01$ versus the steatosis score ≤ 1 group. In (R), $**p < 0.01$ versus the ballooning score = 0 group, $##p < 0.01$ versus the ballooning score = 1 group. In (S), $**p < 0.01$ versus the lobular inflammation = 0 group, $##p < 0.01$ versus the lobular inflammation = 1 group. In (T), $**p < 0.01$ versus the fibrosis score = 0 group, $\#p < 0.05$ versus the fibrosis score = 1 group.



(legend on next page)

Figure S2. *B. uniformis* produces 3-sucCA in a BAS-suc-dependent manner, related to Figures 2 and 3

- (A) Level of GCA and 3-sucCA during incubation in SECs for 3 days ($n = 3$ independent incubations).
- (B) Workflow for the isolation of cultured bacteria from human fecal samples and 3-sucCA-producing bacteria screen. For volunteers with top 3 highest 3-sucCA levels mentioned in Figure 1C, bacterial isolates were recovered and cultured anaerobically in mGAM (with additional 1 μ M CA and 1 μ M succinic acid) for 48 h and identified by 16S rRNA gene sequencing.
- (C) Production of 3-sucCA by different *Bacteroides* spp. for indicated time. Isolates were cultured anaerobically in mGAM (with additional 1 μ M CA and 1 μ M succinic acid) ($n = 3$ independent incubations).
- (D) Production of 3-sucCA by *B. uniformis* for 48 h cultured in different media anaerobically (with additional 1 μ M CA and 1 μ M succinic acid) ($n = 3$ independent incubations).
- (E) Production of 3-sucCA by *B. uniformis* for 4 h cultured in PBS buffer anaerobically (with additional 1 μ M CA and 1 μ M succinic acid) ($n = 3$ independent incubations).
- (F and G) Workflow for the 3-sucCA production ability of *B. uniformis* at multiple strain level (F). (G) The 3-sucCA concentration in different multiple strain groups cultured in mGAM anaerobically (with additional 1 μ M CA and 1 μ M succinic acid) ($n = 3$ independent incubations).
- (H) The information of acyltransferases encoded in *B. uniformis* genome. The sequence similarity for each protein between JC066 and ATCC 8492 was analyzed.
- (I) Representative extracted ion chromatogram of 3-sucCA production by heterologous expression of acyltransferases in *E. coli* BL21 and positive control of enzymatic assay conducted with *Bu* lysate.
- (J) Purification table of activity-guided enzyme purification. 10 μ g protein of each fraction was used to conduct the enzymatic assay for evaluation of specific activity and purification fold. The amount of total protein of each fraction was quantified.
- (K) Coomassie stained SDS-PAGE of protein fractions obtained by hydrophobic interaction chromatography (HIC).
- (L) Extracted ion chromatogram of 3-sucCA of the enzymatic assays catalyzed by different fractions of HIC. The fractions 4 and 5 showed activity on 3-sucCA production.
- (M) Coomassie stained SDS-PAGE of the separated sub-fractions of the fraction 4 using ion-exchange chromatography (IEC).
- (N) Extracted ion chromatogram of 3-sucCA of the enzymatic assays catalyzed by different sub-fractions of the fraction 4 using IEC. The fractions 4–10 and 4–11 showed high activity on 3-sucCA production.
- (O) Schematic diagram showing the workflow of BAS-suc deficient *B. uniformis* constructed by CRISPR-Cas genome editing.
- (P) PCR of counter-selected colonies for the deletion of BAS-suc in *B. uniformis* Δ *bas-suc*. Data presented individual PCR reactions.
- (Q and R) Both wild-type and BAS-suc deficient strains were grown anaerobically 24 h in mGAM (Q) or mGAM with CA (1 μ M) or 3-sucCA (1 μ M) (R).
- (S) Schematic representation showing the workflow of heterologous expression of *bas-suc* in *B. xylanisolvans*. The constructed plasmid was obtained by Gibson assembly of linearized vector and *bas-suc* fragment and electroporated into *E. coli* S17-1 λ pir. Conjugation was carried out with *B. xylanisolvans* and *E. coli* S17-1 λ pir before the strains *B. xylanisolvans* containing constructed plasmids were picked out for heterologous expression of *bas-suc*.
- (T) PCR of counter-selected colonies for the *Bx::bas-suc* strain. Data presented individual PCR reactions.
- (U) The growth curve of wild-type and BAS-suc overexpression *B. xylanisolvans* strains, grown anaerobically 24 h in mGAM (with additional 1 μ M CA and 1 μ M succinic acid).
- (V) Coomassie stained SDS-PAGE of the BAS-suc protein.
- (W) Time-dependence of 3-sucCA production by BAS-suc in the presence of CA and succinic acid.
- All data are presented as the means \pm SEMs. In (E), the p values were determined by two-tailed Mann-Whitney U test. * $p < 0.05$ versus the 0 h group. In (Q) and (U), the p values were determined by two-tailed Mann-Whitney U test. In (R), the p values were determined by Kruskal-Wallis test followed by Dunn's post hoc test.

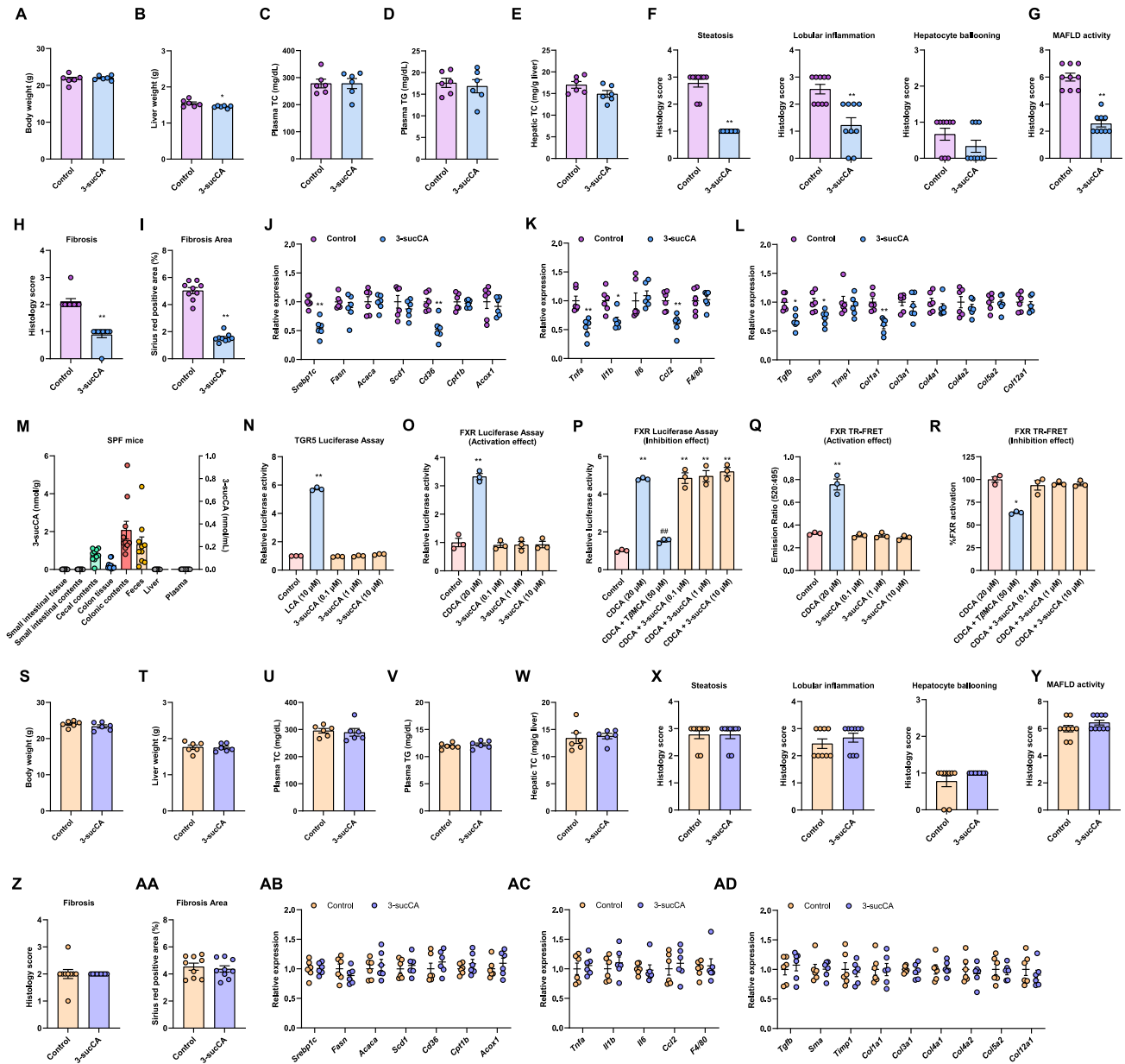


Figure S3. 3-sucCA alleviates MAFL-MASH progression in a gut-microbiota-dependent manner, related to Figure 4

(A–L) CDAA-HFD-fed SPF mice were treated with PBS (control) or 3-sucCA (10 mg/kg) 3 times per week for the last 3 weeks. $n = 6$ mice/group. (A) Body weight. (B) Liver weights. (C) Plasma TC content. (D) Plasma TG content. (E) Hepatic TC content. (F) Histology scores of steatosis, lobular inflammation, and hepatocyte ballooning. (G) MAFLD activity score. (H) Histology scores of fibrosis stage. (I) Sirius Red-positive area. Relative mRNA levels of genes related to hepatic lipid metabolism (J), inflammation (K), and fibrosis (L).

(M) 3-sucCA concentrations in small intestinal tissue and contents, cecal contents, colon tissue and contents, feces, liver, and plasma samples in the 8-week-old SPF mice. $n = 10$ mice/group.

(N) Luciferase activity was performed in HEK-293T cells that constructed for detecting TGR5 activity and were treated with negative control, LCA, and 3-sucCA at the indicated concentrations.

(O) Luciferase activity was detected in HEK-293T cells, which were treated with control, FXR agonist CDCA, and 3-sucCA at the indicated concentrations.

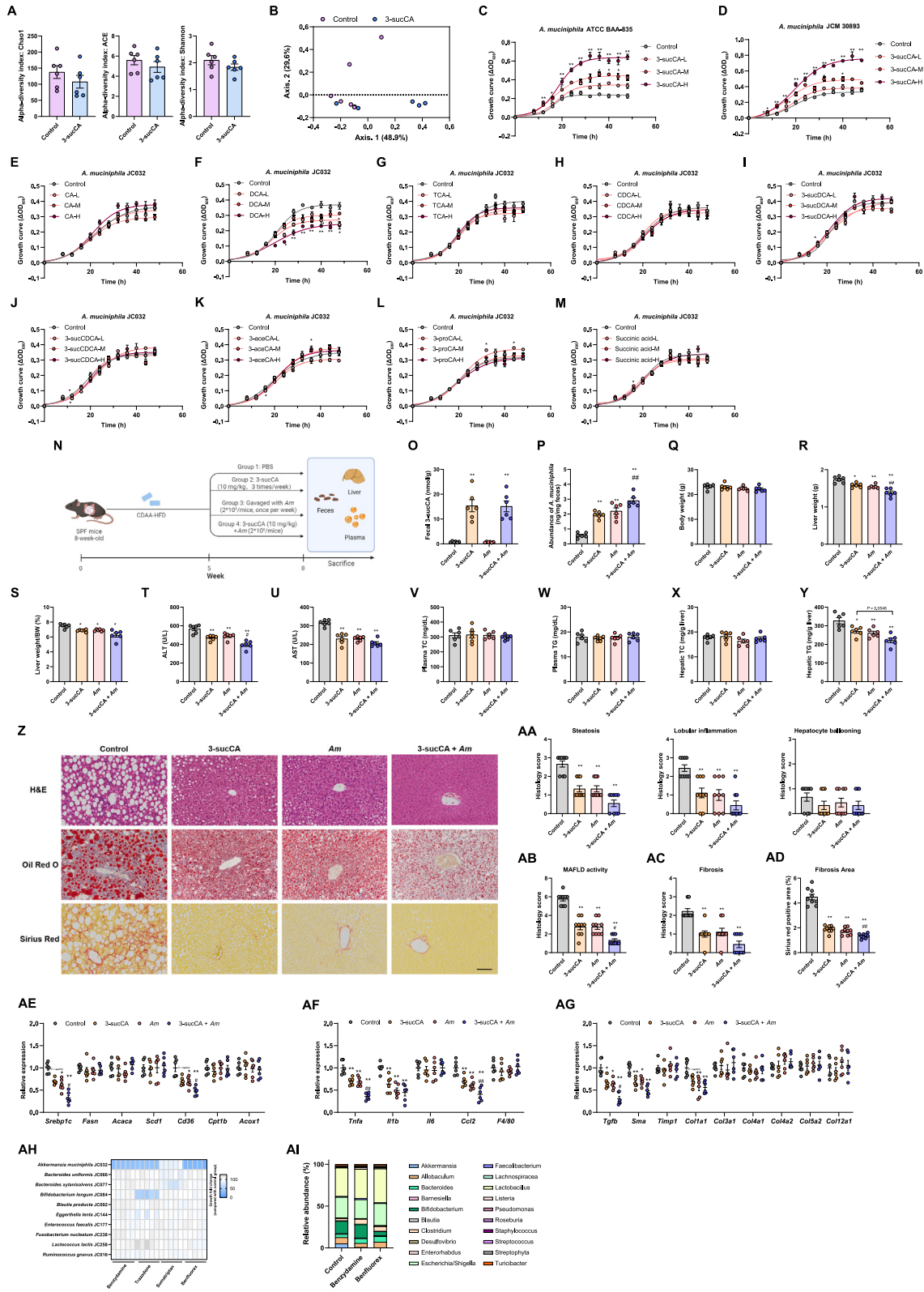
(P) Luciferase activity was detected in HEK-293T cells, which were treated with control, CDCA, and CDCA with different bile acids (3-sucCA, FXR antagonist T β MCA) at the indicated concentrations.

(Q and R) TR-FRET FXR coactivator recruitment assay to assess the effect of 3-sucCA on FXR. $n = 3$ replicates/treatment.

(S–AD) CDAA-HFD-fed GF mice were treated with PBS (control) or 3-sucCA (10 mg/kg) 3 times per week for the last 3 weeks. $n = 6$ mice/group. (S) Body weight. (T) Liver weights. (U) Plasma TC content. (V) Plasma TG content. (W) Hepatic TC content. (X) Histology scores of steatosis, lobular inflammation, and hepatocyte ballooning. (Y) MAFLD activity score. (Z) Histology scores of fibrosis stage. (AA) Sirius Red-positive area. Relative mRNA levels of genes related to hepatic lipid metabolism (AB), inflammation (AC), and fibrosis (AD).

(legend continued on next page)

All data are presented as the means \pm SEMs. In (A)–(E), (I), (J), (S)–(W), (AA), and (AD), the p values were determined by two-tailed Student's t test. In (F)–(H), (K), (L), (X)–(Z), (AB), and (AC), the p values were determined by two-tailed Mann-Whitney U test. In (N) and (R), the p values were determined by one-way ANOVA with Dunnett's T3 test. In (O)–(Q), the p values were determined by one-way ANOVA with Tukey's post hoc test. In (A)–(L), * p < 0.05 and ** p < 0.01 versus the control group. In (N), (O), and (Q), ** p < 0.01 versus the control group. In (P), ** p < 0.01 versus the control group, ## p < 0.01 versus the CDCA (20 μ M) group. In (R), * p < 0.05 versus the CDCA (20 μ M) group.



(legend on next page)

Figure S4. 3-sucCA alleviates MAFL-MASH progression by promoting the expansion of *A. muciniphila*, related to Figure 5

(A and B) CDAA-HFD-fed SPF mice were treated with PBS (control) or 3-sucCA (10 mg/kg) 3 times per week for the last 3 weeks. The fecal samples in the endpoint were collected and performed 16S rRNA gene sequencing. $n = 6$ mice/group. (A) Alpha-diversity indexes of the gut microbiota between the control and 3-sucCA groups as indicated by the Chao1, ACE, and Shannon indexes. (B) Principal coordinates analysis (PCoA) of the gut microbiota between the control and 3-sucCA groups using Jensen-Shannon Divergence distance.

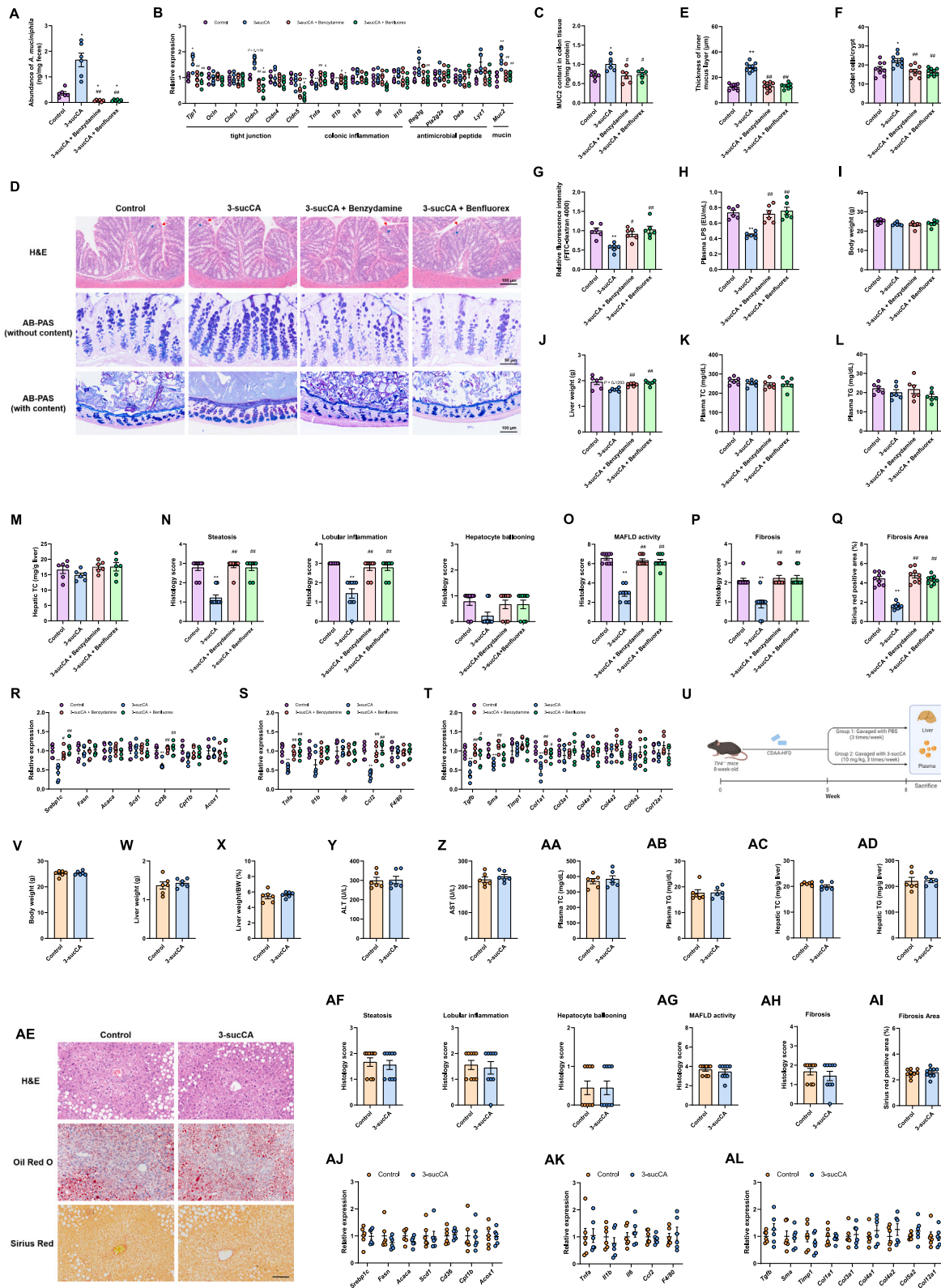
(C and D) The growth curve of the *A. muciniphila* ATCC BAA-835 (C) and *A. muciniphila* JCM 30893 (D) cultured in BHI media supplemented with 3-sucCA at different concentrations (L, M, and H indicate 1 μ M, 10 μ M, and 50 μ M, respectively) or PBS control anaerobically for 48 h. $n = 3$ biological replicates.

(E–M) The growth curve of the *A. muciniphila* JC032 cultured in BHI media supplemented with (E) CA, (F) DCA, (G) TCA, (H) CDCA, (I) 3-sucDCA, (J) 3-sucCDCA, (K) 3-aceCA, (L) 3-proCA, and (M) succinic acid at different concentrations or PBS control anaerobically for 48 h. $n = 3$ biological replicates. (For CA, CDCA, DCA, and succinic acid, L, M, and H indicate 10 μ M, 100 μ M, and 1 mM, respectively; for TCA and acylated bile acids, L, M, and H indicate 1 μ M, 10 μ M, and 50 μ M, respectively).

(N–AG) CDAA-HFD-fed SPF mice were treated with PBS (control), 3-sucCA (10 mg/kg), *Am*, or *Am* plus 3-sucCA (10 mg/kg) for the last 3 weeks. Mice were gavaged with 3-sucCA (10 mg/kg) 3 times per week and *Am* 1 time per week. $n = 6$ mice/group. (N) Experimental scheme for (O)–(AG). (O) Fecal 3-sucCA. (P) *Am* abundance. (Q) Body weights. (R) Liver weights. (S) Ratios of liver mass to body mass. Plasma ALT (T) and AST (U) levels. (V) Plasma TC content. (W) Plasma TG content. (X) Hepatic TC content. (Y) Hepatic TG content. (Z) Representative H&E (top), oil red O (middle), and Sirius red (bottom) staining of liver sections. $n = 3$ mice per group, 3 images per mouse. Scale bar, 100 μ m. (AA) Histology scores of steatosis, lobular inflammation, and hepatocyte ballooning. (AB) MAFLD activity score. (AC) Histology scores of fibrosis stage. (AD) Sirius Red-positive area. Relative mRNA levels of genes related to hepatic lipid metabolism (AE), inflammation (AF), and fibrosis (AG).

(AH) Heatmap showing the effects of different drugs on the growth of *A. muciniphila* JC032. Drugs at 50 μ M or control PBS were added in the BHI media and incubated with *A. muciniphila* JC032 or other isolates at logarithmic phase (inoculum size at 5%) anaerobically for 48 h. Each value represents the ratio of OD₆₀₀ value between treatment group and control group. $n = 5$ biological replicates.

(AI) Genus-level compositions of human SECs cultured in mGAM media supplemented with benzydamine, benfluorex, or PBS control anaerobically for 48 h. All data are presented as the means \pm SEMs. In (A), the p values were determined by two-tailed Student's t test. In (C)–(M), (AA)–(AC), (AE), and (AG), the p values were determined by Kruskal-Wallis test followed by Dunn's post hoc test. In (O), (P), (S), and (AD), the p values were determined by one-way ANOVA with Dunnett's T3 test. In (Q), (R), (T)–(Y), and (AF), the p values were determined by one-way ANOVA with Tukey's post hoc test. In (C)–(M), * $p < 0.05$ and ** $p < 0.01$ versus the control group. In (O)–(Y) and (AA)–(AG), * $p < 0.05$ and ** $p < 0.01$ versus the control group, # $p < 0.05$ and ## $p < 0.01$ versus the 3-sucCA group.



(legend on next page)

Figure S5. *A. muciniphila*-LPS-TLR4 pathway is responsible for the alleviation of MAFL-MASH progression by 3-sucCA, related to Figure 5

(A–T) CDAA-HFD-fed SPF mice were treated with PBS (control), 3-sucCA (10 mg/kg), 3-sucCA plus benzydamine (50 mg/kg), and 3-sucCA plus benfluorex (50 mg/kg) 3 times per week for the last 3 weeks. $n = 6$ mice/group. (A) *A. muciniphila* abundance in feces accessed by qPCR. (B) The relative expression of *Tjp1*, *Ocln*, *Cldn1*, *Cldn3*, *Cldn4*, *Cldn5*, *Tnfa*, *Il1b*, *Il18*, *Il6*, *Il10*, *Reg3g*, *Pla2g2a*, *Defa*, *Lyz1*, and *Muc2* mRNAs in colonic tissue. (C) *Muc2* protein content assayed by ELISA. (D) The representative H&E staining without colonic contents (top), Alcian blue/periodic acid-Schiff (AB-PAS) staining without (middle) or with (bottom) colonic contents of colonic tissue from different groups. Scale bar as indicated. Red and blue arrows indicate epithelial layer and lamina propria, respectively. (E) Blinded colonic mucus layer measurements from AB-PAS-stained sections (with colonic contents). 3 fields/image, 3 images/group. (F) The number of goblet cells was determined from AB-PAS-stained sections (without colonic contents). 3 fields/image, 3 images/group. (G) Intestinal permeability measured by plasma fluorescence intensity after FITC-dextran 4000 gavage. (H) Plasma LPS level. (I) Body weight. (J) Liver weights. (K) Plasma TC content. (L) Plasma TG content. (M) Hepatic TC content. (N) Histology scores of steatosis, lobular inflammation, and hepatocyte ballooning. (O) MAFLD activity score. (P) Histology scores of fibrosis stage. (Q) Sirius Red-positive area. Relative mRNA levels of genes related to hepatic lipid metabolism (R), inflammation (S), and fibrosis (T).

(U–AL) CDAA-HFD-fed *Tlr4*^{-/-} mice were treated with PBS (control) or 3-sucCA (10 mg/kg) 3 times per week for the last 3 weeks. $n = 6$ mice/group. (U) Experimental scheme for (V)–(AL). (V) Body weight. (W) Liver weights. (X) Ratios of liver mass to body mass. Plasma ALT (Y) and AST (Z) levels. (AA) Plasma TC content. (AB) Plasma TG content. (AC) Hepatic TC content. (AD) Hepatic TG content. (AE) Representative H&E (top), oil red O (middle), and Sirius red (bottom) staining of liver sections. $n = 3$ mice per group, 3 images per mouse. Scale bar, 100 μ m. (AF) Histology scores of steatosis, lobular inflammation, and hepatocyte ballooning. (AG) MAFLD activity score. (AH) Histology scores of fibrosis stage. (AI) Sirius Red-positive area. Relative mRNA levels of genes related to hepatic lipid metabolism (AJ), inflammation (AK), and fibrosis (AL).

All data are presented as the means \pm SEMs. In (A), (H), (J), (Q), and (S), the p values were determined by one-way ANOVA with Dunnett's T3 test. In (C), (E)–(G), and (K)–(M), the p values were determined by one-way ANOVA with Tukey's post hoc test. In (B), (I), (N)–(P), (R), and (T), the p values were determined by Kruskal-Wallis test followed by Dunn's post hoc test. In (V)–(X), (Z), (AA), (AC), (AD), (AI), (AK), and (AL), the p values were determined by two-tailed Student's t test. In (Y), (AB), (AF)–(AH), and (AJ), the p values were determined by two-tailed Mann-Whitney U test. In (A)–(C) and (E)–(T), * $p < 0.05$ and ** $p < 0.01$ versus the control group, # $p < 0.05$ and ## $p < 0.01$ versus the 3-sucCA group.

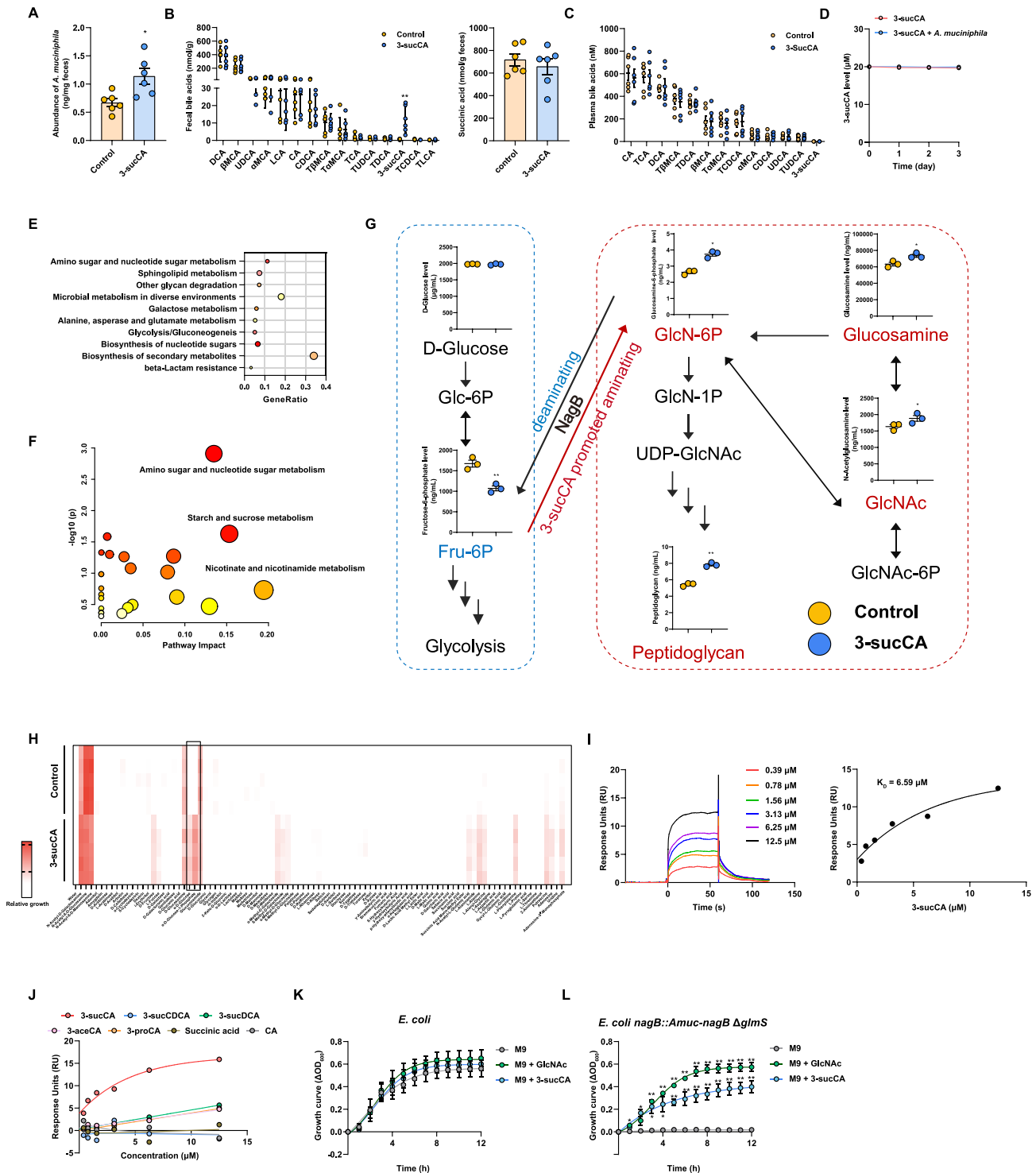


Figure S6. 3-sucCA promotes *A. muciniphila* growth through the enrichment of peptidoglycan synthesis, related to Figure 5 (A–C) CDAA-HFD-fed SPF mice were treated with PBS (control) or 3-sucCA (10 mg/kg) 3 times per week for 1 week. $n = 6$ mice/group. (A) *A. muciniphila* abundance in feces accessed by qPCR. (B) Bile acid and succinic acid levels in the feces. (C) Bile acid levels in plasma. (D) Level of remaining 3-sucCA during 3-sucCA incubation with *A. muciniphila* for 3 days ($n = 3$ independent incubations). (E) RNA-seq analysis of the *A. muciniphila* JC032 cultured in BHI media supplemented with 3-sucCA (10 μM) or PBS control anaerobically for 48 h. KEGG enrichment analysis of the biofunction changes between the 3-sucCA and control groups.

(legend continued on next page)

(F) The enriched pathways calculated from mummichog algorithm based on the non-targeted metabolomics analysis of samples from *A. muciniphila* incubation with 3-sucCA (10 μ M) or control PBS.

(G) Core metabolites related to amino sugar metabolism in *A. muciniphila*. Figure has been adapted from van der Ark et al.⁴² *A. muciniphila* JC032 cultured in BHI media supplemented with 3-sucCA (10 μ M) or PBS control, then grown anaerobically for 48 h. The culture was tested for glycolysis and peptidoglycan related metabolites, including D-glucose, glucosamine, *N*-acetylglucosamine, glucosamine 6-phosphate, and fructose 6-phosphate, which were detected by LC-MS/MS, and peptidoglycan, which was detected by ELISA kit. Metabolites in blue represented decreased in 3-sucCA treatment group and in red meant enriched by 3-sucCA addition.

(H) Heatmap showing the substrate utilization phenotyping of *A. muciniphila* by Biolog *in vitro* assay. The growth of *A. muciniphila* treated with 3-sucCA or PBS control was screened against different substrates as the sole nutrient source. Each value represents the relative growth indicated by crystal violet staining, following the protocol of the commercial kit.

(I) SPR sensorgram (left) and normalized steady-state binding curve (right) for 3-sucCA analytes (2-fold dilutions; 0.39–12.5 μ M) binding to Amuc-NagB. The K_D value is indicated.

(J) Normalized steady-state binding curves from SPR for succinic acid and different bile acids analytes (2-fold dilutions; 0.39–12.5 μ M) binding to Amuc-NagB.

(K) The growth curve of the strain *E. coli* cultured in M9 media supplemented with GlcNAc (0.1 mg/mL), 3-sucCA (10 μ M), or PBS control aerobically for 12 h. $n = 3$ biological replicates.

(L) The growth curve of the strain *E. coli nagB::Amuc-nagB Δ glmS* cultured in M9 media supplemented with GlcNAc (0.1 mg/mL), 3-sucCA (10 μ M), or PBS control aerobically for 12 h. $n = 3$ biological replicates.

All data are presented as the means \pm SEMs. In (A), (B) (right), and (G) (fructose 6-phosphate, D-glucose, and peptidoglycan), the p values were determined by two-tailed Student's *t* test. In (B) (left), (C), and (G) (glucosamine, *N*-acetylglucosamine, and glucosamine 6-phosphate), the p values were determined by two-tailed Mann-Whitney U test. In (K), the p values were determined by Kruskal-Wallis test followed by Dunn's post hoc test. In (L), the p values were determined by one-way ANOVA with Tukey's post hoc test. In (A)–(C), * $p < 0.05$ and ** $p < 0.01$ versus the control group. In (G), * $p < 0.05$ and ** $p < 0.01$ versus the control group. In (L), * $p < 0.05$ and ** $p < 0.01$ versus the M9 group.

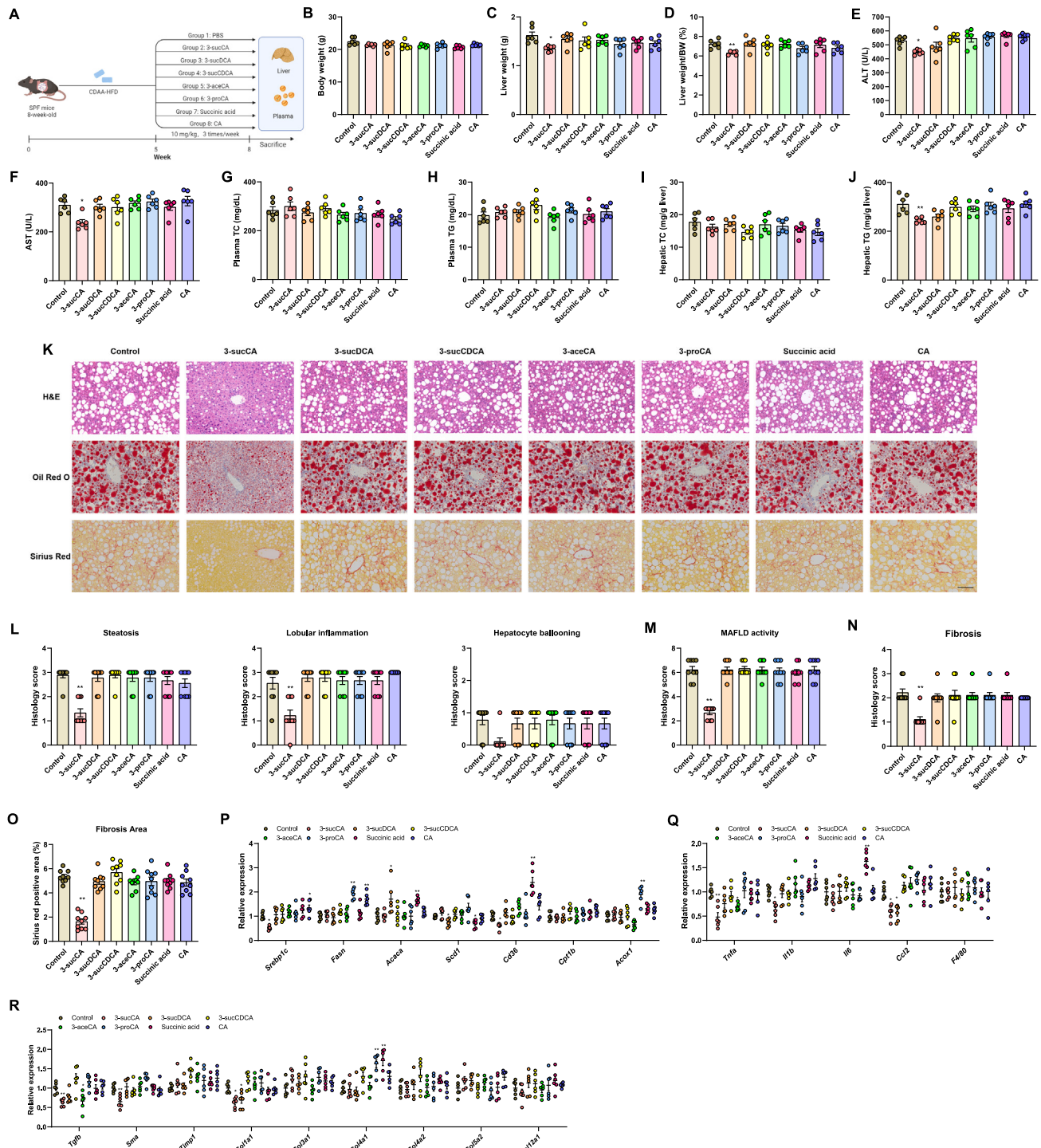
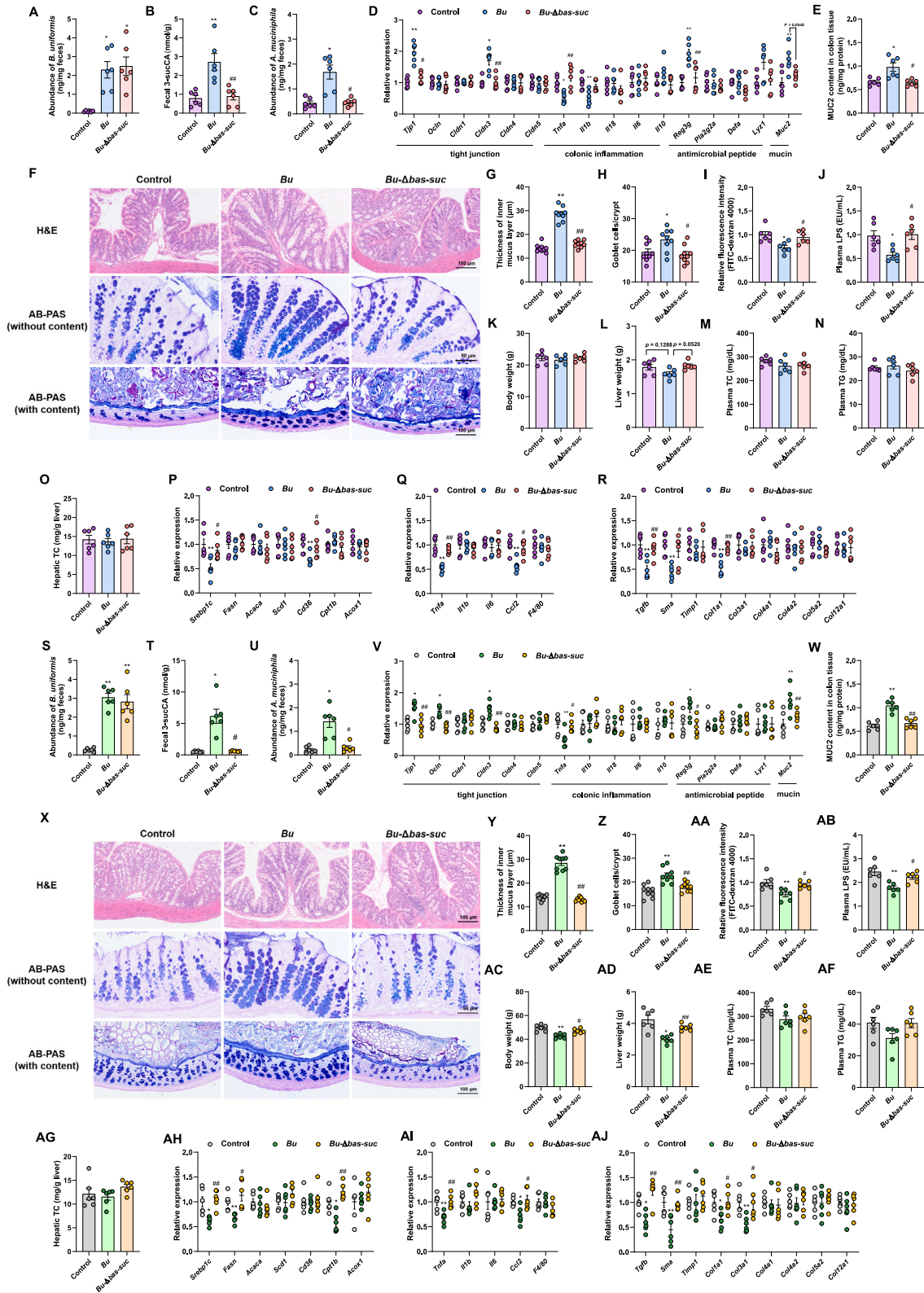


Figure S7. The effect of other related bile acids and derivatives on MAFL-MASH progression, related to Figure 5

(A–R) CDAA-HFD-fed SPF mice were treated with PBS (control), 3-sucCA (10 mg/kg), 3-sucDCA (10 mg/kg), 3-sucCDCA (10 mg/kg), 3-aceCA (10 mg/kg), 3-proCA (10 mg/kg), succinic acid (10 mg/kg), and CA (10 mg/kg) 3 times per week for the last 3 weeks. $n = 6$ mice/group. (A) Experimental scheme for (B)–(R). (B) Body weight. (C) Liver weights. (D) Ratios of liver mass to body mass. Plasma ALT (E) and AST (F) levels. (G) Plasma TC content. (H) Plasma TG content. (I) Hepatic TC content. (J) Hepatic TG content. (K) Representative H&E (top), oil red O (middle), and Sirius red (bottom) staining of liver sections. $n = 3$ mice per group, 3 images per mouse. Scale bar, 100 μ m. (L) Histology scores of steatosis, lobular inflammation, and hepatocyte ballooning. (M) MAFLD activity score. (N) Histology scores of fibrosis stage. (O) Sirius Red-positive area. Relative mRNA levels of genes related to hepatic lipid metabolism (P), inflammation (Q), and fibrosis (R).

(legend continued on next page)

All data are presented as the means \pm SEMs. In (B), the p values were determined by one-way ANOVA with Dunnett's T3 test. In (C), (G)–(J), and (O), the p values were determined by one-way ANOVA with Tukey's post hoc test. In (D)–(F), (L)–(N), and (P)–(R), the p values were determined by Kruskal-Wallis test followed by Dunn's post hoc test. In (B)–(J) and (L)–(R), * p < 0.05 and ** p < 0.01 versus the control group.



(legend on next page)

Figure S8. *B. uniformis* alleviates MAFL-MASH progression in a BAS-suc-dependent manner, related to Figure 6

(A–R) CDAA-HFD-fed SPF mice were treated with PBS (control), *Bu*, or *Bu-Δbas-suc* strain 1 time per week for the last 3 weeks. *n* = 6 mice/group. (A) *B. uniformis* abundance in feces accessed by qPCR. (B) 3-sucCA level in feces. (C) *A. muciniphila* abundance in feces accessed by qPCR. (D) The relative expression of *Tjp1*, *Ocln*, *Cldn1*, *Cldn3*, *Cldn4*, *Cldn5*, *Tnfa*, *Il1b*, *Il18*, *Il6*, *Il10*, *Reg3g*, *Pla2g2a*, *Defa*, *Lyz1*, and *Muc2* mRNAs in colonic tissue. (E) *Muc2* protein content assayed by ELISA. (F) The representative H&E staining without colonic contents (top), Alcian blue/periodic acid-Schiff (AB-PAS) staining without (middle) or with (bottom) colonic contents of colonic tissue from different groups. Scale bar as indicated. (G) Blinded colonic mucus layer measurements from AB-PAS-stained sections (with colonic contents). 3 fields/image, 3 images/group. (H) The number of goblet cells was determined from AB-PAS-stained sections (without colonic contents). 3 fields/image, 3 images/group. (I) Intestinal permeability measured by plasma fluorescence intensity after FITC-dextran 4000 gavage. (J) Plasma LPS level. (K) Body weight. (L) Liver weight. (M) Plasma TC content. (N) Plasma TG content. (O) Hepatic TC content. Relative mRNA levels of genes related to hepatic lipid metabolism (P), inflammation (Q), and fibrosis (R).

(S–AJ) GAN-diet-fed SPF mice were treated with PBS (control), *Bu*, or *Bu-Δbas-suc* strain 1 time per week for the last 4 weeks. *n* = 6 mice/group. (S) *B. uniformis* abundance in feces accessed by qPCR. (T) 3-sucCA level in feces. (U) *A. muciniphila* abundance in feces accessed by qPCR. (V) The relative expression of *Tjp1*, *Ocln*, *Cldn1*, *Cldn3*, *Cldn4*, *Cldn5*, *Tnfa*, *Il1b*, *Il18*, *Il6*, *Il10*, *Reg3g*, *Pla2g2a*, *Defa*, *Lyz1*, and *Muc2* mRNAs in colonic tissue. (W) *Muc2* protein content assayed by ELISA. (X) The representative H&E staining without colonic contents (top), Alcian blue/periodic acid-Schiff (AB-PAS) staining without (middle) or with (bottom) colonic contents of colonic tissue from different groups. Scale bar as indicated. (Y) Blinded colonic mucus layer measurements from AB-PAS-stained sections (with colonic contents). 3 fields/image, 3 images/group. (Z) The number of goblet cells was determined from AB-PAS-stained sections (without colonic contents). 3 fields/image, 3 images/group. (AA) Intestinal permeability measured by plasma fluorescence intensity after FITC-dextran 4000 gavage. (AB) Plasma LPS level. (AC) Body weight. (AD) Liver weights. (AE) Plasma TC content. (AF) Plasma TG content. (AG) Hepatic TC content. Relative mRNA levels of genes related to hepatic lipid metabolism (AH), inflammation (AI), and fibrosis (AJ).

All data are presented as the means ± SEMs. In (A), (C), (E), (R)–(U), (Y), (AD), and (AH), the *p* values were determined by one-way ANOVA with Dunnett's T3 test. In (B), (G)–(M), (O), (W), (Z)–(AC), (AE), and (AF), the *p* values were determined by one-way ANOVA with Tukey's post hoc test. In (D), (N), (P), (Q), (V), (AG), (AI), and (AJ), the *p* values were determined by Kruskal-Wallis test followed by Dunn's post hoc test. **p* < 0.05 and ***p* < 0.01 versus the control group, #*p* < 0.05 and ##*p* < 0.01 versus the *Bu* group.